Fluctuations of anisotropic flow in Pb+Pb collisions at $\sqrt{s_{\text{NN}}} = 5.02\,\text{TeV}$ with the ATLAS detector

The ATLAS collaboration

E-mail: atlas.publications@cern.ch

ABSTRACT: Multi-particle azimuthal cumulants are measured as a function of centrality and transverse momentum using $470\,\mu\text{b}^{-1}$ of Pb+Pb collisions at $\sqrt{s_{\text{NN}}} = 5.02\,\text{TeV}$ with the ATLAS detector at the LHC. These cumulants provide information on the event-by-event fluctuations of harmonic flow coefficients v_n and correlated fluctuations between two harmonics v_n and v_m. For the first time, a non-zero four-particle cumulant is observed for dipolar flow, v_1. The four-particle cumulants for elliptic flow, v_2, and triangular flow, v_3, exhibit a strong centrality dependence and change sign in ultra-central collisions. This sign change is consistent with significant non-Gaussian fluctuations in v_2 and v_3. The four-particle cumulant for quadrangular flow, v_4, is found to change sign in mid-central collisions. Correlations between two harmonics are studied with three- and four-particle mixed-harmonic cumulants, which indicate an anti-correlation between v_2 and v_3, and a positive correlation between v_2 and v_4. These correlations decrease in strength towards central collisions and either approach zero or change sign in ultra-central collisions. To investigate the possible flow fluctuations arising from intrinsic centrality or volume fluctuations, the results are compared between two different event classes used for centrality definitions. In peripheral and mid-central collisions where the cumulant signals are large, only small differences are observed. In ultra-central collisions, the differences are much larger and transverse momentum dependent. These results provide new information to disentangle flow fluctuations from the initial and final states, as well as new insights on the influence of centrality fluctuations.

KEYWORDS: Hadron-Hadron scattering (experiments), Heavy-ion collision, Collective flow, Event-by-event fluctuation, Particle correlations and fluctuations

Contents

1 Introduction

Heavy-ion collisions at RHIC and the LHC create hot, dense matter whose space-time evolution is well described by relativistic viscous hydrodynamics [1–3]. Owing to strong event-by-event energy density fluctuations in the initial state, the distributions of the final-state particles also fluctuate event by event. These fluctuations produce an effect in the

azimuthal angle ϕ distribution of the final-state particles, characterized by a Fourier expansion $\mathrm{d}N/\mathrm{d}\phi \propto 1 + 2\sum_{n=1}^{\infty} v_n \cos n(\phi - \Phi_n)$, where v_n and Φ_n represent the magnitude and event-plane angle of the nth-order harmonic flow. These quantities also are conveniently represented by the 'flow vector' $\boldsymbol{V}_n = v_n \mathrm{e}^{in\Phi_n}$ in each event. The $\boldsymbol{V}_n$ value reflects the hydrodynamic response of the produced medium to the nth-order initial-state eccentricity vector [4, 5], denoted by $\mathcal{E}_n = \epsilon_n \mathrm{e}^{in\Psi_n}$. Model calculations show that $\boldsymbol{V}_n$ is approximately proportional to $\mathcal{E}_n$ in general for $n = 2$ and 3, and for $n = 4$ in the case of central collisions [4, 6, 7]. The measurements of v_n and Φ_n [8–15] place important constraints on the properties of the medium and on the density fluctuations in the initial state [5–7, 16–18].

In order to disentangle the initial- and final-state effects, one needs detailed knowledge of the probability density distribution (or the event-by-event fluctuation) for single harmonics, $p(v_n)$, and two harmonics, $p(v_n, v_m)$. These distributions are often studied through multi-particle azimuthal correlations within the cumulant framework [19–23]. In this framework, the moments of the $p(v_n)$ distributions are measured by the $2k$-particle cumulants, $c_n\{2k\}$, for instance, $c_n\{2\} = \langle v_n^2 \rangle$ and $c_n\{4\} = \langle v_n^4 \rangle - 2\langle v_n^2 \rangle^2$ which are then used to define flow harmonics $v_n\{2k\}$ such as $v_n\{2\} = (c_n\{2\})^{1/2}$ and $v_n\{4\} = (-c_n\{4\})^{1/4}$. The four-particle cumulants $c_2\{4\}$ and $c_3\{4\}$ have been measured at RHIC and the LHC [24–31]. Most models of the initial state of A+A collisions predict a $p(v_n)$ with shape that is close to Gaussian, and these models predict zero or negative values for $c_n\{4\}$ [32, 33]. The values of $c_2\{4\}$ and $c_3\{4\}$ are found to be negative, except that $c_2\{4\}$ in very central Au+Au collisions at RHIC is positive [27]. Six- and eight-particle cumulants for v_2 have also been measured [24, 28, 34].

In the cumulant framework, the $p(v_n, v_m)$ distribution is studied using the four-particle 'symmetric cumulants', $\mathrm{sc}_{n,m}\{4\} = \langle v_n^2 v_m^2 \rangle - \langle v_n^2 \rangle \langle v_m^2 \rangle$ [22], or the three-particle 'asymmetric cumulants', $\mathrm{ac}_n\{3\} = \langle \boldsymbol{V}_n^2 \boldsymbol{V}_{2n}^* \rangle = \langle v_n^2 v_{2n} \cos 2n(\Phi_n - \Phi_{2n}) \rangle$ [35]. The asymmetric cumulants involve both the magnitude and phase of the flow vectors, and are often referred to as the 'event-plane correlators' [13]. The $\mathrm{sc}_{2,3}\{4\}$, $\mathrm{sc}_{2,4}\{4\}$ and $\mathrm{ac}_2\{3\}$ values have been measured in A+A collisions [13–15, 36, 37]. The values of $\mathrm{sc}_{2,3}\{4\}$ are found to be negative, reflecting an anti-correlation between v_2 and v_3, while the positive values of $\mathrm{sc}_{2,4}\{4\}$ and $\mathrm{ac}_2\{3\}$ suggest a positive correlation between v_2 and v_4.

Assuming that the scaling between $\boldsymbol{V}_n$ and $\mathcal{E}_n$ is exactly linear, then $p(v_n)$ and $p(v_n, v_m)$ should be the same as $p(\epsilon_n)$ and $p(\epsilon_n, \epsilon_m)$ up to a global rescaling factor. In order to isolate the initial eccentricity fluctuations, it was proposed in ref. [38] to measure the ratios of two cumulants of different order, for instance $\mathrm{nc}_n\{4\} \equiv c_n\{4\}/(c_n\{2\})^2 = -(v_n\{4\}/v_n\{2\})^4$. Similar cumulant ratios can be constructed for symmetric and asymmetric cumulants such as $\mathrm{nsc}_{n,m}\{4\} \equiv \mathrm{sc}_{n,m}\{4\}/(\langle v_n^2 \rangle \langle v_m^2 \rangle)$ and $\mathrm{nac}_n\{3\} = \mathrm{ac}_n\{3\}/(\langle v_n^4 \rangle \langle v_{2n}^2 \rangle)^{1/2}$. In addition, hydrodynamic model calculations suggest strong p_{T}-dependent fluctuations of v_n and Φ_n even in a single event [39, 40]. Such final-state intra-event flow fluctuations may change the shape of $p(v_n)$ or $p(v_n, v_m)$ in a p_{T}-dependent way and can be quantified by comparing cumulant ratios using particles from different p_{T} ranges.

In heavy-ion collisions, v_n coefficients are calculated for events with similar centrality, defined by the particle multiplicity in a fixed pseudorapidity range, which is also referred to as the reference multiplicity. The event ensemble, selected using a given reference

multiplicity, is referred to as a reference event class. Due to fluctuations in the particle production process, the true centrality for events with the same reference multiplicity still fluctuates from event to event. Since the v_n values vary with centrality, the fluctuations of centrality can lead to additional fluctuations of v_n and change the underlying $p(v_n)$ and $p(v_n, v_m)$ distributions [41]. Consequently, the cumulants $c_n\{2k\}$, $sc_{n,m}\{4\}$, and $ac_n\{3\}$ could be affected by the centrality resolution effects that are associated with the definition of the reference event class. Such centrality fluctuations, also known as volume fluctuations, have been shown to contribute significantly to event-by-event fluctuations of conserved quantities, especially in ultra-central collisions [42–44]. Recently, the centrality fluctuations were found to affect flow fluctuations as indicated by the sign change of $c_2\{4\}$ measured in ultra-central collisions [41]. A detailed study of $c_n\{2k\}$, $sc_{n,m}\{4\}$ and $ac_n\{3\}$ for different choices of the reference event class helps clarify the meaning of centrality and provides insight into the sources of particle production in heavy-ion collisions. In this paper, two reference event-class definitions are used to study the influence of centrality fluctuations on flow cumulants. The total transverse energy in the forward pseudorapidity range $3.2 < |\eta| < 4.9$ is taken as the default definition and a second definition uses the number of reconstructed charged particles in the mid-rapidity range $|\eta| < 2.5$.

This paper presents a measurement of $c_n\{2k\}$ for $n = 2, 3, 4$ and $k = 1, 2, 3$, $c_1\{4\}$, $sc_{2,3}\{4\}$, $sc_{2,4}\{4\}$ and $ac_2\{3\}$ in Pb+Pb collisions at $\sqrt{s_{NN}} = 5.02 \, \text{TeV}$ with the ATLAS detector at the LHC. The corresponding normalized cumulants $nc_n\{2k\}$, cumulant ratios $v_n\{4\}/v_n\{2\}$ and $v_n\{6\}/v_n\{4\}$, as well as normalized mixed-harmonic cumulants $nsc_{n,m}\{4\}$ and $nac_2\{3\}$, are calculated in order to shed light on the nature of $p(v_n)$ and $p(v_n, v_m)$. Results are obtained with the standard cumulant method as well as with the recently proposed three-subevent cumulant method [29, 35] in order to quantify the influence of non-flow correlations such as resonance decays and jets. Results using the two reference event-class definitions are compared in order to understand the role of centrality fluctuations and to probe the particle production mechanism which directly influences the size of centrality fluctuations.

The paper is organized as follows. Sections 2 and 3 describe the detector, trigger and datasets, as well as event and track selections. The mathematical framework for the multi-particle cumulants and the list of cumulant observables are provided in section 4. The correlation analysis and systematic uncertainties are described in sections 5 and 6, respectively. Section 7 first presents the results for various cumulant observables and then investigates the role of centrality fluctuations by making a detailed comparison of the cumulants calculated using two reference event classes. A summary is given in section 8.

2 ATLAS detector and trigger

The ATLAS detector [45] provides nearly full solid-angle coverage with tracking detectors, calorimeters, and muon chambers, and is well suited for measurements of multi-particle azimuthal correlations over a large pseudorapidity range.[1] The measurements are per-

---

[1]ATLAS uses a right-handed coordinate system with its origin at the nominal interaction point (IP) in the centre of the detector and the z-axis along the beam pipe. The x-axis points from the IP to the centre

formed using the inner detector (ID), the forward calorimeters (FCal), and the zero-degree calorimeters (ZDC). The ID detects charged particles within $|\eta| < 2.5$ using a combination of silicon pixel detectors, silicon microstrip detectors (SCT), and a straw-tube transition-radiation tracker, all immersed in a 2 T axial magnetic field [46]. An additional pixel layer, the 'insertable B-layer' [47, 48], was installed during the 2013–2015 shutdown between Run 1 and Run 2, and is used in the present analysis. The FCal consists of three sampling layers, longitudinal in shower depth, and covers $3.2 < |\eta| < 4.9$. The ZDC, positioned at ± 140 m from the IP, detects neutrons and photons with $|\eta| > 8.3$.

The ATLAS trigger system [49] consists of a level-1 (L1) trigger implemented using a combination of dedicated electronics and programmable logic, and a high-level trigger (HLT), which uses software algorithms similar to those applied in the offline event reconstruction. Events for this analysis were selected by two types of trigger. The minimum-bias trigger required either a scalar sum, over the whole calorimeter system, of transverse energy $\Sigma E_{\mathrm{T}}^{\mathrm{tot}}$ greater than 0.05 TeV or the presence of at least one neutron on both sides of the ZDC in coincidence with a track identified by the HLT. This trigger selected $22\,\mu\mathrm{b}^{-1}$ of Pb+Pb data. The number of recorded events from very central Pb+Pb collisions was increased by using a dedicated trigger selecting on the $\Sigma E_{\mathrm{T}}^{\mathrm{tot}}$ at L1 and ΣE_{T}, the total transverse energy in the FCal, at HLT. The combined trigger selects events with ΣE_{T} larger than one of the three threshold values: 4.21 TeV, 4.37 TeV and 4.54 TeV. This ultra-central trigger has a very sharp turn-on as a function of ΣE_{T} and for these thresholds was fully efficient for the 1.3%, 0.5% and 0.1% of events with the highest transverse energy in the FCal. The trigger collected $52\,\mu\mathrm{b}^{-1}$, $140\,\mu\mathrm{b}^{-1}$ and $470\,\mu\mathrm{b}^{-1}$ of Pb+Pb collisions for the three thresholds, respectively.

In the offline data analysis, events from the minimum-bias and ultra-central triggers are combined as a function of ΣE_{T} by applying an event-by-event weight calculated as the ratio of the number of minimum-bias events to the total number of events. This procedure ensures that the weighted distribution as a function of ΣE_{T} for the combined dataset follows the distribution of the minimum-bias events, and the results measured as a function of ΣE_{T} or centrality (see section 3) are not biased in their ΣE_{T} or centrality values.

3 Event and track selection

The analysis uses approximately $470\,\mu\mathrm{b}^{-1}$ of $\sqrt{s_{\mathrm{NN}}} = 5.02$ TeV Pb+Pb data collected in 2015. The offline event selection requires a reconstructed primary vertex with a z position satisfying $|z_{\mathrm{vtx}}| < 100$ mm. A coincidence between the ZDC signals at forward and backward pseudorapidity rejects a variety of background processes such as elastic collisions and non-collision backgrounds, while maintaining high efficiency for inelastic processes. The contribution from events containing more than one inelastic interaction (pile-up) is studied by exploiting the correlation between the transverse energy, ΣE_{T}, measured in

---

of the LHC ring, and the y-axis points upward. Cylindrical coordinates (r, ϕ) are used in the transverse plane, ϕ being the azimuthal angle around the beam pipe. The pseudorapidity is defined in terms of the polar angle θ as $\eta = -\ln\tan(\theta/2)$.

the FCal or the estimated number of neutrons N_n in the ZDC and the number of tracks associated with a primary vertex N_{ch}^{rec}. Since the distribution of ΣE_T or N_n in events with pile-up is broader than that for the events without pile-up, pile-up events are suppressed by rejecting events with an abnormally large ΣE_T or N_n as a function of N_{ch}^{rec}. The remaining pile-up contribution after this procedure is estimated to be less than 0.1% in the most central collisions.

The Pb+Pb event centrality [50] is characterized by the ΣE_T deposited in the FCal over the pseudorapidity range $3.2 < |\eta| < 4.9$. The FCal ΣE_T distribution is divided into a set of centrality intervals. A centrality interval refers to a percentile range, starting at 0% relative to the most central collisions at the largest ΣE_T value. Thus the 0–5% centrality interval, for example, corresponds to the most central 5% of the events. The ultra-central trigger mentioned in section 2 enhances the number of events in the 0–1.3%, 0–0.5% and 0–0.1% centrality intervals with full efficiency for the three L1 ΣE_T thresholds, respectively. Centrality percentiles are set by using a Monte Carlo Glauber analysis [50, 51] to provide a correspondence between the ΣE_T distribution and the sampling fraction of the total inelastic Pb+Pb cross section.

Charged-particle tracks [52] are reconstructed from hits in the ID and are then used to construct the primary vertices. Tracks are required to have $p_T > 0.5$ GeV and $|\eta| < 2.5$. They are required to have at least one pixel hit, with the additional requirement of a hit in the first pixel layer when one is expected, and at least six SCT hits. In order to reduce contribution from resonance decays, each track must have transverse and longitudinal impact parameters relative to the primary vertex which satisfy $|d_0| < 1.5$ mm and $|z_0 \sin\theta| < 1.5$ mm, respectively [53].

The efficiency $\epsilon(p_T, \eta)$ of the track reconstruction and track selection criteria is evaluated using Pb+Pb Monte Carlo events produced with the HIJING event generator [54]. The generated particles in each event are rotated in azimuthal angle according to the procedure described in ref. [55] in order to produce a harmonic flow that is consistent with the previous ATLAS measurements [10, 53]. The response of the detector is simulated using GEANT4 [56, 57] and the resulting events are reconstructed with the same algorithms as are applied to the data. For peripheral collisions, the efficiency ranges from 75% at $\eta \approx 0$ to about 50% for $|\eta| > 2$ for charged particles with $p_T > 0.8$ GeV. The efficiency falls by about 5% for a p_T of 0.5 GeV. The efficiency in central collisions ranges from 71% at $\eta \approx 0$ to about 40% for $|\eta| > 2$ for charged particles with $p_T > 0.8$ GeV, falling by about 8% for a p_T of 0.5 GeV. The rate of falsely reconstructed tracks ('fake' tracks) is also estimated and found to be significant only at $p_T < 1$ GeV in central collisions where it ranges from 2% for $|\eta| < 1$ to 8% at larger $|\eta|$. The fake-track rate drops rapidly for higher p_T and for more peripheral collisions. The fake-track rate is accounted for in the tracking efficiency correction following the procedure in ref. [24].

4 Observables

Both the standard cumulant method [20] and the three-subevent cumulant method [29, 35, 58, 59] are used to calculate the cumulants $c_n\{4\}$, $sc_{n,m}\{4\}$ and $ac_n\{3\}$. However, only the standard method is used to calculate the six-particle cumulants $c_n\{6\}$.

4.1 Cumulants in the standard method

The standard cumulant method calculates the $2k$-particle ($k = 1,2\ldots$) cumulants $c_n\{2k\}$ from the $2m$-particle ($m = 1,2\ldots k$) azimuthal correlations $\langle\{2m\}_n\rangle$, which are calculated for each event as [21, 22]

$$\langle\{2\}_n\rangle = \left\langle \mathrm{e}^{\mathrm{i}n(\phi_1-\phi_2)} \right\rangle, \quad \langle\{4\}_n\rangle = \left\langle \mathrm{e}^{\mathrm{i}n(\phi_1+\phi_2-\phi_3-\phi_4)} \right\rangle, \quad \langle\{6\}_n\rangle = \left\langle \mathrm{e}^{\mathrm{i}n(\phi_1+\phi_2+\phi_3-\phi_4-\phi_5-\phi_6)} \right\rangle, \tag{4.1}$$

where '$\langle\rangle$' denotes a single-event average over all pairs, quadruplets or sextuplets, respectively. The averages from eq. (4.1) can be expressed in terms of per-particle normalized flow vectors $\boldsymbol{q}_{n;l}$ with $l = 1, 2\ldots$ in each event [21]

$$\boldsymbol{q}_{n;l} \equiv \sum_j (w_j)^l\, \mathrm{e}^{\mathrm{i}n\phi_j} \left/ \sum_j (w_j)^l \right., \tag{4.2}$$

where the sum runs over all particles in the event and w_j is a weight assigned to the jth particle. This weight is constructed to correct for both detector non-uniformity and tracking inefficiency as explained in section 5.

The multi-particle cumulants are obtained from the azimuthal correlations using

$$\begin{aligned}
c_n\{2\} &= \langle\!\langle\{2\}_n\rangle\!\rangle = \left\langle v_n^2 \right\rangle, \\
c_n\{4\} &= \langle\!\langle\{4\}_n\rangle\!\rangle - 2\langle\!\langle\{2\}_n\rangle\!\rangle^2 = \left\langle v_n^4 \right\rangle - 2\left\langle v_n^2 \right\rangle^2, \\
c_n\{6\} &= \langle\!\langle\{6\}_n\rangle\!\rangle - 9\langle\!\langle\{4\}_n\rangle\!\rangle\langle\!\langle\{2\}_n\rangle\!\rangle + 12\langle\!\langle\{2\}_n\rangle\!\rangle^3 = \left\langle v_n^6 \right\rangle - 9\left\langle v_n^4 \right\rangle\left\langle v_n^2 \right\rangle + 12\left\langle v_n^2 \right\rangle^3,
\end{aligned} \tag{4.3}$$

where '$\langle\!\langle\rangle\!\rangle$' represents a weighted average of $\langle\{2k\}_n\rangle$ over an event ensemble with similar ΣE_{T} or $N_{\mathrm{ch}}^{\mathrm{rec}}$. In the absence of non-flow correlations, the $c_n\{2k\}$ values are related to the moments of the $p(v_n)$ distribution by the expression given in the last part of each equation chain. In particular, the higher moments of $p(v_n)$ can be obtained by combining the cumulants of different order, for example $\left\langle v_n^4 \right\rangle = 2c_n\{2\}^2 + c_n\{4\}$. If the amplitude of the flow vector does not fluctuate event by event, then eq. (4.3) gives a negative $c_n\{4\} = -v_n^4$ and a positive $c_n\{2\} = v_n^2$ and $c_n\{6\} = 4v_n^6$, which directly measure the true v_n. Flow coefficients from multi-particle cumulants $v_n\{2k\}$ are defined in this analysis as

$$v_n\{2\} = \sqrt{c_n\{2\}}, \quad v_n\{4\} = \begin{cases} \sqrt[4]{-c_n\{4\}} & c_n\{4\} \leq 0 \\ -\sqrt[4]{c_n\{4\}} & c_n\{4\} > 0, \end{cases} \quad v_n\{6\} = \begin{cases} \sqrt[6]{\frac{1}{4}c_n\{6\}} & c_n\{6\} \geq 0 \\ -\sqrt[6]{-\frac{1}{4}c_n\{6\}} & c_n\{6\} < 0, \end{cases} \tag{4.4}$$

which extends the standard definition [20] of $v_n\{2k\}$ to regions where $c_n\{4\} > 0$ and $c_n\{6\} < 0$.

If the fluctuation of the event-by-event flow-vector $\boldsymbol{V}_n = v_n\mathrm{e}^{\mathrm{i}n\Phi_n}$ is described in the plane transverse to the beam by a two-dimensional Gaussian function[2] given by

$$p(\boldsymbol{V}_n) = \frac{1}{\pi\delta_n^2}\mathrm{e}^{-\left|\boldsymbol{V}_n-v_n^0\right|^2 \big/ \left(\delta_n^2\right)}, \tag{4.5}$$

---

[2]Also known as a Bessel-Gaussian function.

then $v_n\{2\} = \sqrt{(v_n^0)^2 + \delta_n^2}$ and $v_n\{4\} = v_n\{6\} = v_n^0$ [12, 60]. The parameter δ_n is the width of the Gaussian function and v_n^0 is related to the average geometry of the overlap region. However, if the shape of $p(v_n)$ has significant non-Gaussian fluctuations at large v_n, both $c_n\{4\}$ and $c_n\{6\}$ may change sign, giving negative values for $v_n\{4\}$ and $v_n\{6\}$ [61].

The four-particle symmetric cumulants $\mathrm{sc}_{n,m}\{4\}$ and three-particle asymmetric cumulants $\mathrm{ac}_n\{3\}$ are related to multi-particle azimuthal correlations for two flow harmonics of different order by [22, 58]

$$\langle\{4\}_{n,m}\rangle = \left\langle \mathrm{e}^{\mathrm{i}n(\phi_1-\phi_2)+\mathrm{i}m(\phi_3-\phi_4)} \right\rangle, \qquad\qquad \langle\{3\}_n\rangle = \left\langle \mathrm{e}^{\mathrm{i}(n\phi_1+n\phi_2-2n\phi_3)} \right\rangle,$$

$$\mathrm{sc}_{n,m}\{4\} = \langle\!\langle\{4\}_{n,m}\rangle\!\rangle - \langle\!\langle\{2\}_n\rangle\!\rangle\langle\!\langle\{2\}_m\rangle\!\rangle, \quad \mathrm{ac}_n\{3\} = \langle\!\langle\{3\}_n\rangle\!\rangle = \langle\!\langle\mathrm{e}^{\mathrm{i}(n\phi_1+n\phi_2-2n\phi_3)}\rangle\!\rangle.$$

The first average is over all distinct quadruplets, triplets or pairs in one event to obtain $\langle\{4\}_{n,m}\rangle$, $\langle\{3\}_n\rangle$, $\langle\{2\}_n\rangle$ and $\langle\{2\}_m\rangle$, and the second average is over an event ensemble with the same ΣE_T or $N_\mathrm{ch}^\mathrm{rec}$ to obtain $\mathrm{sc}_{n,m}\{4\}$ and $\mathrm{ac}_n\{3\}$. In the absence of non-flow correlations, $\mathrm{sc}_{n,m}\{4\}$ and $\mathrm{ac}_n\{3\}$ are related to the correlation between v_n and v_m or between v_n and v_{2n}, respectively:

$$\mathrm{sc}_{n,m}\{4\} = \langle v_n^2 v_m^2\rangle - \langle v_n^2\rangle\langle v_m^2\rangle, \qquad \mathrm{ac}_n\{3\} = \langle v_n^2 v_{2n} \cos 2n(\Phi_n - \Phi_{2n})\rangle. \qquad (4.6)$$

Note that $\mathrm{ac}_n\{3\}$ is also related to the correlation between Φ_n and Φ_{2n}. This analysis measures three types of cumulants defined by eq. (4.6): $\mathrm{sc}_{2,3}\{4\}$, $\mathrm{sc}_{2,4}\{4\}$ and $\mathrm{ac}_2\{3\}$.

All the observables discussed above can be similarly defined for eccentricities by replacing v_n and Φ_n with ϵ_n and Ψ_n respectively. Denoted by $c_n\{2k, \epsilon\}$, $v_n\{2k, \epsilon\}$, $\mathrm{sc}_{n,m}\{4, \epsilon\}$ and $\mathrm{ac}_n\{3, \epsilon\}$, they describe the properties of $p(\epsilon_n)$ and $p(\epsilon_n, \epsilon_m)$. For example, $c_n\{4, \epsilon\} \equiv \langle\epsilon_2^4\rangle - 2\langle\epsilon_2^2\rangle^2$ and $\mathrm{ac}_n\{3, \epsilon\} = \langle\epsilon_n^2 \epsilon_{2n} \cos 2n(\Psi_n - \Psi_{2n})\rangle$.

4.2 Cumulants in the subevent method

In the 'standard' cumulant method described so far, all the k-particle multiplets involved in $\langle\{k\}_n\rangle$ and $\langle\{k\}_{n,m}\rangle$ are selected using charged tracks that are in the entire ID acceptance of $|\eta| < 2.5$. In order to further suppress the non-flow correlations that typically involve particles emitted within a localized region in η, the charged tracks are grouped into three subevents, labelled a, b and c, that each cover a unique η range [35]:

$$-2.5 < \eta_a < -\frac{2.5}{3}, \quad |\eta_b| < \frac{2.5}{3}, \quad \frac{2.5}{3} < \eta_c < 2.5.$$

Various subevent cumulants are then constructed by correlating particles between different subevents:

$$c_n^{a|c}\{2\} \equiv \langle\!\langle\{2\}_n\rangle\!\rangle_{a|c},$$

$$c_n^{2a|b,c}\{4\} \equiv \langle\!\langle\{4\}_n\rangle\!\rangle_{2a|b,c} - 2\langle\!\langle\{2\}_n\rangle\!\rangle_{a|b}\langle\!\langle\{2\}_n\rangle\!\rangle_{a|c},$$

$$\mathrm{sc}_{n,m}^{2a|b,c}\{4\} \equiv \langle\!\langle\{4\}_{n,m}\rangle\!\rangle_{2a|b,c} - \langle\!\langle\{2\}_n\rangle\!\rangle_{a|b}\langle\!\langle\{2\}_m\rangle\!\rangle_{a|c},$$

$$\mathrm{ac}_n^{a,b|c}\{3\} \equiv \langle\!\langle\{3\}_n\rangle\!\rangle_{a,b|c},$$

where

$$\langle\{2\}_n\rangle_{a|b} = \left\langle e^{in(\phi_1^a - \phi_2^b)}\right\rangle, \qquad\qquad \langle\{4\}_n\rangle_{2a|b,c} = \left\langle e^{in(\phi_1^a + \phi_2^a - \phi_3^b - \phi_4^c)}\right\rangle,$$

$$\langle\{4\}_{n,m}\rangle_{2a|b,c} = \left\langle e^{in(\phi_1^a - \phi_2^b) + im(\phi_3^a - \phi_4^c)}\right\rangle, \qquad \langle\{3\}_n\rangle_{a,b|c} = \left\langle e^{i(n\phi_1^a + n\phi_2^b - 2n\phi_3^c)}\right\rangle.$$

The statistical precision is enhanced by interchanging the η range for subevent a with that for subevent b or c which results in three independent measurements for each of $c_n\{4\}$, $\mathrm{sc}_{n,m}\{4\}$ and $\mathrm{ac}_n\{3\}$. They are averaged to obtain the final result.

It is well known that the values of $c_n\{2\}$ and $v_n\{2\}$ calculated using the standard cumulant method have a significant contribution from non-flow effects [60]. Therefore, in this analysis, they are measured using the two-subevent method following the expressions used in previous publications [62]:

$$c_n\{2\} \equiv c_n^{a|c}\{2\}, \qquad\qquad v_n\{2\} \equiv \sqrt{c_n^{a|c}\{2\}}. \tag{4.7}$$

This definition ensures that the non-flow correlations in $v_n\{2\}$ are greatly reduced by requiring a minimum pseudorapidity gap of 1.67 between subevents a and c. For k-particle cumulants with $k > 2$, the standard method is used as the default since they are less influenced by non-flow correlations, and this assumption is additionally verified with the three-subevent method [35, 63, 64].

4.3 Normalized cumulants and cumulant ratios

Any quantity which is linearly proportional to v_n has the same cumulants, up to a global factor. Therefore the shapes of $p(v_n)$ and $p(v_n, v_m)$ can be more directly probed using the ratio of the cumulants [65, 66]:

$$\mathrm{nc}_n\{4\} = \frac{c_n\{4\}}{c_n^{a|c}\{2\}^2} = \frac{\langle v_n^4\rangle}{\langle v_n^2\rangle^2} - 2, \tag{4.8}$$

$$\mathrm{nc}_n\{6\} = \frac{c_n\{6\}}{4c_n^{a|c}\{2\}^3}, \tag{4.9}$$

$$\mathrm{nsc}_{n,m}\{4\} = \frac{\mathrm{sc}_{n,m}\{4\}}{c_n^{a|c}\{2\}c_m^{a|c}\{2\}} = \frac{\langle v_n^2 v_m^2\rangle}{\langle v_n^2\rangle \langle v_m^2\rangle} - 1, \tag{4.10}$$

$$\mathrm{nac}_n\{3\} = \frac{\mathrm{ac}_n\{3\}}{\sqrt{\left(2c_n^{a|c}\{2\}^2 + c_n\{4\}\right)c_{2n}^{a|c}\{2\}}} = \frac{\langle v_n^2 v_{2n} \cos 2n(\Phi_n - \Phi_{2n})\rangle}{\sqrt{\langle v_n^4\rangle \langle v_{2n}^2\rangle}}, \tag{4.11}$$

where the two-particle cumulants $c_n\{2\}$ in the denominator of these equations are calculated from subevents a and c using eq. (4.7). If v_n is exactly proportional to ϵ_n, the normalized cumulants defined above would be the same as the normalized cumulants calculated from eccentricities in the initial state, i.e. $\mathrm{nc}_n\{2k\} = \mathrm{nc}_n\{2k, \epsilon\}$, $\mathrm{nsc}_{n,m}\{4\} = \mathrm{nsc}_{n,m}\{4, \epsilon\}$ and $\mathrm{nac}_n\{3\} = \mathrm{nac}_n\{3, \epsilon\}$. In practice, final-state effects, such as p_T-dependent fluctuations of v_n and Φ_n [39, 40], hydrodynamic noise [67] and non-linear mode-mixing between harmonics of different order [4, 68] can break this equality. Therefore, studying the p_T

dependence of these normalized cumulants can help in understanding the influence of dynamical effects from the final state.

The $\mathrm{nc}_n\{4\}$ and $\mathrm{nc}_n\{6\}$ cumulants defined above contain the same information as the previously proposed ratios of $v_n\{4\}$ to $v_n\{2\}$ and $v_n\{6\}$ to $v_n\{2\}$ [38] given by,

$$\frac{v_n\{4\}}{v_n\{2\}} \equiv \begin{cases} \sqrt[4]{-\mathrm{nc}_n\{4\}} & \mathrm{nc}_n\{4\} \leq 0 \\ -\sqrt[4]{\mathrm{nc}_n\{4\}} & \mathrm{nc}_n\{4\} > 0 \end{cases}, \qquad \frac{v_n\{6\}}{v_n\{2\}} = \begin{cases} \sqrt[6]{\mathrm{nc}_n\{6\}} & \mathrm{nc}_n\{6\} \geq 0 \\ -\sqrt[6]{-\mathrm{nc}_n\{6\}} & \mathrm{nc}_n\{6\} < 0 \end{cases}. \qquad (4.12)$$

The $\mathrm{nc}_n\{4\}$ and $\mathrm{nc}_n\{6\}$ values still vary smoothly as a function of centrality even if the $c_n\{4\}$ or $c_n\{6\}$ values change sign as a function of centrality. However, due to the fractional power in eq. (4.12), this is not true for $v_n\{4\}$ and $v_n\{6\}$ in the region where the sign changes. For this reason, the results in this paper are often presented using $\mathrm{nc}_n\{4\}$ and $\mathrm{nc}_n\{6\}$ instead of $v_n\{4\}$ and $v_n\{6\}$.

5 Data analysis

The cumulants are calculated in three steps following examples from refs. [29, 58] using the standard and subevent methods. Since these steps are the same for $c_n\{2k\}$, $\mathrm{sc}_{n,m}\{4\}$ and $\mathrm{ac}_n\{3\}$, they are explained using $c_n\{2k\}$ as an example.

In the first step, the multi-particle correlators $\langle\{2k\}_n\rangle$ are calculated for each event from particles in one of four p_{T} ranges: $0.5 < p_{\mathrm{T}} < 5\,\mathrm{GeV}$, $1.0 < p_{\mathrm{T}} < 5\,\mathrm{GeV}$, $1.5 < p_{\mathrm{T}} < 5\,\mathrm{GeV}$, and $2 < p_{\mathrm{T}} < 5\,\mathrm{GeV}$. The upper p_{T} cutoff is required to reduce the contribution from jet fragmentation. In the second step, the correlators $\langle\{2k\}_n\rangle$ are averaged over an event ensemble, defined as events in either a narrow interval of ΣE_{T} ($0.002\,\mathrm{TeV}$) or a narrow interval of $N_{\mathrm{ch}}^{\mathrm{rec}}$ (track bin width is 1) taken as the number of reconstructed charged particles in the range $0.5 < p_{\mathrm{T}} < 5\,\mathrm{GeV}$. The $c_n\{2k\}$ values are then calculated separately for these two types of reference event classes, denoted by $c_n\{2k, \Sigma E_{\mathrm{T}}\}$ and $c_n\{2k, N_{\mathrm{ch}}^{\mathrm{rec}}\}$, respectively. In order to obtain statistically significant results, in the final step the $c_n\{2k\}$ values from several neighbouring ΣE_{T} or $N_{\mathrm{ch}}^{\mathrm{rec}}$ intervals are combined, weighted by the number of events in each interval. The p_{T} dependence of the cumulants is studied by simultaneously varying the p_{T} range for all particles in each $2k$-multiplet in the cumulant analysis. This approach is different from previous studies where the p_{T} range of only one particle in the multiplet is varied [20, 22, 24, 28, 69].

The left panel of figure 1 shows the correlation between ΣE_{T} and $N_{\mathrm{ch}}^{\mathrm{rec}}$. The two quantities have an approximately linear correlation, but events with the same ΣE_{T} have significant fluctuations in $N_{\mathrm{ch}}^{\mathrm{rec}}$ and vice versa. Due to these relative fluctuations, the reference event class based on $N_{\mathrm{ch}}^{\mathrm{rec}}$ may have centrality fluctuations that differ from those of the reference event class based on ΣE_{T}, even if both are matched to have the same $\langle\Sigma E_{\mathrm{T}}\rangle$ or the same $\langle N_{\mathrm{ch}}^{\mathrm{rec}}\rangle$.

The correlation between ΣE_{T} and $N_{\mathrm{ch}}^{\mathrm{rec}}$ is studied using events divided into narrow intervals in either ΣE_{T} or $N_{\mathrm{ch}}^{\mathrm{rec}}$. The mean and root-mean-square values of the $N_{\mathrm{ch}}^{\mathrm{rec}}$ (ΣE_{T}) distributions are calculated for each ΣE_{T} ($N_{\mathrm{ch}}^{\mathrm{rec}}$) interval, and the results are shown in the middle and right panels of figure 1, respectively. A linear relation is observed between $\langle N_{\mathrm{ch}}^{\mathrm{rec}}\rangle$ and ΣE_{T} over the full ΣE_{T} range, while a significant non-linear relation is observed

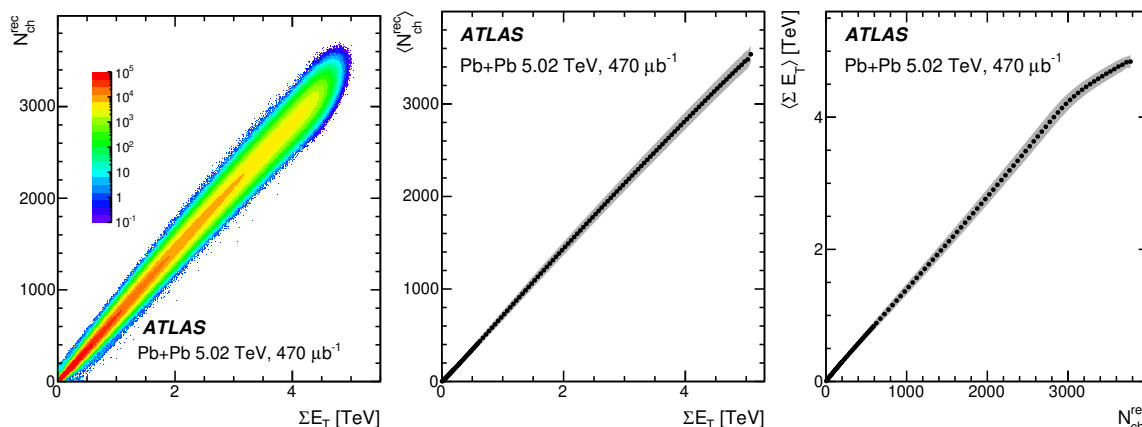**Figure 1**. The correlation between N_{ch}^{rec} and ΣE_T (left panel), and the mean (solid points) and root-mean-square (shaded bands) of either the N_{ch}^{rec} distributions for events in narrow slices of ΣE_T (middle panel) or the ΣE_T distributions for events in narrow slices of N_{ch}^{rec} (right panel).

between $\langle \Sigma E_T \rangle$ and N_{ch}^{rec} at large N_{ch}^{rec}. This latter behaviour suggests that, in ultra-central collisions, ΣE_T retains sensitivity to the $\langle N_{ch}^{rec} \rangle$ of the events, while N_{ch}^{rec} has relatively poorer sensitivity to the $\langle \Sigma E_T \rangle$ of the events. This implies that the true centrality is more smeared for events with the same N_{ch}^{rec} than for events with the same ΣE_T.

Since v_n changes with centrality, any centrality fluctuations could lead to additional fluctuation of v_n, and subsequently to a change in the flow cumulants. Indeed, previous ATLAS studies [29, 58, 62] have shown that the $c_n\{2k\}$ values depend on the definition of the reference event class used for averaging. A comparison of the results based on these two reference event classes can shed light on the details of flow fluctuations and how they are affected by centrality fluctuations.

Figure 2 shows the distributions of N_{ch}^{rec} and ΣE_T obtained from the projections of the two-dimensional correlation shown in the left panel of figure 1. The inserted panels show the local first-order derivatives of the one-dimensional ΣE_T or N_{ch}^{rec} distributions in the most central collisions. The derivative for the ΣE_T distribution is relatively independent of ΣE_T up to 4.1 TeV and then decreases and reaches a local minimum at around 4.4 TeV. The derivative for the N_{ch}^{rec} distribution is mostly flat up to 2800 and then decreases and reaches a local minimum at around 3100. The locations where the derivative starts to depart from a constant are defined as the knee of the ΣE_T or N_{ch}^{rec} distribution and is given by $(\Sigma E_T)_{knee} = 4.1$ TeV and $(N_{ch}^{rec})_{knee} = 2800$. Events with $\Sigma E_T > (\Sigma E_T)_{knee}$ correspond to the top 1.9% centrality and events with $N_{ch}^{rec} > (N_{ch}^{rec})_{knee}$ correspond to top 2.7% centrality when mapped to the equivalent $\langle \Sigma E_T \rangle$. The knees mark the locations where multiplicity distributions start to decrease sharply and the underlying centrality fluctuations are expected to deviate significantly from a Gaussian distribution [41, 44]. The knee values are important in discussing the trends of cumulants in ultra-central collisions in section 7.3.

The particle weights used in eq. (4.2) that account for detector inefficiencies and non-uniformity are defined as [62]

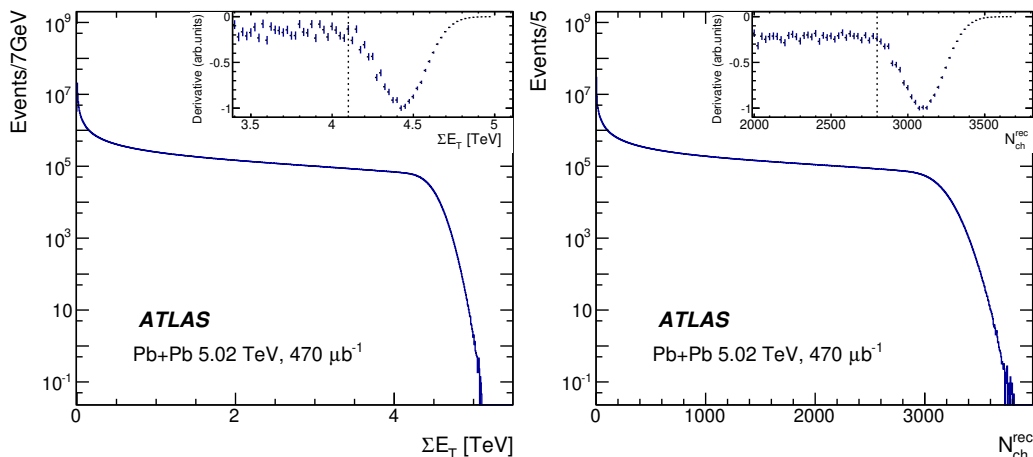$$w_j(\phi, \eta, p_T) = d(\phi, \eta)/\epsilon(\eta, p_T), \tag{5.1}$$

Figure 2. The distribution of ΣE_T (left panel) and the distribution of N_{ch}^{rec} (right panel) for the Pb+Pb collisions. The insert panels show the first-order derivative of the corresponding one-dimensional distributions. The vertical dashed line indicates the location, $(\Sigma E_T)_{knee} = 4.1$ TeV and $(N_{ch}^{rec})_{knee} = 2800$ respectively, where the derivatives for ΣE_T and N_{ch}^{rec} start to decrease. The values of the derivatives have been rescaled to a minimum value of -1.

where $\epsilon(\eta, p_T)$ is the efficiency for reconstructing charged particles from Monte Carlo. The additional weight factor $d(\phi, \eta)$, determined from data, accounts for non-uniformities in the efficiency as a function of ϕ in each η range. All reconstructed charged particles with $p_T > 0.5$ GeV are entered into a two-dimensional histogram $N(\phi, \eta)$, and the weight factor is then obtained as $d(\phi, \eta) \equiv \langle N(\eta) \rangle / N(\phi, \eta)$, where $\langle N(\eta) \rangle$ is the track density averaged over ϕ in the given η interval. This procedure corrects most of the ϕ-dependent non-uniformity that results from track reconstruction [62].

6 Systematic uncertainties

The systematic uncertainties of the measurements presented in this paper are evaluated by varying different aspects of the analysis and comparing $c_n\{2k\}$, $sc_{2,3}\{4\}$, $sc_{2,4}\{4\}$ and $ac_2\{3\}$ with their baseline values. The main sources of systematic uncertainty are track selection, the track reconstruction efficiency, the pile-up contribution, and differences between data and Monte Carlo simulation. The uncertainties are generally small when the absolute values of the cumulants are large. The relative uncertainties are larger in central or very peripheral collisions where the signal is small. The uncertainties also decrease rapidly with increasing p_T, due to a larger flow signal at higher p_T and are typically less than a few percent for $p_T > 1$ GeV. Therefore, the following discussion focuses mainly on the results obtained for charged particles in the $0.5 < p_T < 5$ GeV range. The systematic uncertainties are also found to be similar between the standard method and the three-subevent method.

The systematic uncertainty associated with track selection is evaluated by applying more restrictive requirements. The requirement on $|d_0|$ and $|z_0 \sin\theta|$ is changed to be less than 1.0 mm instead of the nominal value of 1.5 mm. The numbers of pixel and SCT hits required are also increased, to two and eight respectively, to further reduce the fake-track

rates. The uncertainties are less than 2% for $c_n\{2\}$, less than 3% for $c_2\{4\}$, $c_2\{6\}$ and $c_3\{4\}$, less than 5% for $c_1\{4\}$ and $c_4\{4\}$, and are in the range of 1–5% for $\mathrm{sc}_{2,3}\{4\}$, $\mathrm{sc}_{2,4}\{4\}$ and $\mathrm{ac}_2\{3\}$.

Previous measurements [10] show that the v_n signal has a strong dependence on p_T but a relatively weak dependence on η. Therefore, a p_T-dependent uncertainty in the track reconstruction efficiency $\epsilon(\eta, p_\mathrm{T})$ could affect the measured cumulants through the particle weights in eqs. (4.2) and (5.1). The uncertainty of $\epsilon(\eta, p_\mathrm{T})$ arises from differences in the detector conditions and known differences in the material between data and simulations. This uncertainty varies between 1% and 4%, depending on η and p_T [24]. Its impact on cumulants is evaluated by repeating the analysis with the tracking efficiency varied up and down by its corresponding uncertainty. The impact on cumulants is in the range of 1–5% for $c_n\{2\}$, 0.5–12% for $c_n\{4\}$ and $c_n\{6\}$, and in the range of 2–8% for $\mathrm{sc}_{n,m}\{4\}$ and $\mathrm{ac}_2\{3\}$.

Pile-up events are suppressed by exploiting the correlation, discussed in section 3, between ΣE_T measured in the FCal and the number of neutrons N_n in the ZDC. In the ultra-central collisions, where the pile-up fraction is the largest, the residual pile-up is estimated to be less than 0.1%. The impact of the pile-up is evaluated by tightening and relaxing pile-up rejection criteria, and the resulting variation is included in the systematic uncertainty. The uncertainty is in the range of 0.1–1% for all cumulants.

The analysis procedure is also validated through Monte Carlo studies by comparing the observables calculated with generated particles with those obtained from reconstructed particles, using the same analysis chain and correction procedure as for data. In the low p_T region, where tracking performance suffers from low efficiency and high fake-track rates, systematic differences are observed between the cumulants calculated at the generator level and at the reconstruction level. These differences are included as part of the systematic uncertainty. They amount to 0.1–3% in mid-central and peripheral collisions and up to 10% in the most central collisions.

The systematic uncertainties from different sources are added in quadrature to determine the total systematic uncertainties. These uncertainties for two-particle cumulants are in the range of 1–5% for $c_2\{2\}$, 2–7% for $c_3\{2\}$ and 4–9% for $c_4\{2\}$. For multi-particle cumulants, the total uncertainties are in the range of 8–12% for $c_1\{4\}$, 2–7% for $c_2\{4\}$, 1–9% for $c_3\{4\}$, 4–15% for $c_4\{4\}$ and 4–15% for $c_2\{6\}$. For symmetric and asymmetric cumulants, the total uncertainties are in the range of 2–7% for $\mathrm{sc}_{2,3}\{4\}$, 2–9% for $\mathrm{sc}_{2,4}\{4\}$ and 2–7% for $\mathrm{ac}_2\{3\}$. The total systematic uncertainties for the three-subevent cumulant method are comparable. The uncertainties in the flow coefficients $v_n\{2k\}$ are obtained from the total uncertainties of $c_n\{2k\}$ by using eq. (4.3).

The uncertainties for normalized cumulants, $\mathrm{nc}_n\{4\}$, $\mathrm{nc}_2\{6\}$, $\mathrm{nsc}_{2,3}\{4\}$, $\mathrm{nsc}_{2,4}\{4\}$ and $\mathrm{nac}_2\{3\}$, are calculated separately for each source of systematic uncertainty discussed above, and are similar to the baseline results. Most of the systematic uncertainties cancel out in these ratios. In mid-central and peripheral collisions, the total uncertainties are in the range of 1–5% depending on the observables. However, the total uncertainties are larger in ultra-central collisions, reaching as high as 10% for $\mathrm{nc}_2\{6\}$ and $\mathrm{nac}_2\{3\}$.

7 Results

The results for various cumulant observables are presented in sections 7.1 and 7.2. The cumulants are calculated using the reference event class based on ΣE_T and with the procedure discussed in section 5. The results are presented as a function of centrality calculated from ΣE_T. Section 7.1 discusses the cumulants related to single harmonics: $c_n\{2k, \Sigma E_\mathrm{T}\}$, $v_n\{2k, \Sigma E_\mathrm{T}\}$, and $\mathrm{nc}_n\{2k, \Sigma E_\mathrm{T}\}$. Section 7.2 presents correlations between two flow harmonics: $\mathrm{nsc}_{2,3}\{4, \Sigma E_\mathrm{T}\}$, $\mathrm{nsc}_{2,4}\{4, \Sigma E_\mathrm{T}\}$ and $\mathrm{nac}_2\{3, \Sigma E_\mathrm{T}\}$. The results are shown for four p_T ranges: $0.5 < p_\mathrm{T} < 5\,\mathrm{GeV}$, $1.0 < p_\mathrm{T} < 5\,\mathrm{GeV}$, $1.5 < p_\mathrm{T} < 5\,\mathrm{GeV}$, and $2 < p_\mathrm{T} < 5\,\mathrm{GeV}$. The default results are obtained using the standard cumulant method and are compared with those obtained using the three-subevent cumulant method. The comparisons are shown only if significant differences are observed; otherwise, they are included in appendix B.

Section 7.3 discusses the influence of centrality fluctuations on flow cumulants. Each cumulant observable is calculated using both the ΣE_T-based reference event class and the $N_\mathrm{ch}^\mathrm{rec}$-based reference event class. The results from the two reference event classes, for example $c_n\{2k, \Sigma E_\mathrm{T}\}$ and $c_n\{2k, N_\mathrm{ch}^\mathrm{rec}\}$, are compared as a function of $\langle \Sigma E_\mathrm{T}\rangle$ or $\langle N_\mathrm{ch}^\mathrm{rec}\rangle$. The differences are sensitive to the centrality fluctuations.

While most of the results are presented for $v_n\{2\}$, $\mathrm{nc}_n\{2k\}$, $\mathrm{nsc}_{n,m}\{4\}$ and $\mathrm{nac}_2\{3\}$, the results for $c_n\{4\}$, $c_n\{6\}$, $v_n\{4\}$ and $v_n\{6\}$, as well as $\mathrm{sc}_{2,3}\{4\}$, $\mathrm{sc}_{2,4}\{4\}$ and $\mathrm{ac}_2\{3\}$, are not shown explicitly (although some are included in appendix A). However, they can be obtained directly from $v_n\{2\}$, normalized cumulants and normalized mixed-harmonic cumulants according to eqs. (4.8)–(4.12).

7.1 Flow cumulants for $p(v_n)$

Figure 3 shows the $v_n\{2\}$ values for $n = 2, 3, 4$ for charged particles in several p_T ranges, calculated for the event class based on FCal ΣE_T and then plotted as a function of centrality. The $v_n\{2\}$ values are obtained from two-particle cumulants with a pseudorapidity gap according to eq. (4.7). For all p_T ranges, $v_2\{2\}$ first increases and then decreases toward central collisions, reflecting the typical centrality dependence behaviour of the eccentricity ϵ_2 [60]. The magnitude of $v_2\{2\}$ also increases strongly with p_T. The centrality and p_T dependences of $v_3\{2\}$ and $v_4\{2\}$ are similar, but the tendency to decrease from mid-central toward central collisions is less pronounced.

Figure 4 shows the centrality dependence of normalized four-particle cumulants $\mathrm{nc}_2\{4\}$, $\mathrm{nc}_3\{4\}$, and $\mathrm{nc}_4\{4\}$ in four p_T ranges using the standard method (top row) and the three-subevent method (bottom row). The advantage of using $\mathrm{nc}_n\{4\}$ instead of $c_n\{4\}$ is that the p_T dependence of v_n, seen in figure 3, is largely cancelled out and that $\mathrm{nc}_n\{4\}$ directly reflects the shape of the $p(v_n)$ distributions [12]. Overall, the results based on the three-subevent method behave similarly to those from the standard cumulant method, implying that the influence of non-flow correlations is small. Therefore, the remaining discussion is focused on the standard method in the top row.

Figure 4 shows that the values of $\mathrm{nc}_2\{4\}$ and $\mathrm{nc}_3\{4\}$ are negative in most of the centrality range. The values of $|\mathrm{nc}_2\{4\}|$ increase and then decrease toward central colli-
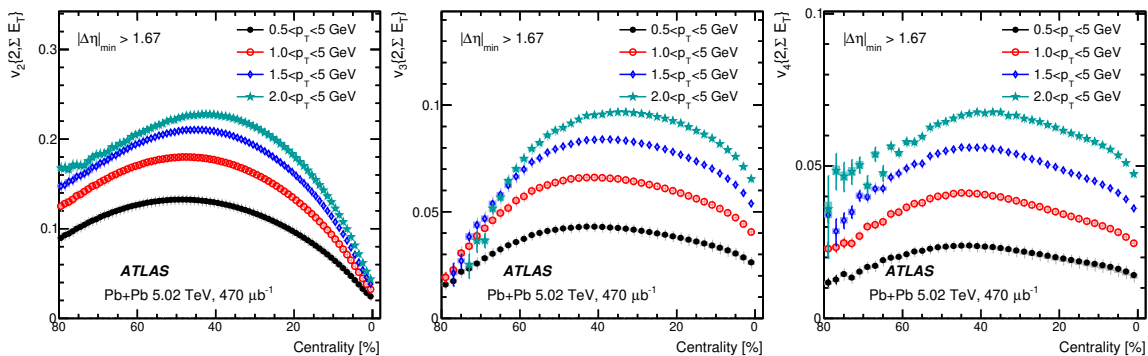
Figure 3. The centrality dependence of $v_2\{2, \Sigma E_T\}$ (left panel), $v_3\{2, \Sigma E_T\}$ (middle panel) and $v_4\{2, \Sigma E_T\}$ (right panel) for four p_T ranges. The error bars and shaded boxes represent the statistical and systematic uncertainties, respectively.
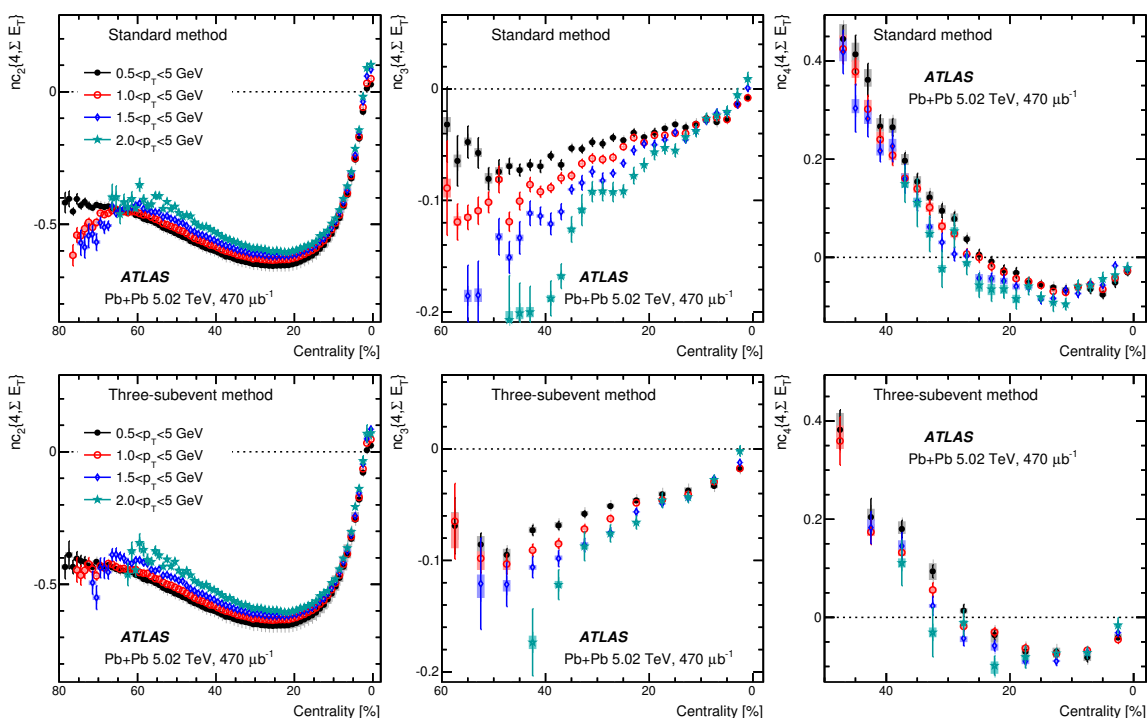

Figure 4. The centrality dependence of normalized four-particle cumulants $\mathrm{nc}_2\{4, \Sigma E_T\}$ (left panel), $\mathrm{nc}_3\{4, \Sigma E_T\}$ (middle panel), and $\mathrm{nc}_4\{4, \Sigma E_T\}$ (right panel) obtained with the standard method (top row) and the three-subevent method (bottom row) for four p_T ranges. The error bars and shaded boxes represent the statistical and systematic uncertainties, respectively. Zero is indicated by a dotted line.

sions, while the values of $|\mathrm{nc}_3\{4\}|$ decrease continuously toward central collisions. These centrality-dependent trends are shown in refs. [24, 25, 70] to be driven by the centrality dependence of the four-particle cumulants for ϵ_2 and ϵ_3, respectively. The normalized cumulants still show some residual dependence on p_T. Namely, the $|\mathrm{nc}_2\{4\}|$ values are smaller for the higher-p_T particles, while the values of $|\mathrm{nc}_3\{4\}|$ are larger for the higher p_T range.

Furthermore, the values of $\mathrm{nc}_2\{4\}$ are also observed to change sign in ultra-central collisions and the pattern of these sign changes also has significant p_T dependence. The observed behaviour of $\mathrm{nc}_n\{4\}$ in ultra-central collisions is closely related to centrality fluctuations and is discussed further in section 7.3.

The $\mathrm{nc}_4\{4\}$ values, as shown in the right panels of figure 4, are negative in central collisions but change sign around a centrality range of 25–30%. The centrality value at which the sign change occurs shifts towards more peripheral collisions as the p_T of the particles increases. It is well established that $\boldsymbol{V}_4$ in Pb+Pb collisions contains a linear contribution associated with the initial geometry and a mode-mixing contribution from lower-order harmonics due to the non-linear hydrodynamic response [4, 13, 14, 17, 68],

$$\boldsymbol{V}_4 = \boldsymbol{V}_{4\mathrm{L}} + \chi_2 \boldsymbol{V}_2^2 \,, \tag{7.1}$$

where the linear component $\boldsymbol{V}_{4\mathrm{L}}$ is driven by the corresponding eccentricity ϵ_4 in the initial geometry [6], and χ_2 is a constant. Previous measurements [13, 14] show that the $\boldsymbol{V}_{4\mathrm{L}}$ term dominates in central collisions, while the $\boldsymbol{V}_2^2$ term dominates in more peripheral collisions. Therefore, the sign change of $\mathrm{nc}_4\{4\}$ could reflect an interplay between these two contributions [71]. In central collisions, $\mathrm{nc}_4\{4\}$ is dominated by a negative contribution from $p(v_{4\mathrm{L}})$, while in peripheral collisions $\mathrm{nc}_4\{4\}$ is dominated by a positive contribution from $p(v_2^2)$. The change of the crossing point with p_T suggests that the relative contribution from these two sources is also a function of p_T.

If the v_n value is driven only by ϵ_n, then $p(v_n)$ should have the same shape as $p(\epsilon_n)$. On the other hand, the significant p_T dependence of $\mathrm{nc}_n\{4\}$ in figure 4 suggests that the shape of $p(v_n)$ also changes with p_T. Such p_T-dependent behaviour implies that the eccentricity fluctuations in the initial state are not the only source for flow fluctuations. Dynamical fluctuations in the momentum space in the initial or final state may also change $p(v_n)$.

Figure 5 shows the cumulant ratio, $v_n\{4\}/v_n\{2\}$, obtained from the $\mathrm{nc}_n\{4\}$ data shown in figure 4 using eq. (4.12). This ratio is directly related to the magnitude of the relative fluctuation of the $p(v_n)$ distribution. For the Gaussian fluctuation model given in eq. (4.5), it is $v_n\{4\}/v_n\{2\} = v_n^0/\sqrt{(v_n^0)^2 + \delta_n^2}$. A ratio close to one suggests a small flow fluctuation $\delta_n \ll v_n^0$, while a ratio close to zero implies a large fluctuation $\delta_n \gg v_n^0$. The results for $v_2\{4\}/v_2\{2\}$ imply that flow fluctuations are small relative to v_2^0, but become larger in the most central collisions. The results for $v_3\{4\}/v_3\{2\}$ suggest that the relative fluctuation of $p(v_3)$ grows gradually from peripheral to central collisions. The values of $v_4\{4\}/v_4\{2\}$ are around 0.4–0.5 in the 0–20% centrality range, comparable to slightly larger than the values of $v_3\{4\}/v_3\{2\}$. In peripheral collisions, $v_4\{4\}/v_4\{2\}$ is negative and its magnitude increases and reaches minus one in very peripheral collisions, suggesting a significant departure of $p(v_4)$ from a Gaussian shape. The large statistical uncertainties around the sign-change region is due to the divergence in the first derivative of the function $\sqrt[4]{|x|}$ around $x \equiv \mathrm{nc}_4\{4\} = 0$.

Figure 6 shows the centrality dependence of normalized six-particle cumulants $\mathrm{nc}_2\{6\}$, $\mathrm{nc}_3\{6\}$ and $\mathrm{nc}_4\{6\}$. According to eq. (4.12), these quantities are directly related to the cumulant ratios $v_n\{6\}/v_n\{2\}$. The values of $\mathrm{nc}_2\{6\}$ are positive over most of the centrality range, but reach zero in ultra-central collisions. The centrality dependence of $|\mathrm{nc}_2\{6\}|$ is
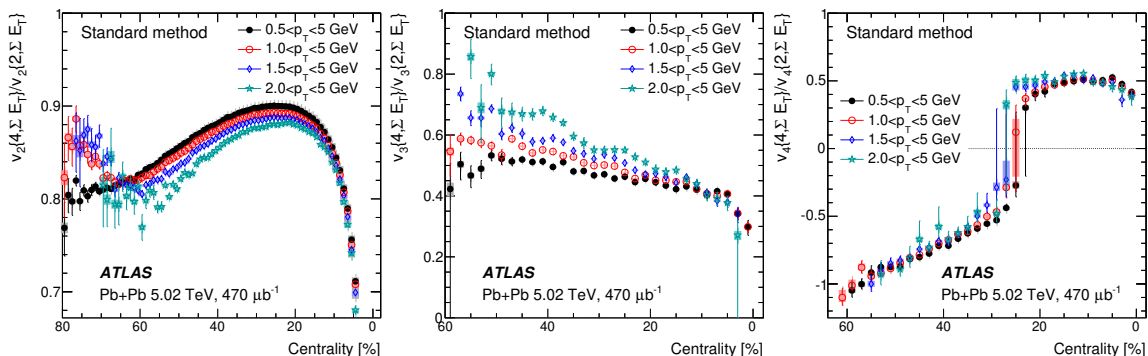
Figure 5. The centrality dependence of cumulant ratios $v_n\{4,\Sigma E_T\}/v_n\{2,\Sigma E_T\}$ for $n=2$ (left panel), $n=3$ (middle panel), and $n=4$ (right panel) for four p_T ranges. The error bars and shaded boxes represent the statistical and systematic uncertainties, respectively. Zero is indicated by a dotted line.
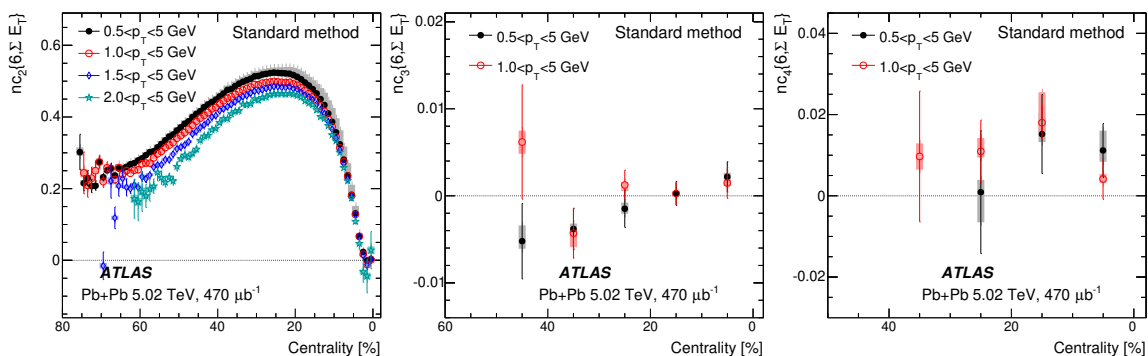

Figure 6. The centrality dependence of normalized six-particle cumulants $nc_2\{6,\Sigma E_T\}$ (left panel), $nc_3\{6,\Sigma E_T\}$ (middle panel), and $nc_4\{6,\Sigma E_T\}$ (right panel) obtained with the standard method for several p_T ranges. The error bars and shaded boxes represent the statistical and systematic uncertainties, respectively. Zero is indicated by a dotted line.

very similar to that of $|nc_2\{4\}|$ in the left panel of figure 4. The values of $nc_3\{6\}$ and $nc_4\{6\}$ are much smaller and have larger statistical uncertainties. Therefore, only the results from the two p_T ranges with lower p_T thresholds, which have the best statistical precision, are shown. The values are smaller than 0.005 and 0.01 for $nc_3\{6\}$ and $nc_4\{6\}$, which correspond to an upper limit of $|v_3\{6\}/v_3\{2\}| \lesssim \sqrt[6]{0.005} = 0.38$ and $|v_4\{6\}/v_4\{2\}| \lesssim \sqrt[6]{0.01} = 0.46$, respectively.

From the measured $nc_2\{6\}$ and $nc_2\{4\}$, the ratio of the six-particle cumulant to the fourth-particle cumulant, $v_2\{6\}/v_2\{4\}$, can be obtained. The results are shown in the left panel of figure 7. For the Gaussian fluctuation model in eq. (4.5), this ratio is expected to be one. The apparent deviation of the ratio from one suggests non-Gaussianity of $p(v_2)$ over a broad centrality range. The results for different p_T ranges are close to each other, but nevertheless show systematic- and centrality-dependent differences. In general, the results from higher p_T are larger in central collisions and smaller in peripheral collisions than those from lower p_T. The middle panel of figure 7 compares the results for $0.5 < p_T < 5\,\mathrm{GeV}$
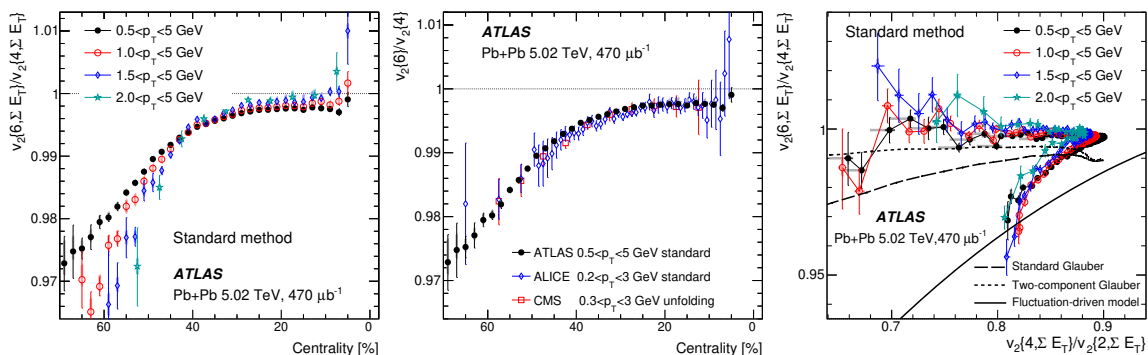
Figure 7. The centrality dependence of the cumulant ratio $v_2\{6, \Sigma E_{\rm T}\}/v_2\{4, \Sigma E_{\rm T}\}$ for four $p_{\rm T}$ ranges (left panel) and comparison with results obtained with the standard method from ALICE collaboration [34] and unfolding technique from the CMS collaboration [30] (middle panel), and correlation between $v_2\{6, \Sigma E_{\rm T}\}/v_2\{4, \Sigma E_{\rm T}\}$ and $v_2\{4, \Sigma E_{\rm T}\}/v_2\{2, \Sigma E_{\rm T}\}$ compared with models based on initial-state eccentricities (right panel). The error bars and shaded boxes represent the statistical and systematic uncertainties, respectively. One is indicated by a dotted line.

with those obtained from ALICE and CMS collaborations. Despite slight differences in the $p_{\rm T}$ selections, good consistency is observed, although the ATLAS results have much smaller statistical and systematic uncertainties.

To further understand the nature of the $p(v_2)$ and its relation to $p(\epsilon_2)$, the right panel of figure 7 shows directly the correlation between $v_2\{6\}/v_2\{4\}$ and $v_2\{4\}/v_2\{2\}$. Each data point is obtained by combining the information from the left panels of figures 5 and 7 from the same centrality range. The central region corresponds to the left-most points, while peripheral region corresponds to points near the bottom-middle of the panel. If v_2 values are driven by ϵ_2, this correlation should be directly comparable to analogous correlation calculated directly from initial-state elliptic eccentricity: $v_2\{6, \epsilon\}/v_2\{4, \epsilon\}$ vs. $v_2\{4, \epsilon\}/v_2\{2, \epsilon\}$. The data are compared to correlations from three initial state models: the standard Glauber model with ϵ_2 calculated from the participating nucleons (long-dashed line) [41, 51], a two-component Glauber model with ϵ_2 calculated from a combination of participating nucleons and binary nucleon-nucleon collisions (short-dashed line) [41, 51], or a fluctuation-driven model with ϵ_2 calculated from random sources (solid line) [32]. These models fail to describe quantitatively the overall correlation pattern, although the two-component Glauber model is closest to the data in central collisions, while the fluctuation-driven model is closest to the data in peripheral collisions.

The multi-particle correlations are also calculated to obtain cumulants for the dipolar flow, v_1. Figure 8 shows the centrality dependence of $c_1\{4\}$ in several $p_{\rm T}$ ranges, which is obtained from the reference event class based on $\Sigma E_{\rm T}$. In the hydrodynamic picture, $c_1\{4\}$ is sensitive to event-by-event fluctuations of the dipolar eccentricity ϵ_1 associated with initial-state geometry [6]. This measurement has a large uncertainty because both $\langle\!\langle\{4\}_1\rangle\!\rangle$ and $\langle\!\langle\{2\}_1\rangle\!\rangle$ in eq. (4.3) contain a significant contribution from global momentum-conservation effects [10, 72]. This contribution cancels out for $c_1\{4\}$ but leads to a large statistical uncertainty. A negative $c_1\{4\}$ for $p_{\rm T} > 1.5\,{\rm GeV}$ is observed in both the standard and three-subevent cumulant methods, which reflects the event-by-event fluctuations of the dipolar eccentricity.
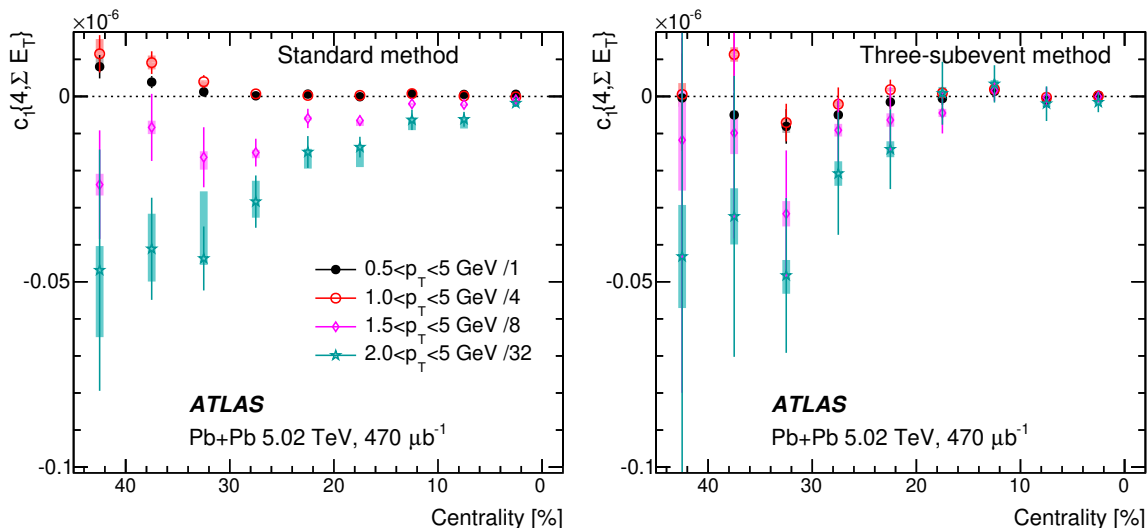
Figure 8. The centrality dependence of $c_1\{4\}$ calculated for charged particles in several p_T ranges with the standard method (left panel) and three-subevent method (right panel). The error bars and shaded boxes represent the statistical and systematic uncertainties, respectively. The data for each p_T range are scaled by a constant factor indicated in the legend for the purpose of presentation. Zero is indicated by a dotted line.

Previously, ATLAS measured v_1 using the two-particle correlation method in Pb+Pb collisions at $\sqrt{s_{NN}} = 2.76\,\text{TeV}$ where an explicit procedure was employed to subtract the global momentum-conservation effects [10]. The $v_1\{2\}$ values was observed to be negative at low p_T, change sign at $p_T \approx 1.2\,\text{GeV}$ and increase quickly for higher p_T. Therefore, a $c_1\{4\}$ signal is expected to be larger and easier to measure at higher p_T. Figure 9 shows the $v_1\{4\}$ values calculated from $c_1\{4\}$ for the two highest p_T ranges: $1.5 < p_T < 5\,\text{GeV}$ and $2 < p_T < 5\,\text{GeV}$. The $v_1\{4\}$ values increase both with p_T and in more peripheral collisions, and are in the range of 0.02–0.04 for $2 < p_T < 5\,\text{GeV}$.

7.2 Flow cumulants for $p(v_n, v_m)$

The correlation between flow harmonics of different order is studied using the four-particle normalized symmetric cumulant $nsc_{2,3}\{4\}$ and $nsc_{2,4}\{4\}$, and the three-particle normalized asymmetric cumulant $nac_3\{3\}$. Figure 10 shows the centrality dependence of $nsc_{2,3}\{4\}$ in several p_T ranges which probes the correlation between the v_2 and v_3. The $nsc_{2,3}\{4\}$ is negative in most of the centrality range, indicating an anti-correlation between the v_2 and v_3. This anti-correlation has been observed in previous studies based on the same observable [15] and using an event-shape engineering technique [14]. The strength of the anti-correlation has significant p_T dependence. For higher-p_T particles, the anti-correlation is stronger in peripheral collisions and weaker in central collisions. In the ultra-central collisions, $nsc_{2,3}\{4\}$ changes sign and becomes positive. This positive correlation is related to centrality fluctuations and is discussed further in section 7.3. The behaviour of the overall centrality and p_T dependence is also found to be similar between the standard cumulant
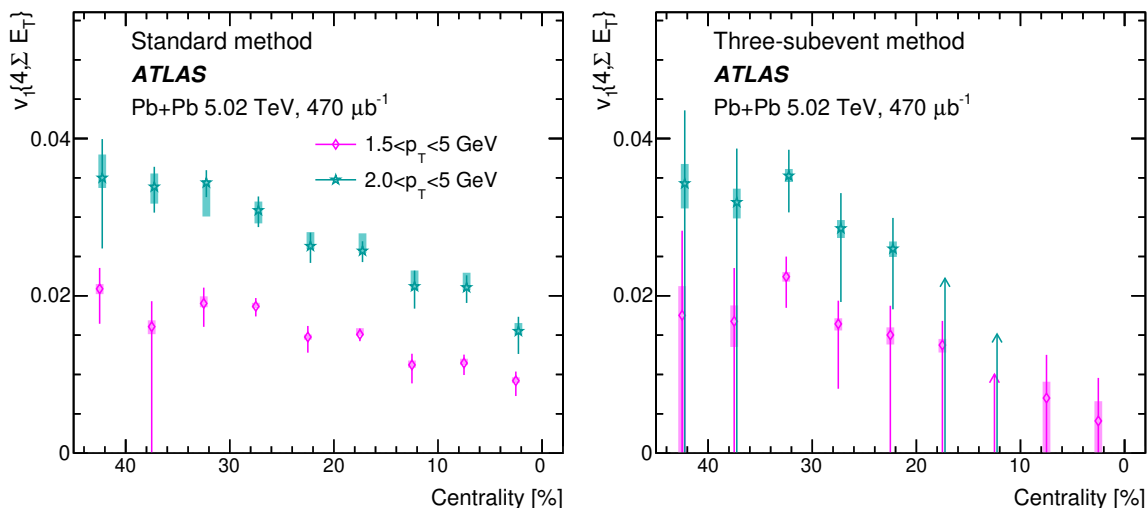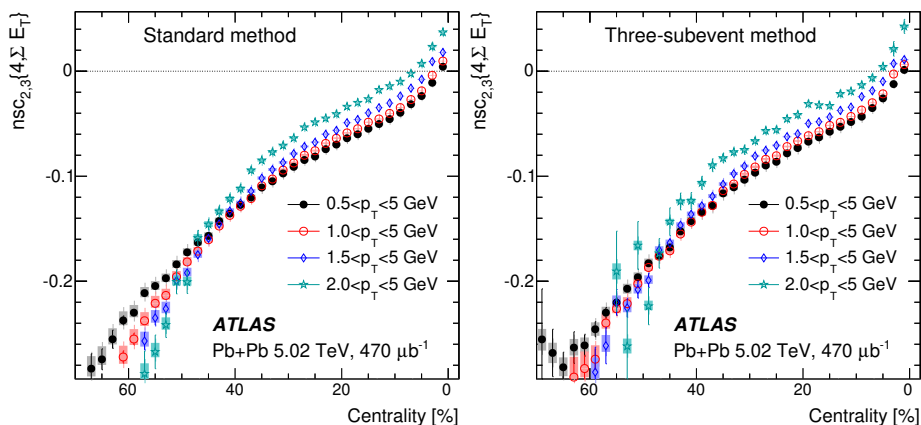
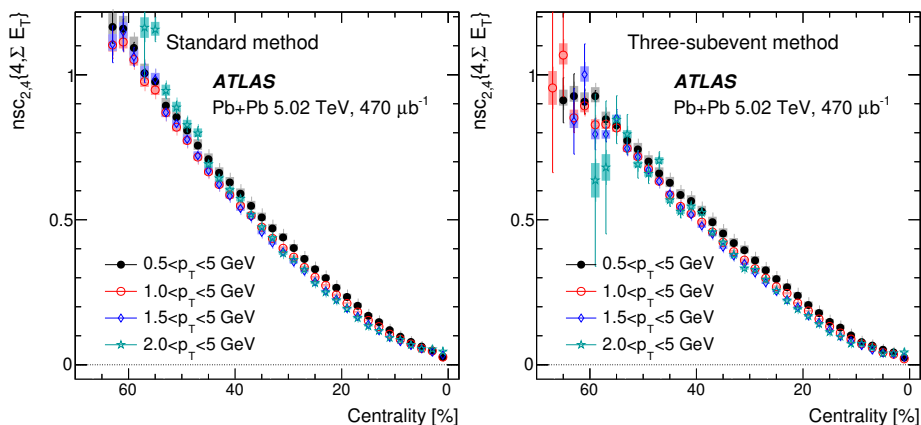**Figure 9**. The centrality dependence of $v_1\{4\}$ calculated for charged particles in two p_T ranges with the standard method (left panel) and three-subevent method (right panel). The error bars and shaded boxes represent the statistical and systematic uncertainties, respectively.

Figure 10. The centrality dependence of $nsc_{2,3}\{4\}$ calculated for charged particles in four p_T ranges with the standard method (left panel) and three-subevent method (right panel). The error bars and shaded boxes represent the statistical and systematic uncertainties, respectively. Zero is indicated by a dotted line.

method and the three-subevent cumulant method. This suggests that these features are not caused by non-flow correlations.

Figure 11 shows the centrality dependence of $nsc_{2,4}\{4\}$ in several p_T ranges which probes the correlation between v_2 and v_4. The $nsc_{2,4}\{4\}$ value is positive over the entire centrality range, indicating a positive correlation between v_2 and v_4. The signal is very small in central collisions but increases rapidly towards peripheral collisions. The correlations are similar among different p_T ranges in central collisions but are slightly weaker for higher-p_T particles in mid-central collisions. This behaviour is also predicted by hydrodynamic models [7, 73]. Compared with the three-subevent method, the $nsc_{2,4}\{4\}$ values from the standard method have better statistical precision but slightly higher values in

Figure 11. The centrality dependence of $\mathrm{nsc}_{2,4}\{4\}$ calculated for charged particles in four p_{T} ranges with the standard method (left panel) and three-subevent method (right panel). The error bars and shaded boxes represent the statistical and systematic uncertainties, respectively. Zero is indicated by a dotted line.

peripheral collisions, indicating that the non-flow effects may become significant for events beyond 60% centrality.

Figure 12 shows the centrality dependence of $\mathrm{nac}_2\{3\}$ in several p_{T} ranges which also probes the correlation between v_2 and v_4. The $\mathrm{nac}_2\{3\}$ value is positive over the entire centrality range. The correlation is weak in the central collisions, increases rapidly as the centrality approaches about 20–30% and then increases slowly toward more peripheral collisions. The correlation patterns for different p_{T} ranges are similar in central collisions but are slightly weaker for higher-p_{T} particles in mid-central collisions. Compared with results obtained from the three-subevent method, the results from the standard method are slightly larger in peripheral collisions, indicating that non-flow fluctuations may contribute for events beyond 60% centrality. The similar p_{T} and centrality dependences for $\mathrm{nsc}_{2,4}\{4\}$ and $\mathrm{nac}_2\{3\}$ are related to the non-linear mode-mixing effects between v_2 and v_4 described by eq. (7.1) [65].

7.3 Dependence on reference event class and the role of centrality fluctuations

This section presents the $\langle \Sigma E_{\mathrm{T}} \rangle$ or $\langle N_{\mathrm{ch}}^{\mathrm{rec}} \rangle$ dependence of various cumulants for the two reference event classes. Section 5 describes how the role of centrality fluctuations associated with the reference event class used in the calculation of the cumulants can be understood by extracting the results for each observable in narrow ranges of ΣE_{T} and $N_{\mathrm{ch}}^{\mathrm{rec}}$. These results are presented as a function of $\langle \Sigma E_{\mathrm{T}} \rangle / (\Sigma E_{\mathrm{T}})_{\mathrm{knee}}$ and $\langle N_{\mathrm{ch}}^{\mathrm{rec}} \rangle / (N_{\mathrm{ch}}^{\mathrm{rec}})_{\mathrm{knee}}$, where $(\Sigma E_{\mathrm{T}})_{\mathrm{knee}} = 4.1\,\mathrm{TeV}$ and $(N_{\mathrm{ch}}^{\mathrm{rec}})_{\mathrm{knee}} = 2800$ are the knee values of the ΣE_{T} and $N_{\mathrm{ch}}^{\mathrm{rec}}$ distributions shown in figure 2. It should be noted that $c_n\{2k, \Sigma E_{\mathrm{T}}\}$ (and other observables as well) as a function of $\langle \Sigma E_{\mathrm{T}} \rangle / (\Sigma E_{\mathrm{T}})_{\mathrm{knee}}$ contains the same information as the centrality dependence of $c_n\{2k, \Sigma E_{\mathrm{T}}\}$ shown in two previous sections. However, x-axes based on $\langle \Sigma E_{\mathrm{T}} \rangle / (\Sigma E_{\mathrm{T}})_{\mathrm{knee}}$ and $\langle N_{\mathrm{ch}}^{\mathrm{rec}} \rangle / (N_{\mathrm{ch}}^{\mathrm{rec}})_{\mathrm{knee}}$ more naturally characterize the size of the overlap region in Pb+Pb collisions and allow a more detailed visualization of the ultra-central region, where the impacts of centrality fluctuations is strongest.
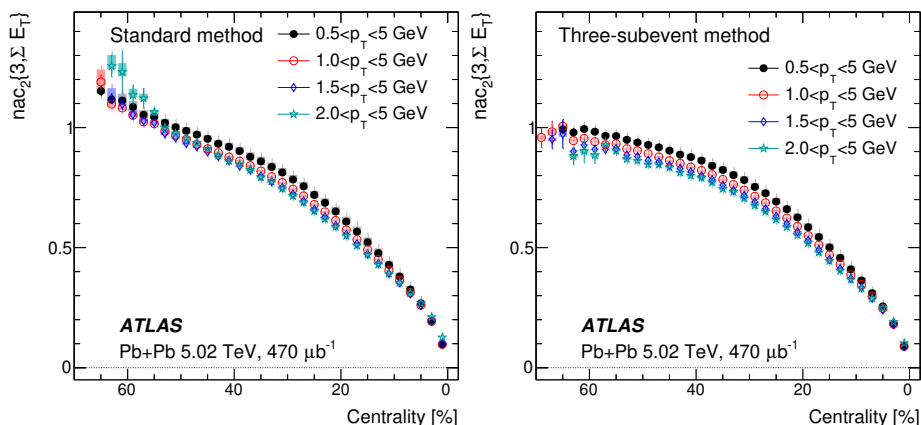
Figure 12. The centrality dependence of nac$_2${3} calculated for charged particles in four p_T ranges with the standard method (left panel) and three-subevent method (right panel). The error bars and shaded boxes represent the statistical and systematic uncertainties, respectively. Zero is indicated by a dotted line.

7.3.1 Two-particle cumulants

The top panels of figure 13 show $v_n\{2, \Sigma E_T\}$ as a function of $\langle \Sigma E_T \rangle$. The $v_n\{2, \Sigma E_T\}$ values are reflecting the same centrality and p_T dependence behaviour already shown in figure 3. In ultra-central collisions, the $v_n\{2, \Sigma E_T\}$ values are nearly constant. Similar trends are also observed for $v_n\{2, N_{ch}^{rec}\}$ which are shown in the bottom panels of figure 13 as a function of $\langle N_{ch}^{rec} \rangle$. These results suggest that the underlying initial geometry, in terms of $\langle \epsilon_n^2 \rangle$, is quite similar between the two reference event classes.

In order to quantify differences between the two reference event classes, $v_n\{2, N_{ch}^{rec}\}$ is mapped to a $\langle \Sigma E_T \rangle$ dependence and $v_n\{2, \Sigma E_T\}$ is mapped to a $\langle N_{ch}^{rec} \rangle$ dependence. The ratio $v_n\{2, N_{ch}^{rec}\}/v_n\{2, \Sigma E_T\}$ is then calculated at a given $\langle \Sigma E_T \rangle$ or at a given $\langle N_{ch}^{rec} \rangle$. The top row of figure 14 shows $v_n\{2, N_{ch}^{rec}\}/v_n\{2, \Sigma E_T\}$ as a function of $\langle \Sigma E_T \rangle$. The ratios are very close to unity for v_3 and v_4 but show a few percent deviation in ultra-central collisions for v_2, i.e $v_2\{2, N_{ch}^{rec}\} > v_2\{2, \Sigma E_T\}$. This result implies that events in a narrow N_{ch}^{rec} range have slightly larger v_2 than events in a narrow ΣE_T, when the two ensembles have the same $\langle \Sigma E_T \rangle$. This would be the case if the centrality resolution of N_{ch}^{rec} was poorer than the centrality resolution of ΣE_T. Consequently, $v_2\{2, N_{ch}^{rec}\}$ is expected to contain more events from less central regions, where v_2 is larger.

The bottom row of figure 14 shows the same ratio, $v_n\{2, N_{ch}^{rec}\}/v_n\{2, \Sigma E_T\}$, but instead as a function of $\langle N_{ch}^{rec} \rangle$. Compared with the upper row of figure 14, the ratio for v_2 shows a larger deviation from unity which reaches 7% in ultra-central collisions. Smaller, but significant differences are also observed for v_3 and v_4 in ultra-central collisions. This is probably because $v_n\{2, N_{ch}^{rec}\}$ has even more contributions from less central events than $v_n\{2, \Sigma E_T\}$ when both are matched to the same $\langle N_{ch}^{rec} \rangle$ instead of the same $\langle \Sigma E_T \rangle$. This is consistent with the hypothesis in which N_{ch}^{rec} has poorer centrality resolution and therefore larger centrality fluctuations than ΣE_T, when mapped to the same average event activity in the final state.
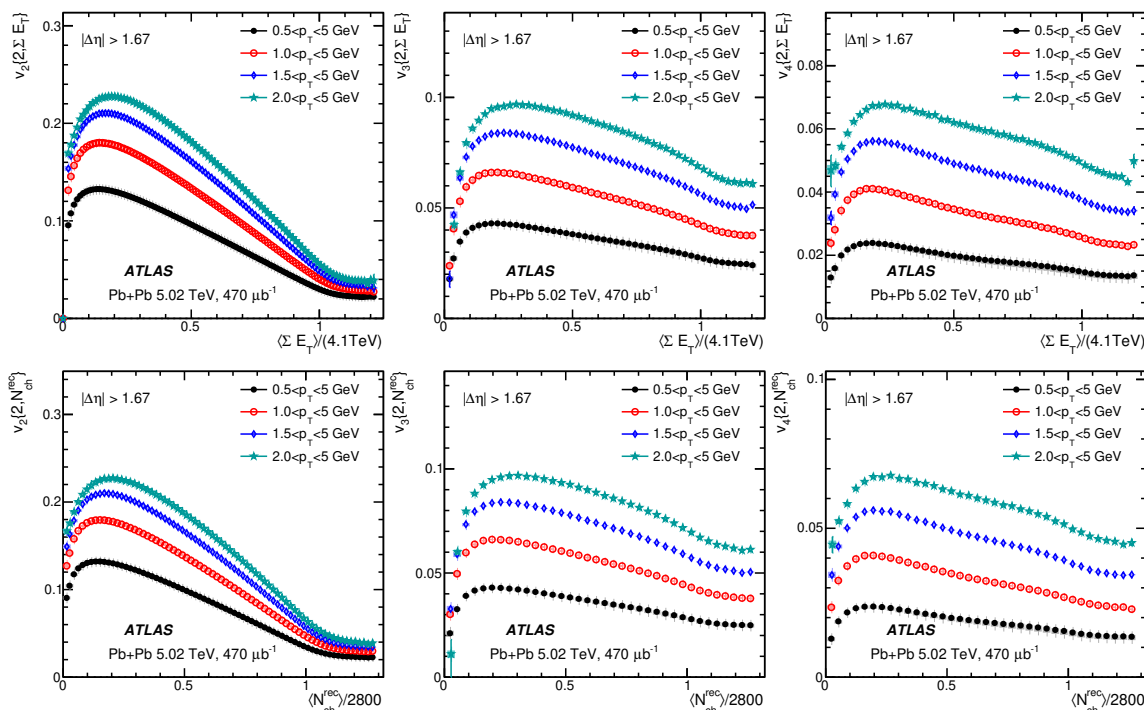
Figure 13. The $\langle \Sigma E_T \rangle$ (top row) and $\langle N_{ch}^{rec} \rangle$ (bottom row) dependence of $v_2\{2, \Sigma E_T\}$ (left panel), $v_3\{2, \Sigma E_T\}$ (middle panel) and $v_4\{2, \Sigma E_T\}$ (right panel) for four p_T ranges. The error bars and shaded boxes represent the statistical and systematic uncertainties, respectively.

Due to the steep decrease of the ΣE_T and N_{ch}^{rec} distributions in the ultra-central region, the centrality fluctuations and the shapes of the $p(\epsilon_n)$ and $p(v_n)$ distributions are expected to exhibit a significant departure from a Gaussian shape [41, 42]. The flow cumulants with four or more particles are more sensitive to a non-Gaussian shape of $p(v_n)$ than the two-particle cumulants. Therefore, they are expected to exhibit larger differences between the two reference event classes. This is the topic of the next section.

7.3.2 Multi-particle cumulants

The top panels of figure 15 show $nc_n\{4, \Sigma E_T\}$ as a function of $\langle \Sigma E_T \rangle$. This figure contains the same information as the results shown in figure 4, except for a change in the scale of the x-axis which shows the central region in more detail. The $nc_2\{4, \Sigma E_T\}$ value changes sign for $\langle \Sigma E_T \rangle \gtrsim (\Sigma E_T)_{knee}$, where it first increases, reaches a maximum and then decreases to close to zero. The value of the maximum also increases with the p_T of the particles. The $nc_3\{4, \Sigma E_T\}$ value is negative and approaches zero in ultra-central collisions and only changes sign for the highest p_T range used in this analysis. The $nc_4\{4, \Sigma E_T\}$ value changes from positive in peripheral collisions to negative in mid-central collisions, reaches a minimum and then turns back and approaches zero in the ultra-central collisions.

The bottom panels of figure 15 show $nc_n\{4, N_{ch}^{rec}\}$ as a function of $\langle N_{ch}^{rec} \rangle$. The overall $\langle N_{ch}^{rec} \rangle$ and p_T-dependent trends are similar to those in the top panels. However, the maximum of $nc_2\{4, N_{ch}^{rec}\}$ is more than a factor of two larger, and $nc_3\{4, N_{ch}^{rec}\}$ shows a clear
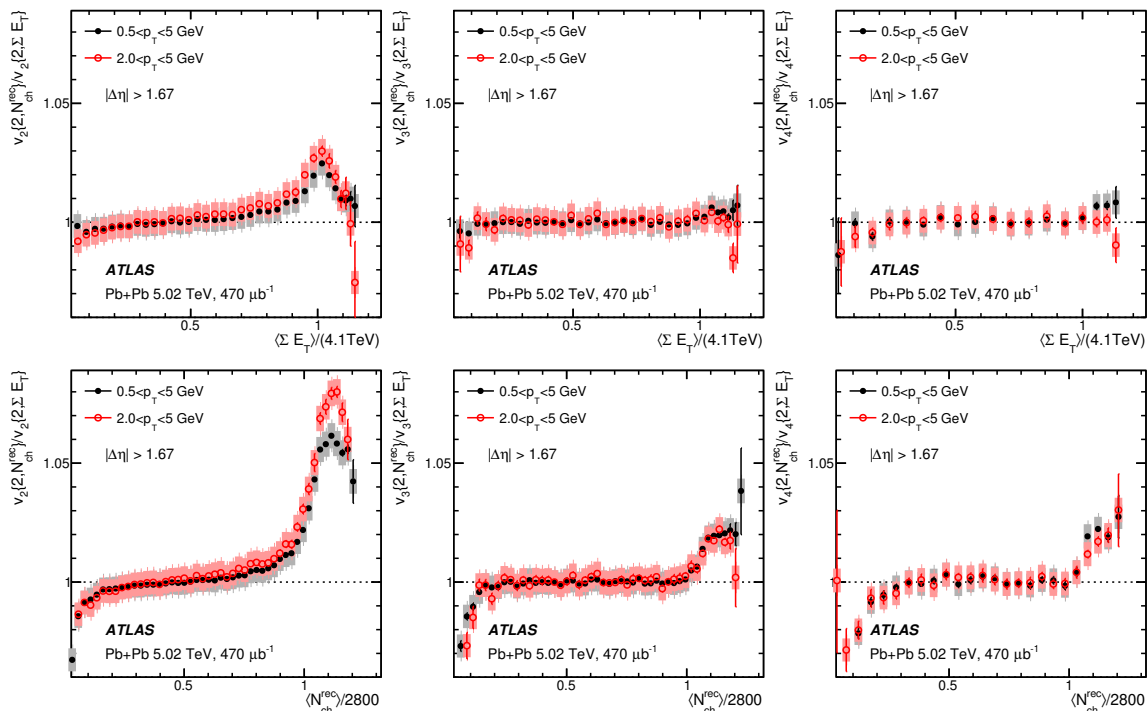
Figure 14. The ratios of flow harmonics between the two event-class definitions $v_n\{2, N_{\rm ch}^{\rm rec}\}/$ $v_n\{2, \Sigma E_{\rm T}\}$ as a function of $\langle \Sigma E_{\rm T} \rangle$ (top row) and $\langle N_{\rm ch}^{\rm rec} \rangle$ (bottom row) for $n = 2$ (left panel), $n = 3$ (middle panel), and $n = 4$ (right panel) for charged particles in two $p_{\rm T}$ ranges. The error bars and shaded boxes represent the statistical and systematic uncertainties, respectively. Unity is indicated by a dotted line. See text for detailed description.

sign change for the two highest $p_{\rm T}$ ranges used in this analysis. Furthermore, $nc_4\{4, N_{\rm ch}^{\rm rec}\}$ shows a local maximum in ultra-central collisions, a feature absent for $nc_4\{4, \Sigma E_{\rm T}\}$.

If $\boldsymbol{V}_n \propto \mathcal{E}_n$ is valid, then the shape of $p(v_n)$ should be the same as the shape of $p(\epsilon_n)$ and $nc_n\{4\} = nc_n\{4, \epsilon\}$ [38, 41]. The $c_n\{4, \epsilon\}$ values can be estimated from a simple Glauber model framework using participating nucleons in the overlap region. The $c_n\{4, \epsilon\}$ value is found to be always negative when the reference event class is defined using the number of participating nucleons $N_{\rm part}$ or the impact parameter of the collisions [70]. However, a positive $nc_n\{4, \epsilon\}$ is observed in ultra-central collisions when the reference event class is defined using the final-state particle multiplicity [41, 74]. Due to multiplicity smearing, events with the same final-state multiplicity can have different $N_{\rm part}$, and therefore different ϵ_n. The positive $nc_n\{4, \epsilon\}$ reflects the non-Gaussian shape of $p(\epsilon_n)$ due to the smearing in $N_{\rm part}$ for events with the same final-state multiplicity. The larger values of $nc_n\{4, N_{\rm ch}^{\rm rec}\}$ in comparison with $nc_n\{4, \Sigma E_{\rm T}\}$ in ultra-central collisions could be due to stronger multiplicity smearing for $nc_n\{4, N_{\rm ch}^{\rm rec}\}$. Figure 16 compares $nc_n\{4, \Sigma E_{\rm T}\}$ and $nc_n\{4, N_{\rm ch}^{\rm rec}\}$ as a function of $\langle \Sigma E_{\rm T} \rangle$ obtained for $1.5 < p_{\rm T} < 5\,{\rm GeV}$. In both cases, the normalized cumulants for v_2 and v_3 show significant differences between the two reference event classes, while the difference is smaller for v_4. The values of $nc_n\{4, N_{\rm ch}^{\rm rec}\}$ for $n = 2$ and 3 are significantly larger than those for $nc_n\{4, \Sigma E_{\rm T}\}$ over a broad centrality range, not only limited to the ultra-central collisions. This implies that the influence of centrality fluctuations on flow fluctuations is potentially important even in mid-central collisions.
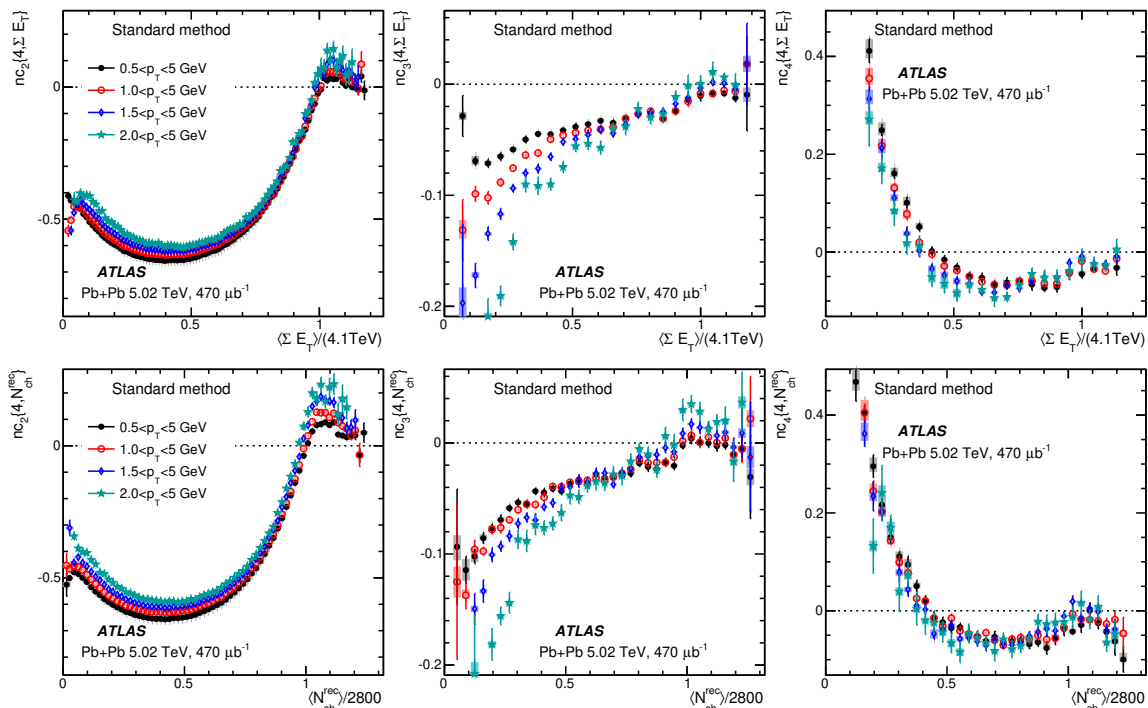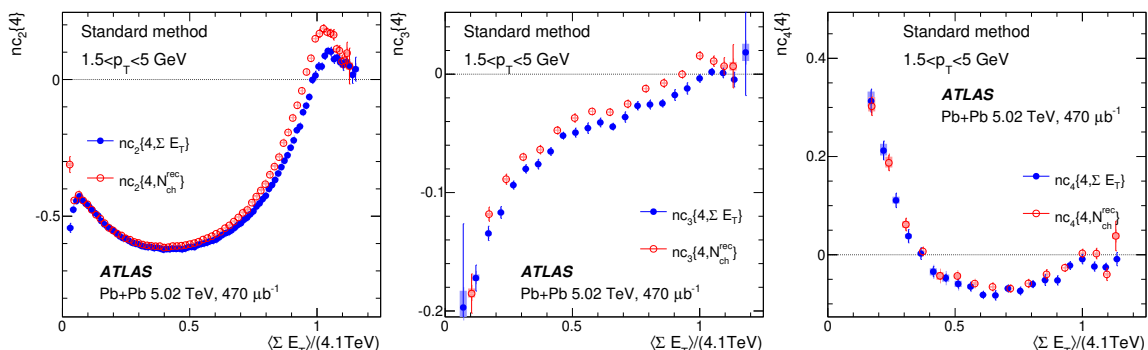
Figure 15. The normalized four-particle cumulants $nc_n\{4, \Sigma E_T\}$ as a function of $\langle \Sigma E_T \rangle$ (top row) and $nc_n\{4, N_{ch}^{rec}\}$ as a function of $\langle N_{ch}^{rec} \rangle$ (bottom row) for $n = 2$ (left panel), $n = 3$ (middle panel), and $n = 4$ (right panel) for four p_T ranges. The error bars and shaded boxes represent the statistical and systematic uncertainties, respectively. Zero is indicated by a dotted line.

Figure 16. The comparison of normalized four-particle cumulants $nc_n\{4, \Sigma E_T\}$ and $nc_n\{4, N_{ch}^{rec}\}$ as a function of $\langle \Sigma E_T \rangle$ for $n = 2$ (left panel), $n = 3$ (middle panel), and $n = 4$ (right panel) for charged particles $1.5 < p_T < 5\,\text{GeV}$. The error bars and shaded boxes represent the statistical and systematic uncertainties, respectively. Zero is indicated by a dotted line.

The left two panels of figure 17 show the six-particle normalized cumulants for v_2 obtained using the two reference event classes, $nc_2\{6, \Sigma E_T\}$ and $nc_2\{6, N_{ch}^{rec}\}$, respectively. The $nc_2\{6\}$ values are positive in most of the centrality range but decrease to zero at around $\langle \Sigma E_T \rangle = (\Sigma E_T)_{knee}$ or $\langle N_{ch}^{rec} \rangle = (N_{ch}^{rec})_{knee}$ and stay close to zero above that. The right panel of figure 17 compares $nc_2\{6, \Sigma E_T\}$ and $nc_2\{6, N_{ch}^{rec}\}$ as a function of $\langle \Sigma E_T \rangle$. The values of $nc_2\{6, N_{ch}^{rec}\}$ are smaller than those for $nc_2\{6, \Sigma E_T\}$ in central and mid-central
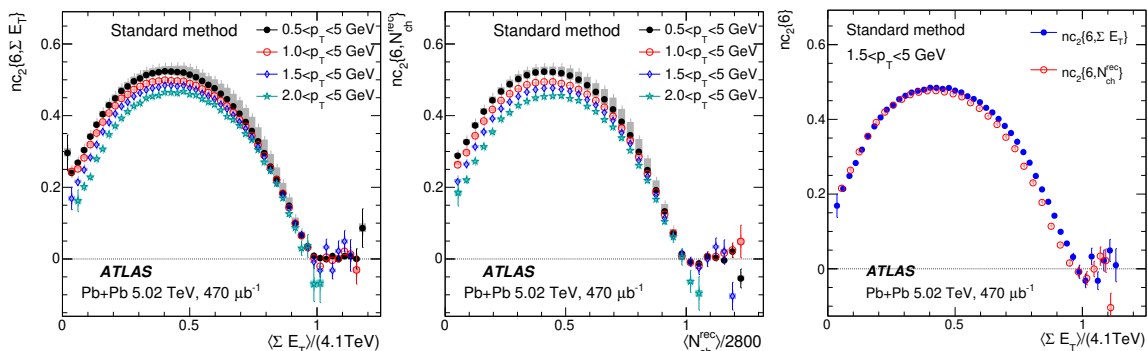
Figure 17. The normalized six-particle cumulants $nc_2\{6, \Sigma E_T\}$ as a function of $\langle \Sigma E_T \rangle$ (left panel) and $nc_2\{6, N_{ch}^{rec}\}$ as a function of $\langle N_{ch}^{rec} \rangle$ (middle panel) in four p_T ranges. The $nc_2\{6, \Sigma E_T\}$ and $nc_6\{4, N_{ch}^{rec}\}$ results for $1.5 < p_T < 5\,\text{GeV}$ are also compared directly as a function of $\langle \Sigma E_T \rangle$ (right panel). The error bars and shaded boxes represent the statistical and systematic uncertainties, respectively. Zero is indicated by a dotted line.

collisions, suggesting that the centrality fluctuations influence the multi-particle cumulants of $p(v_2)$ over a broad centrality range.

The left panel in figure 18 shows the cumulant ratio $v_2\{6\}/v_2\{4\}$ obtained using the event class based on ΣE_T. This panel contains the same information as shown in figure 7 except for a change in the scale of the x-axis made in order to show more detail in the central region. The data show significant differences between the four p_T ranges. The value of $v_2\{6\}/v_2\{4\}$ is larger for higher p_T and even exceeds one in ultra-central collisions. This behaviour is expected, as $c_2\{4\}$ and therefore $v_2\{4\}$, changes sign in ultra-central collisions. The right panel of figure 18 shows $v_2\{6\}/v_2\{4\}$ obtained using the event class based on N_{ch}^{rec} but then mapped onto $\langle \Sigma E_T \rangle$. The differences between the results for the various p_T ranges are larger for most of the centrality range, which again implies that the centrality fluctuations influence the ratios between multi-particle cumulants over a broad centrality range.

7.3.3 Multi-particle mixed-harmonic cumulants

The sensitivity to the choice of reference event class is also studied for the symmetric cumulants $nsc_{2,3}\{4\}$ and $nsc_{2,4}\{4\}$ and the asymmetric cumulant $nac_2\{3\}$. The results obtained with the event class based on ΣE_T are shown in the top row of figure 19 as a function of $\langle \Sigma E_T \rangle$. The $nsc_{2,3}\{4, \Sigma E_T\}$ values change sign and become positive in ultra-central collisions, and are larger for higher p_T. At the largest $\langle \Sigma E_T \rangle$ values, $nsc_{2,4}\{4, \Sigma E_T\}$ reaches zero or even becomes slightly negative while $nac_2\{3, \Sigma E_T\}$ reaches a value of around 0.05. The bottom three panels of figure 19 show the results obtained with the event class based on N_{ch}^{rec} for $nsc_{2,3}\{4, N_{ch}^{rec}\}$, $nsc_{2,4}\{4, N_{ch}^{rec}\}$ and $nac_2\{3, N_{ch}^{rec}\}$, respectively. The positive $nsc_{2,3}\{4, N_{ch}^{rec}\}$ values in the ultra-central region are larger than those for $nsc_{2,3}\{4, \Sigma E_T\}$. The trends of the other two cumulants are similar to those obtained with the event class based on ΣE_T.

The direct comparison of $nsc_{2,3}\{4\}$, $nsc_{2,4}\{4\}$ and $nac_2\{3\}$ obtained with the two reference event classes is shown in figure 20 as a function of $\langle \Sigma E_T \rangle$ for particles with
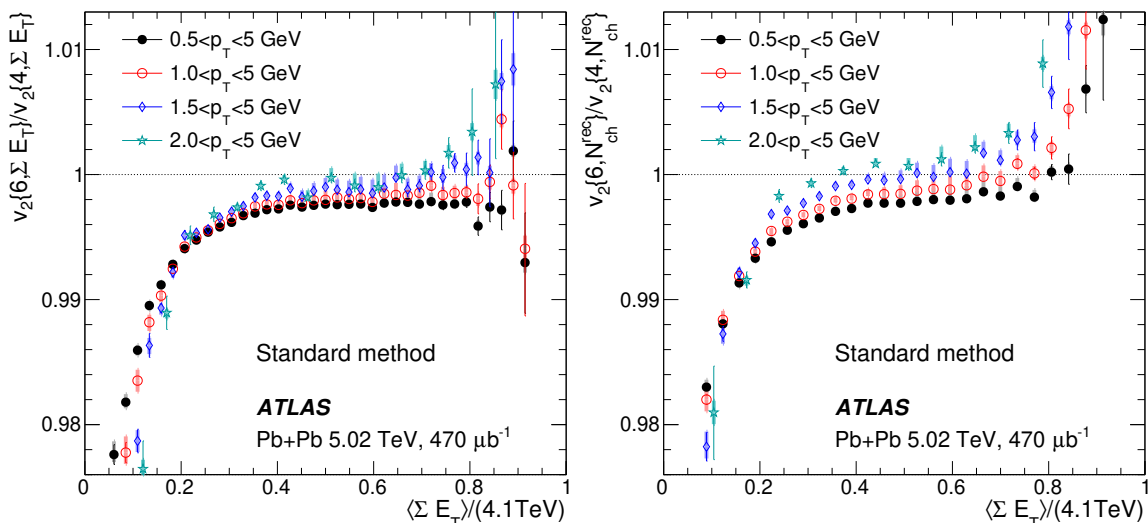
Figure 18. The $\langle \Sigma E_T \rangle$ dependence of cumulant ratio $v_2\{6, \Sigma E_T\}/v_2\{4, \Sigma E_T\}$ (left panel) and $v_2\{6, N_{ch}^{rec}\}/v_2\{4, N_{ch}^{rec}\}$ (right panel) for charged particles in four p_T ranges. The error bars and shaded boxes represent the statistical and systematic uncertainties, respectively. Unity is indicated by a dotted line.
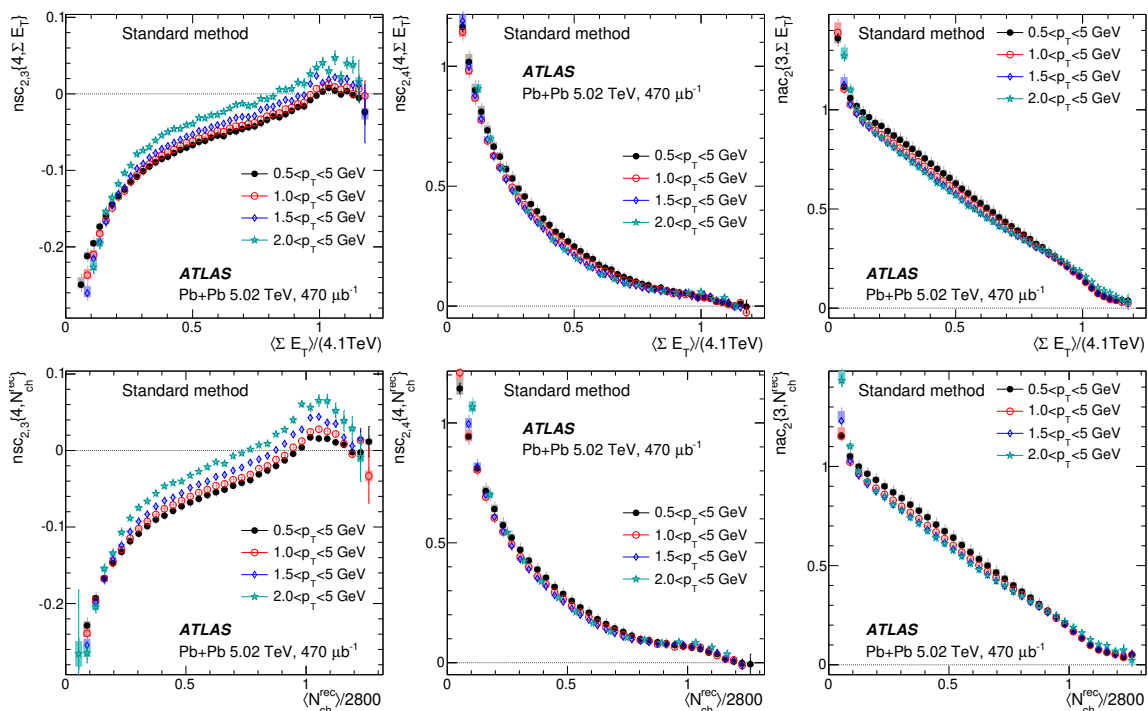

Figure 19. The top row shows the $\langle \Sigma E_T \rangle$ dependence of normalized cumulants $\mathrm{nsc}_{2,3}\{4, \Sigma E_T\}$ (left panel), $\mathrm{nsc}_{2,4}\{4, \Sigma E_T\}$ (middle panel) and $\mathrm{nac}_2\{3, \Sigma E_T\}$ (right panel) for four p_T ranges. The bottom row shows the $\langle N_{ch}^{rec} \rangle$ dependence of normalized cumulants $\mathrm{nsc}_{2,3}\{4, N_{ch}^{rec}\}$ (left panel), $\mathrm{nsc}_{2,4}\{4, N_{ch}^{rec}\}$ (middle panel) and $\mathrm{nac}_2\{3, N_{ch}^{rec}\}$ (right panel) for four p_T ranges. The error bars and shaded boxes represent the statistical and systematic uncertainties, respectively. Zero is indicated by a dotted line.
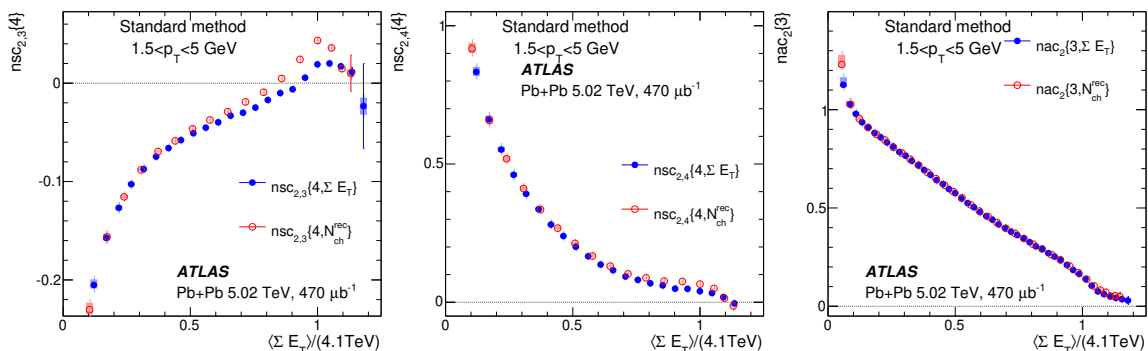
Figure 20. Comparison of $\mathrm{nsc}_{2,3}\{4,\Sigma E_\mathrm{T}\}$ and $\mathrm{nsc}_{2,3}\{4, N_\mathrm{ch}^\mathrm{rec}\}$ (left panels), $\mathrm{nsc}_{2,4}\{4,\Sigma E_\mathrm{T}\}$ and $\mathrm{nsc}_{2,4}\{4, N_\mathrm{ch}^\mathrm{rec}\}$ (middle panels), and $\mathrm{nac}_2\{3,\Sigma E_\mathrm{T}\}$ and $\mathrm{nac}_2\{3, N_\mathrm{ch}^\mathrm{rec}\}$ (right panels) as a function of $\langle \Sigma E_\mathrm{T}\rangle$. The error bars and shaded boxes represent the statistical and systematic uncertainties, respectively. Zero is indicated by a dotted line.

$1.5 < p_\mathrm{T} < 5\,\mathrm{GeV}$. The values of $\mathrm{nsc}_{2,3}\{4, N_\mathrm{ch}^\mathrm{rec}\}$ are larger than those for $\mathrm{nsc}_{2,3}\{4, \Sigma E_\mathrm{T}\}$ in central and mid-central collisions. However, the values of the other two cumulants are similar between the two reference event classes.

8 Summary

Measurements of multi-particle cumulants for harmonic flow coefficients v_n are presented using $470\,\mu\mathrm{b}^{-1}$ of Pb+Pb collisions at $\sqrt{s_\mathrm{NN}} = 5.02$ TeV with the ATLAS detector at the LHC. The cumulants are designed to provide information about the event-by-event fluctuations of one harmonic, $p(v_n)$, and two different harmonics, $p(v_n, v_m)$. The $p(v_n)$ distribution is studied using $2k$-particle cumulants $c_n\{2k\}$ and normalized cumulants $\mathrm{nc}_n\{2k\}$, which provide an estimate of the flow coefficients $v_n\{2k\}$ and cumulant ratios $v_n\{4\}/v_n\{2\}$ and $v_n\{6\}/v_n\{4\}$. The $p(v_n, v_m)$ distribution is studied using the so-called normalized symmetric cumulant $\mathrm{nsc}_{n,m}\{4\}$ and asymmetric cumulant $\mathrm{nac}_2\{3\}$. These normalized cumulants are directly sensitive to fluctuations of the collision geometry in the initial state. In order to investigate the influence of centrality fluctuations on the flow fluctuations, the cumulants are calculated using events selected with two different reference event-class definitions.

A first observation of a negative $c_1\{4\}$, and therefore a positive $v_1\{4\}$ is presented, which sheds light on the nature of the dipolar-eccentricity fluctuation in the initial-state geometry. The values of $c_4\{4\}$ are found to be negative in central collisions but change sign around a centrality of 20–25% and increase quickly for more peripheral collisions. This behaviour is consistent with a non-linear contribution to v_4 that is proportional to v_2^2. This non-linear contribution increases for more peripheral collisions and makes a positive contribution to $c_4\{4\}$. Over most of the centrality range the $c_2\{4\}$ and $c_3\{4\}$ values are found to be negative but change sign towards the most central collisions, suggesting that the $p(v_2)$ and $p(v_3)$ distributions deviate significantly from a Gaussian shape. The cumulant ratios, $v_2\{4\}/v_2\{2\}$, $v_3\{4\}/v_3\{2\}$, $v_4\{4\}/v_4\{2\}$ and $v_2\{6\}/v_2\{4\}$ exhibit a small but significant p_T dependence, suggesting flow fluctuations may also arise directly in the momentum space through the initial-state correlations or final-state interactions.

This paper also presents a detailed measurement of the four-particle symmetric cumulants $\mathrm{nsc}_{2,3}\{4\}$ and $\mathrm{nsc}_{2,4}\{4\}$ and the three-particle asymmetric cumulant $\mathrm{nac}_2\{3\}$. The symmetric cumulants probe the correlation between the magnitudes of two flow harmonics, while the asymmetric cumulant is sensitive to correlations involving both the magnitude and phase of flow. Over most of the centrality range, $\mathrm{nsc}_{2,3}\{4\}$ is found to be negative, reflecting an anti-correlation between v_2 and v_3. The $\mathrm{nsc}_{2,4}\{4\}$ and $\mathrm{nac}_2\{3\}$ values are found to be positive, and their dependence on centrality is consistent with non-linear mode-mixing effects between v_2 and v_4.

In experimental measurements, the flow cumulants are always calculated for events with similar activity. However, for a given activity measure, fluctuations in the particle production process lead to irreducible centrality fluctuations, also known as volume fluctuations. Since v_n changes with centrality, centrality fluctuations lead to an additional fluctuation of v_n, and consequently a change in the flow cumulants. In order to study the influence of centrality fluctuations, cumulant observables are calculated for two reference event classes with different centrality resolution: the total transverse energy in $3.2 < |\eta| < 4.9$, and number of reconstructed charged particles with $|\eta| < 2.5$ and $0.5 < p_{\mathrm{T}} < 5\,\mathrm{GeV}$. In ultra-central collisions, the cumulants $\mathrm{nc}_2\{4\}$, $\mathrm{nc}_3\{4\}$, and $\mathrm{nsc}_{2,3}\{4\}$ are observed to change sign, indicating a significant influence of centrality fluctuations on the multi-particle cumulants of $p(v_2)$, $p(v_3)$ and $p(v_2, v_3)$. The sign change patterns are more pronounced for the event class based on $\langle N_{\mathrm{ch}}^{\mathrm{rec}} \rangle$, consistent with larger centrality fluctuations. The differences between the two event classes are found to extend, with decreasing magnitude, to mid-central collisions, which may suggest that the centrality fluctuations influence the flow fluctuations over a broad centrality range. The sign-change patterns are found to be more pronounced at higher p_{T}, which may indicate that the flow fluctuations have significant p_{T} dependence. Such p_{T} dependence cannot be explained by considering only fluctuations in the initial geometry.

These results provide comprehensive information about the nature of flow fluctuations and the contributions coming from both the initial state and the final state. They also shed light on the influence of centrality fluctuations on flow fluctuations, especially in the ultra-central collisions, which can help to clarify the meaning of centrality and provide insights into the sources of particle production in heavy-ion collisions.

A Flow harmonics $v_n\{2k\}$ from $2k$-particle correlations

Figures 21–23 show the flow coefficients from the four-particle cumulants $v_2\{4\}$, $v_3\{4\}$ and $v_4\{4\}$, respectively. Figure 24 shows the elliptic flow coefficient from the six-particle cumulant, $v_2\{6\}$. They are all obtained from eq. (4.4) and are shown as a function of centrality, ΣE_{T} and $N_{\mathrm{ch}}^{\mathrm{rec}}$. The apparent discontinuities correspond to the locations where the corresponding $c_n\{2k\}$ changes sign.

B Comparison between standard method and three-subevent method

This appendix shows a comparison between the standard cumulant method and the three-subevent method for various cumulant observables. Figures 25–28 show this comparison for
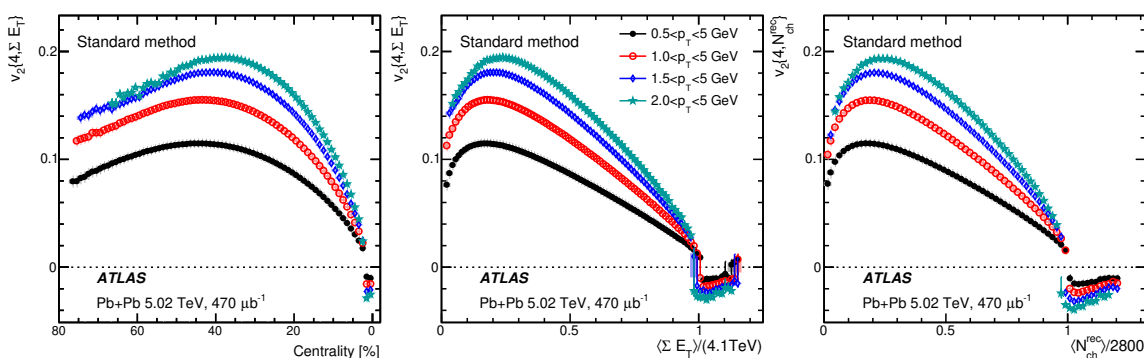
Figure 21. The $v_2\{4\}$ values calculated for charged particles in four p_T ranges as a function of centrality (left panel), ΣE_T (middle panel), and N_{ch}^{rec} (right panel). The error bars and shaded boxes represent the statistical and systematic uncertainties, respectively. Zero is indicated by a dotted line.
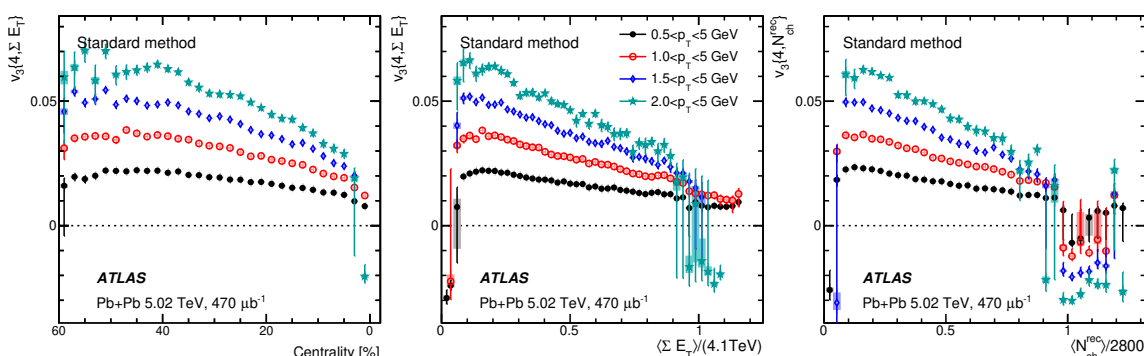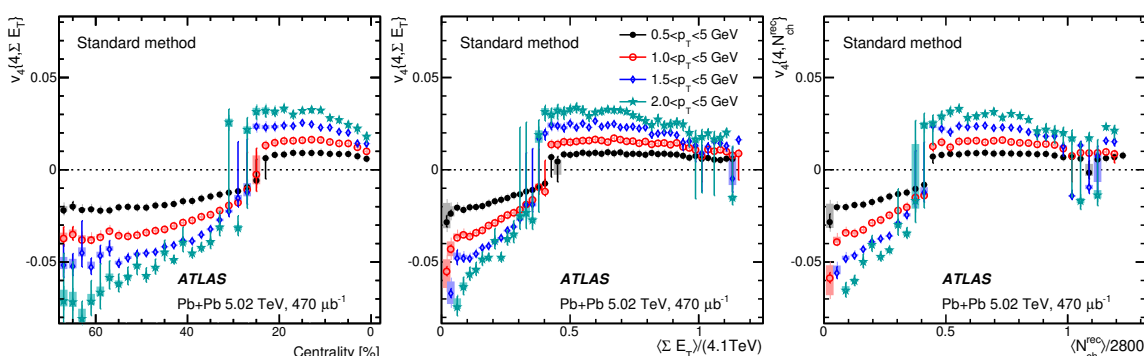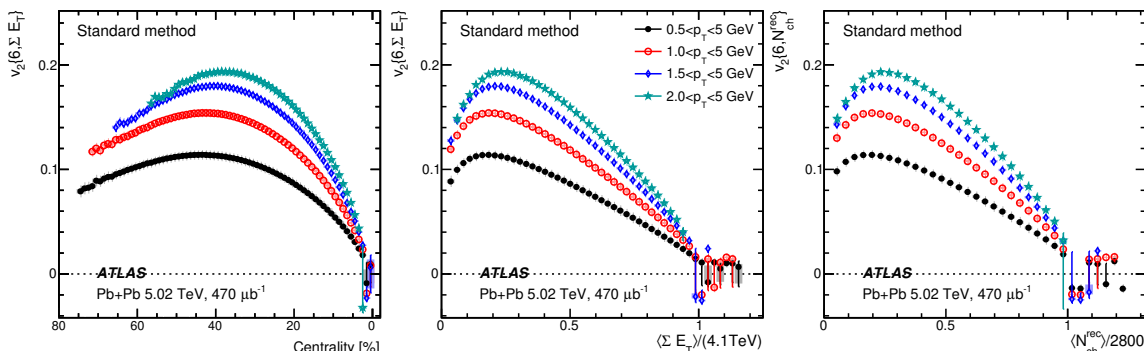

Figure 22. The $v_3\{4\}$ values calculated for charged particles in four p_T ranges as a function of centrality (left panel), ΣE_T (middle panel), and N_{ch}^{rec} (right panel). The error bars and shaded boxes represent the statistical and systematic uncertainties, respectively. Zero is indicated by a dotted line.
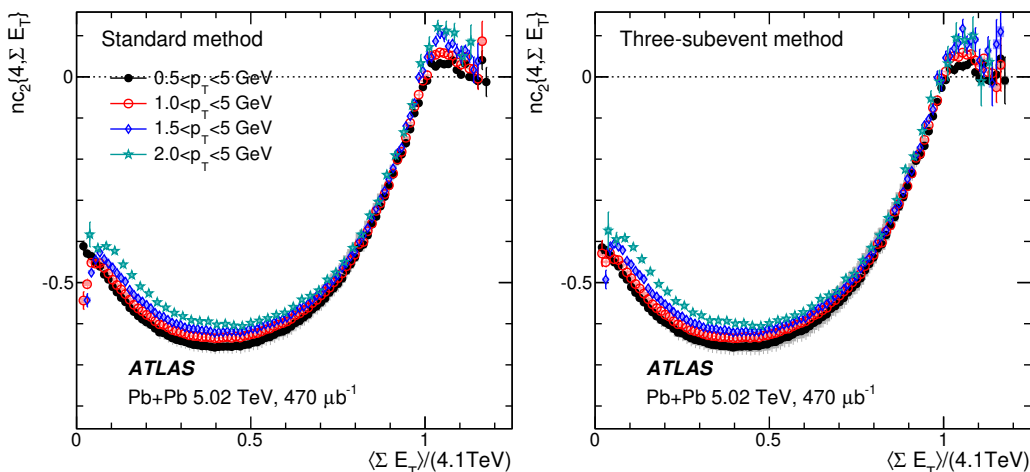

Figure 23. The $v_4\{4\}$ values calculated for charged particles in four p_T ranges as a function of centrality (left panel), ΣE_T (middle panel), and N_{ch}^{rec} (right panel). The error bars and shaded boxes represent the statistical and systematic uncertainties, respectively. Zero is indicated by a dotted line.

Figure 24. The $v_2\{6\}$ values calculated for charged particles in four p_T ranges as a function of centrality (left panel), ΣE_T (middle panel), and N_{ch}^{rec} (right panel). The error bars and shaded boxes represent the statistical and systematic uncertainties, respectively. Zero is indicated by a dotted line.

Figure 25. The $nc_2\{4\}$ values calculated for charged particles in several p_T ranges with the standard cumulant method (left) and three-subevent method (right). The error bars and shaded boxes represent the statistical and systematic uncertainties, respectively. Zero is indicated by a dotted line.

the normalized cumulants $nc_2\{4\}$, $nc_3\{4\}$, and $nc_4\{4\}$ calculated with event class based on ΣE_T. Figures 29–31 show the comparisons for $sc_{2,3}\{4\}$, $sc_{2,4}\{4\}$ and $ac_2\{3\}$, respectively. Figures 32 and 33 compares the standard method and different types of subevent methods. As discussed in [58], part of the differences between the standard method and subevent methods can be partially attributed to longitudinal flow decorrelations [75].

C   Correlation of cumulant ratios

This appendix shows the correlation between different cumulant ratios. Figure 34 shows the correlation between $v_2\{6\}/v_2\{4\}$ and $v_2\{4\}/v_2\{2\}$ for event class based on N_{ch}^{rec}; and this is a complementary plot to the right panel of figure 7. Figures 35 and 36 show the correlation
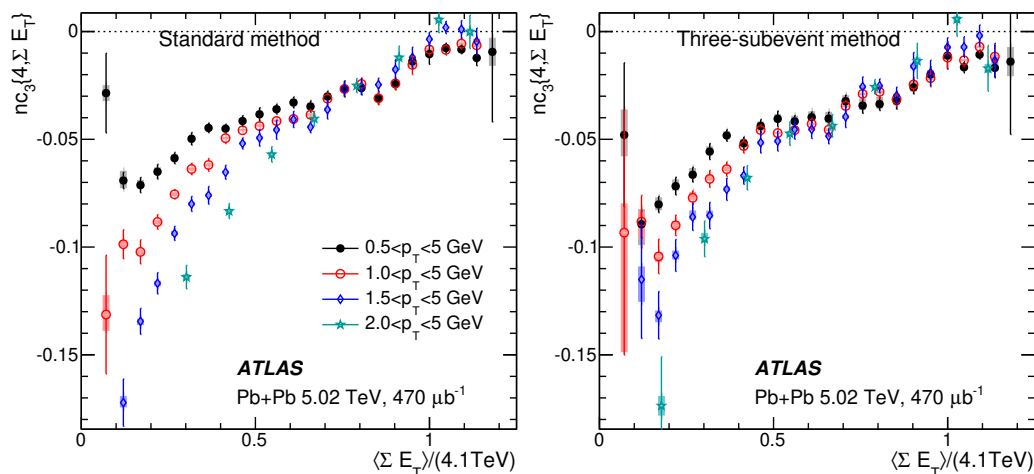
Figure 26. The $nc_3\{4\}$ values calculated for charged particles in several p_T ranges with the standard cumulant method (left) and three-subevent method (right). The error bars and shaded boxes represent the statistical and systematic uncertainties, respectively. Zero is indicated by a dotted line.
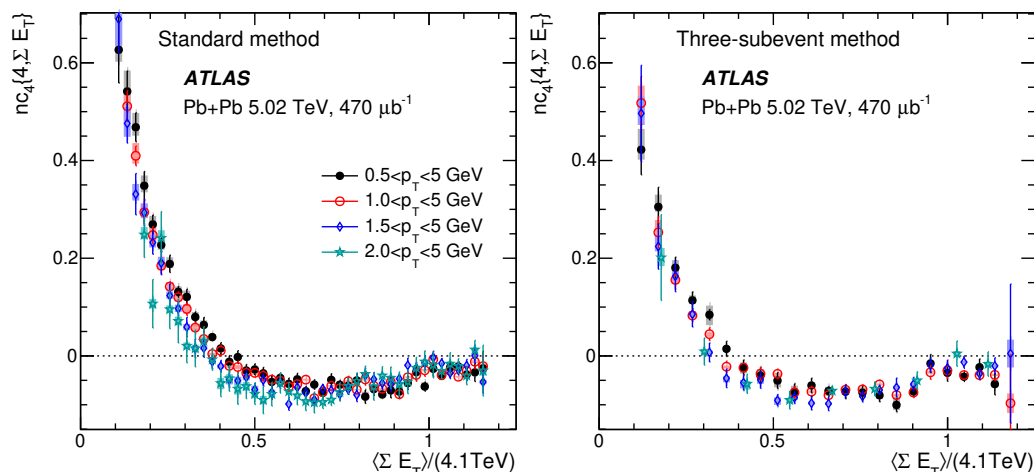

Figure 27. The $nc_4\{4\}$ values calculated for charged particles in several p_T ranges with the standard cumulant method (left) and three-subevent method (right). The error bars and shaded boxes represent the statistical and systematic uncertainties, respectively. Zero is indicated by a dotted line.

between normalized cumulants $nc_n\{4\}$ and $nc_2\{4\}$, these correlations are compared directly with model calculations based on initial-state eccentricities [32, 41, 51].
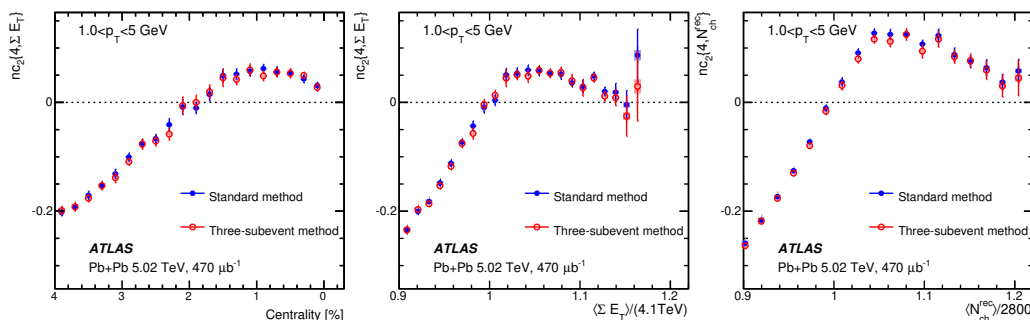
Acknowledgments

Figure 28. The nc$_2\{4, \Sigma E_T\}$ in ultra-central collisions calculated for charged particles as a function of centrality (left panel), ΣE_T (middle panel), and N_{ch}^{rec} (right panel) with the standard cumulant method and the three-subevent method. The error bars and shaded boxes represent the statistical and systematic uncertainties, respectively.
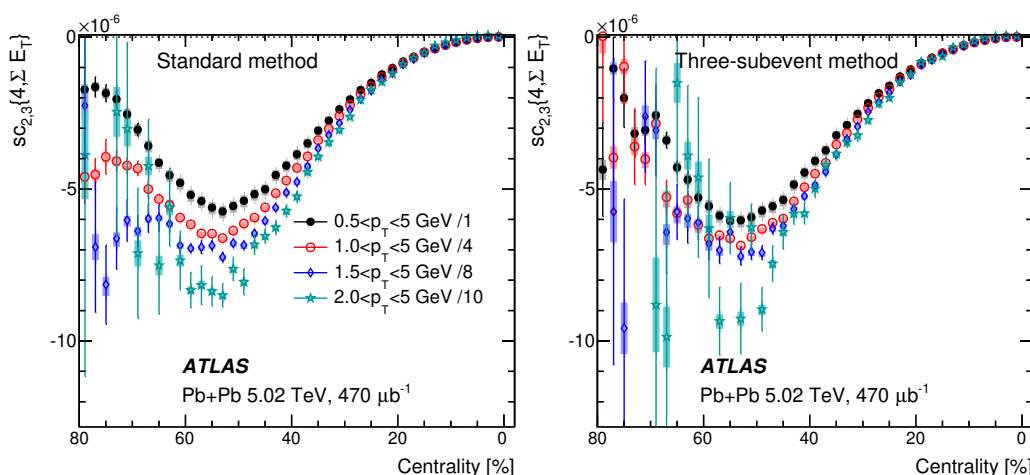

Figure 29. The sc$_{2,3}\{4\}$ values calculated for charged particles in four p_T ranges as a function of centrality for the standard method (left panel) and three-subevent method (right panel). The error bars and shaded boxes represent the statistical and systematic uncertainties, respectively.

Figure 30. The $sc_{2,4}\{4\}$ values calculated for charged particles in four p_T ranges as a function of centrality for the standard method (left panel) and three-subevent method (right panel). The error bars and shaded boxes represent the statistical and systematic uncertainties, respectively.
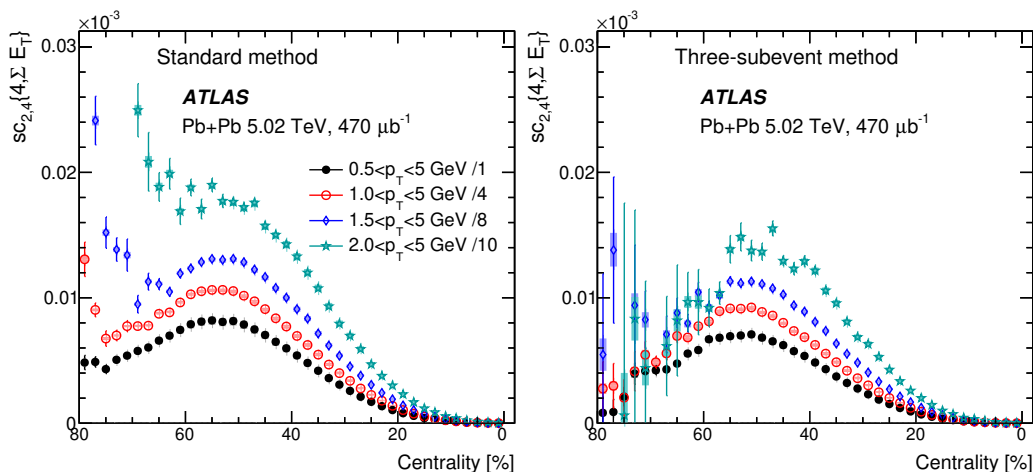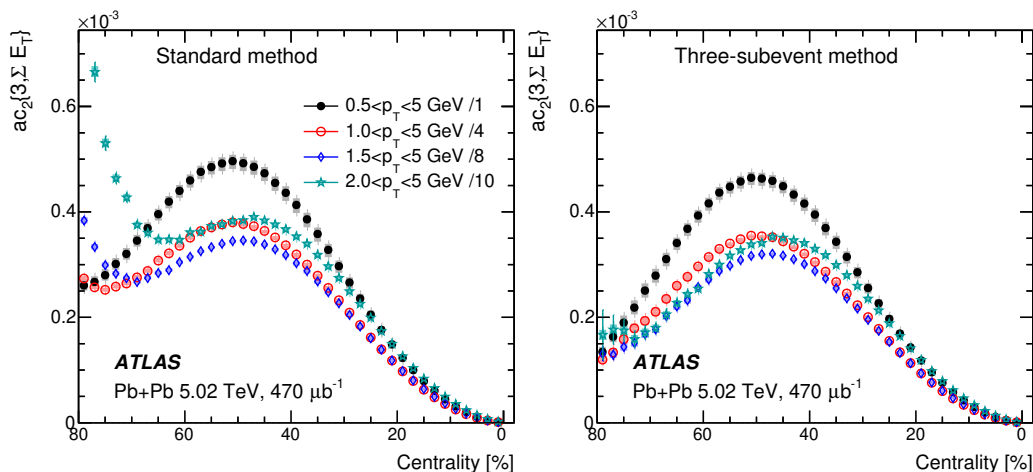

Figure 31. The $ac_2\{3\}$ values calculated for charged particles in four p_T ranges as a function of centrality for the standard method (left panel) and three-subevent method (right panel). The error bars and shaded boxes represent the statistical and systematic uncertainties, respectively.

Figure 32. The nac$_2$\{3\} from the standard method (solid circles), three-subevent method with $\textbf{V}_4$ defined in subevent a or c (solid squares) and three-subevent method with $\textbf{V}_4$ defined in subevent b (open circles). Different panels correspond to different p_T ranges. Only statistical uncertainties are shown.
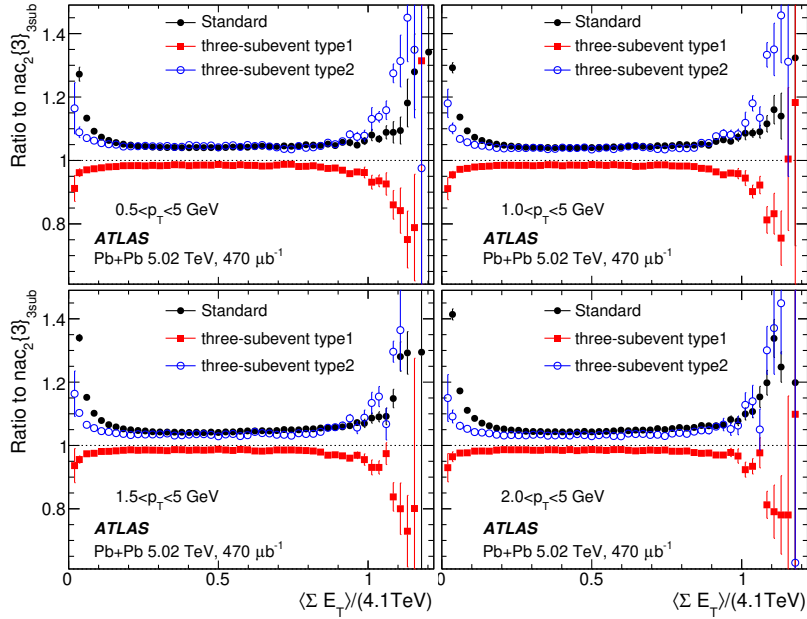
Figure 33. The ratio of nac$_2$\{3\} from the standard method (solid circles), three-subevent method with $\textbf{V}_4$ defined in subevent a or c (solid squares, type1) and three-subevent method with $\textbf{V}_4$ defined in subevent b (open circles, type2) to nac$_2$\{3\} from the three-subevent method combined. Different panels correspond to different p_T ranges. Only statistical uncertainties are shown.
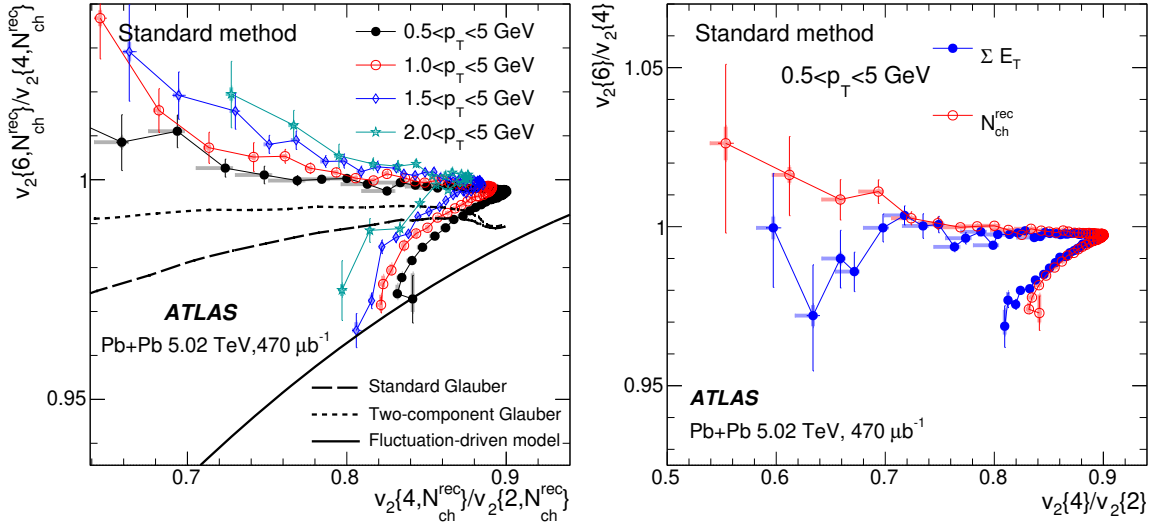
Figure 34. The correlation between $v_2\{6\}/v_2\{4\}$ and $v_2\{4\}/v_2\{2\}$ for four p_T ranges calculated with event class based on N_{ch}^{rec} with models based on initial-state eccentricies (left panel), as well as the correlation compared between the ΣE_T event class and N_{ch}^{rec} event class for $0.5 < p_T < 5\,\mathrm{GeV}$ (right panel). The error bars and shaded boxes represent the statistical and systematic uncertainties, respectively.
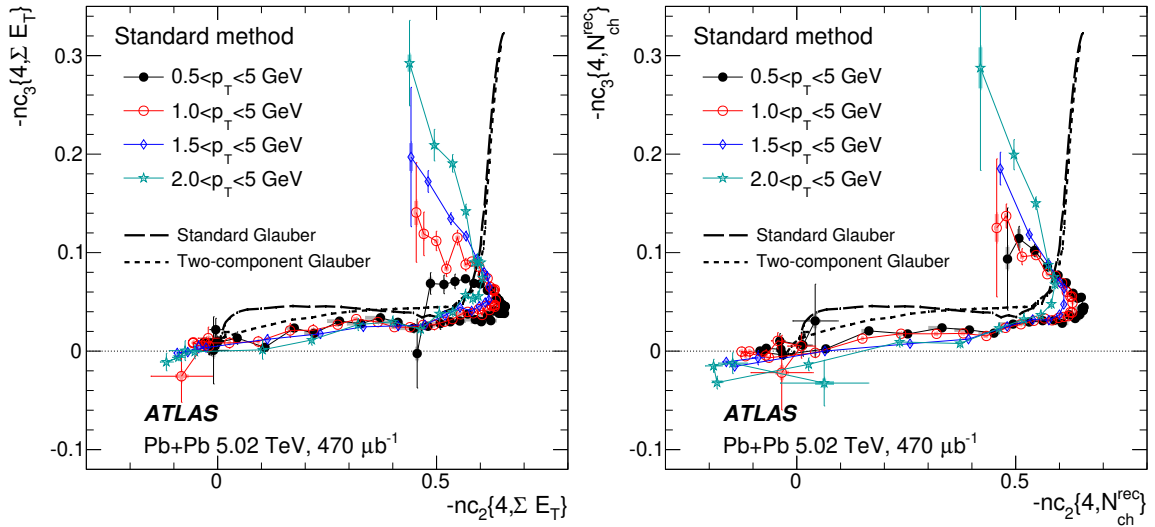
Figure 35. The correlation between $-nc_3\{4\}$ and $-nc_2\{4\}$ compared with Glauber model predictions [41] in four p_T ranges with event class based on ΣE_T (left panel) and N_{ch}^{rec} (right panel). The error bars and shaded boxes represent the statistical and systematic uncertainties, respectively.
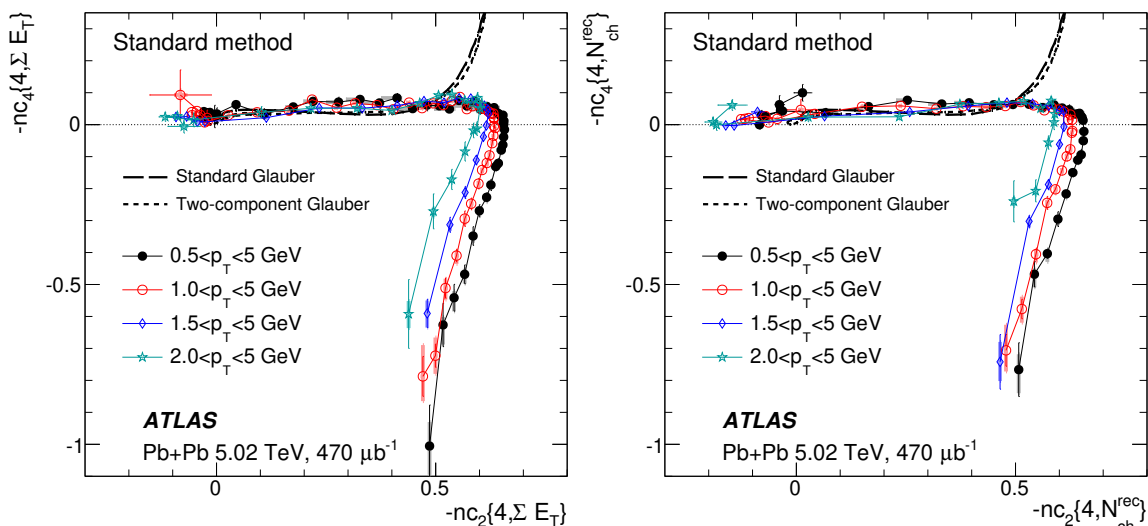
Figure 36. The correlation between $-nc_4\{4\}$ and $-nc_2\{4\}$ compared with Glauber model predictions [41] in four p_T ranges with event class based on ΣE_T (left panel) and N_{ch}^{rec} (right panel). The error bars and shaded boxes represent the statistical and systematic uncertainties, respectively.

References

[1] C. Gale, S. Jeon and B. Schenke, *Hydrodynamic Modeling of Heavy-Ion Collisions*, *Int. J. Mod. Phys.* **A 28** (2013) 1340011 [arXiv:1301.5893] [INSPIRE].

[2] U. Heinz and R. Snellings, *Collective flow and viscosity in relativistic heavy-ion collisions*, *Ann. Rev. Nucl. Part. Sci.* **63** (2013) 123 [arXiv:1301.2826] [INSPIRE].

[3] W. Busza, K. Rajagopal and W. van der Schee, *Heavy Ion Collisions: The Big Picture and the Big Questions*, *Ann. Rev. Nucl. Part. Sci.* **68** (2018) 339 [arXiv:1802.04801] [INSPIRE].

[4] F.G. Gardim, F. Grassi, M. Luzum and J.-Y. Ollitrault, *Mapping the hydrodynamic response to the initial geometry in heavy-ion collisions*, *Phys. Rev.* **C 85** (2012) 024908 [arXiv:1111.6538] [INSPIRE].

[5] C. Gale, S. Jeon, B. Schenke, P. Tribedy and R. Venugopalan, *Event-by-event anisotropic flow in heavy-ion collisions from combined Yang-Mills and viscous fluid dynamics*, *Phys. Rev. Lett.* **110** (2013) 012302 [arXiv:1209.6330] [INSPIRE].

[6] D. Teaney and L. Yan, *Triangularity and Dipole Asymmetry in Heavy Ion Collisions*, *Phys. Rev.* **C 83** (2011) 064904 [arXiv:1010.1876] [INSPIRE].

[7] H. Niemi, G.S. Denicol, H. Holopainen and P. Huovinen, *Event-by-event distributions of azimuthal asymmetries in ultrarelativistic heavy-ion collisions*, *Phys. Rev.* **C 87** (2013) 054901 [arXiv:1212.1008] [INSPIRE].

[8] PHENIX collaboration, *Measurements of Higher-Order Flow Harmonics in Au + Au Collisions at $\sqrt{s_{\mathrm{NN}}} = 200\,GeV$*, *Phys. Rev. Lett.* **107** (2011) 252301 [arXiv:1105.3928] [INSPIRE].

[9] ALICE collaboration, *Higher harmonic anisotropic flow measurements of charged particles in Pb-Pb collisions at $\sqrt{s_{\mathrm{NN}}} = 2.76\,TeV$*, *Phys. Rev. Lett.* **107** (2011) 032301 [arXiv:1105.3865] [INSPIRE].

[10] ATLAS collaboration, *Measurement of the azimuthal anisotropy for charged particle production in $\sqrt{s_{\mathrm{NN}}} = 2.76\,TeV$ lead-lead collisions with the ATLAS detector*, *Phys. Rev.* **C 86** (2012) 014907 [arXiv:1203.3087] [INSPIRE].

[11] CMS collaboration, *Measurement of Higher-Order Harmonic Azimuthal Anisotropy in PbPb Collisions at $\sqrt{s_{\mathrm{NN}}} = 2.76\,TeV$*, *Phys. Rev.* **C 89** (2014) 044906 [arXiv:1310.8651] [INSPIRE].

[12] ATLAS collaboration, *Measurement of the distributions of event-by-event flow harmonics in lead-lead collisions at $\sqrt{s_{\mathrm{NN}}} = 2.76\,TeV$ with the ATLAS detector at the LHC*, *JHEP* **11** (2013) 183 [arXiv:1305.2942] [INSPIRE].

[13] ATLAS collaboration, *Measurement of event-plane correlations in $\sqrt{s_{\mathrm{NN}}} = 2.76\,TeV$ lead-lead collisions with the ATLAS detector*, *Phys. Rev.* **C 90** (2014) 024905 [arXiv:1403.0489] [INSPIRE].

[14] ATLAS collaboration, *Measurement of the correlation between flow harmonics of different order in lead-lead collisions at $\sqrt{s_{\mathrm{NN}}} = 2.76\,TeV$ with the ATLAS detector*, *Phys. Rev.* **C 92** (2015) 034903 [arXiv:1504.01289] [INSPIRE].

[15] ALICE collaboration, *Correlated event-by-event fluctuations of flow harmonics in Pb-Pb collisions at $\sqrt{s_{\mathrm{NN}}} = 2.76\,TeV$*, *Phys. Rev. Lett.* **117** (2016) 182301 [arXiv:1604.07663] [INSPIRE].

[16] M. Luzum and J.-Y. Ollitrault, *Extracting the shear viscosity of the quark-gluon plasma from flow in ultra-central heavy-ion collisions*, *Nucl. Phys.* **A904–905** (2013) 377c [arXiv:1210.6010] [INSPIRE].

[17] Z. Qiu and U. Heinz, *Hydrodynamic event-plane correlations in Pb + Pb collisions at $\sqrt{s} = 2.76\,A\,TeV$*, *Phys. Lett.* **B 717** (2012) 261 [arXiv:1208.1200] [INSPIRE].

[18] D. Teaney and L. Yan, *Event-plane correlations and hydrodynamic simulations of heavy ion collisions*, *Phys. Rev.* **C 90** (2014) 024902 [arXiv:1312.3689] [INSPIRE].

[19] N. Borghini, P.M. Dinh and J.-Y. Ollitrault, *A New method for measuring azimuthal distributions in nucleus-nucleus collisions*, *Phys. Rev.* **C 63** (2001) 054906 [nucl-th/0007063] [INSPIRE].

[20] N. Borghini, P.M. Dinh and J.-Y. Ollitrault, *Flow analysis from multiparticle azimuthal correlations*, *Phys. Rev.* **C 64** (2001) 054901 [nucl-th/0105040] [INSPIRE].

[21] A. Bilandzic, R. Snellings and S. Voloshin, *Flow analysis with cumulants: Direct calculations*, *Phys. Rev.* **C 83** (2011) 044913 [arXiv:1010.0233] [INSPIRE].

[22] A. Bilandzic, C.H. Christensen, K. Gulbrandsen, A. Hansen and Y. Zhou, *Generic framework for anisotropic flow analyses with multiparticle azimuthal correlations*, *Phys. Rev.* **C 89** (2014) 064904 [arXiv:1312.3572] [INSPIRE].

[23] J. Jia, *Event-shape fluctuations and flow correlations in ultra-relativistic heavy-ion collisions*, *J. Phys.* **G 41** (2014) 124003 [arXiv:1407.6057] [ɪɴSPIRE].

[24] ATLAS collaboration, *Measurement of flow harmonics with multi-particle cumulants in Pb + Pb collisions at $\sqrt{s_{NN}} = 2.76\,TeV$ with the ATLAS detector*, *Eur. Phys. J.* **C 74** (2014) 3157 [arXiv:1408.4342] [ɪɴSPIRE].

[25] ALICE collaboration, *Multiparticle azimuthal correlations in p-Pb and Pb-Pb collisions at the CERN Large Hadron Collider*, *Phys. Rev.* **C 90** (2014) 054901 [arXiv:1406.2474] [ɪɴSPIRE].

[26] CMS collaboration, *Multiplicity and Transverse Momentum Dependence of Two- and Four-Particle Correlations in pPb and PbPb Collisions*, *Phys. Lett.* **B 724** (2013) 213 [arXiv:1305.0609] [ɪɴSPIRE].

[27] STAR collaboration, *Azimuthal anisotropy in U + U and Au + Au collisions at RHIC*, *Phys. Rev. Lett.* **115** (2015) 222301 [arXiv:1505.07812] [ɪɴSPIRE].

[28] CMS collaboration, *Azimuthal anisotropy of charged particles with transverse momentum up to $100\,GeV/c$ in PbPb collisions at $\sqrt{s_{NN}} = 5.02\,TeV$*, *Phys. Lett.* **B 776** (2018) 195 [arXiv:1702.00630] [ɪɴSPIRE].

[29] ATLAS collaboration, *Measurement of long-range multiparticle azimuthal correlations with the subevent cumulant method in pp and p + Pb collisions with the ATLAS detector at the CERN Large Hadron Collider*, *Phys. Rev.* **C 97** (2018) 024904 [arXiv:1708.03559] [ɪɴSPIRE].

[30] CMS collaboration, *Non-Gaussian elliptic-flow fluctuations in PbPb collisions at $\sqrt{s_{NN}} = 5.02\,TeV$*, *Phys. Lett.* **B 789** (2019) 643 [arXiv:1711.05594] [ɪɴSPIRE].

[31] ALICE collaboration, *Investigations of Anisotropic Flow Using Multiparticle Azimuthal Correlations in pp, p-Pb, Xe-Xe and Pb-Pb Collisions at the LHC*, *Phys. Rev. Lett.* **123** (2019) 142301 [arXiv:1903.01790] [ɪɴSPIRE].

[32] L. Yan and J.-Y. Ollitrault, *Universal fluctuation-driven eccentricities in proton-proton, proton-nucleus and nucleus-nucleus collisions*, *Phys. Rev. Lett.* **112** (2014) 082301 [arXiv:1312.6555] [ɪɴSPIRE].

[33] L. Yan, J.-Y. Ollitrault and A.M. Poskanzer, *Azimuthal Anisotropy Distributions in High-Energy Collisions*, *Phys. Lett.* **B 742** (2015) 290 [arXiv:1408.0921] [ɪɴSPIRE].

[34] ALICE collaboration, *Energy dependence and fluctuations of anisotropic flow in Pb-Pb collisions at $\sqrt{s_{NN}} = 5.02$ and $2.76\,TeV$*, *JHEP* **07** (2018) 103 [arXiv:1804.02944] [ɪɴSPIRE].

[35] J. Jia, M. Zhou and A. Trzupek, *Revealing long-range multiparticle collectivity in small collision systems via subevent cumulants*, *Phys. Rev.* **C 96** (2017) 034906 [arXiv:1701.03830] [ɪɴSPIRE].

[36] ALICE collaboration, *Systematic studies of correlations between different order flow harmonics in Pb-Pb collisions at $\sqrt{s_{NN}} = 2.76\,TeV$*, *Phys. Rev.* **C 97** (2018) 024906 [arXiv:1709.01127] [ɪɴSPIRE].

[37] STAR collaboration, *Correlation Measurements Between Flow Harmonics in Au + Au Collisions at RHIC*, *Phys. Lett.* **B 783** (2018) 459 [arXiv:1803.03876] [ɪɴSPIRE].

[38] G. Giacalone, J. Noronha-Hostler and J.-Y. Ollitrault, *Relative flow fluctuations as a probe of initial state fluctuations*, *Phys. Rev.* **C 95** (2017) 054910 [arXiv:1702.01730] [ɪɴSPIRE].

[39] F.G. Gardim, F. Grassi, M. Luzum and J.-Y. Ollitrault, *Breaking of factorization of two-particle correlations in hydrodynamics*, *Phys. Rev.* **C 87** (2013) 031901 [arXiv:1211.0989] [INSPIRE].

[40] U. Heinz, Z. Qiu and C. Shen, *Fluctuating flow angles and anisotropic flow measurements*, *Phys. Rev.* **C 87** (2013) 034913 [arXiv:1302.3535] [INSPIRE].

[41] M. Zhou and J. Jia, *Centrality fluctuations in heavy-ion collisions*, *Phys. Rev.* **C 98** (2018) 044903 [arXiv:1803.01812] [INSPIRE].

[42] V. Skokov, B. Friman and K. Redlich, *Volume Fluctuations and Higher Order Cumulants of the Net Baryon Number*, *Phys. Rev.* **C 88** (2013) 034911 [arXiv:1205.4756] [INSPIRE].

[43] X. Luo, J. Xu, B. Mohanty and N. Xu, *Volume fluctuation and auto-correlation effects in the moment analysis of net-proton multiplicity distributions in heavy-ion collisions*, *J. Phys.* **G 40** (2013) 105104 [arXiv:1302.2332] [INSPIRE].

[44] H.-j. Xu, *Cumulants of multiplicity distributions in most-central heavy-ion collisions*, *Phys. Rev.* **C 94** (2016) 054903 [arXiv:1602.07089] [INSPIRE].

[45] ATLAS collaboration, *The ATLAS Experiment at the CERN Large Hadron Collider*, 2008 *JINST* **3** S08003 [INSPIRE].

[46] ATLAS collaboration, *The ATLAS Inner Detector commissioning and calibration*, *Eur. Phys. J.* **C 70** (2010) 787 [arXiv:1004.5293] [INSPIRE].

[47] ATLAS collaboration, *ATLAS Insertable B-Layer Technical Design Report*, ATLAS-TDR-19 (2010) [*Addendum* ATLAS-TDR-19-ADD-1 (2012)] [INSPIRE].

[48] ATLAS IBL collaboration, *Production and Integration of the ATLAS Insertable B-Layer*, 2018 *JINST* **13** T05008 [arXiv:1803.00844] [INSPIRE].

[49] ATLAS collaboration, *Performance of the ATLAS Trigger System in 2015*, *Eur. Phys. J.* **C 77** (2017) 317 [arXiv:1611.09661] [INSPIRE].

[50] ATLAS collaboration, *Measurement of the centrality dependence of the charged particle pseudorapidity distribution in lead-lead collisions at $\sqrt{s_{NN}} = 2.76\,TeV$ with the ATLAS detector*, *Phys. Lett.* **B 710** (2012) 363 [arXiv:1108.6027] [INSPIRE].

[51] M.L. Miller, K. Reygers, S.J. Sanders and P. Steinberg, *Glauber modeling in high energy nuclear collisions*, *Ann. Rev. Nucl. Part. Sci.* **57** (2007) 205 [nucl-ex/0701025] [INSPIRE].

[52] ATLAS collaboration, *Measurement of charged-particle spectra in $Pb + Pb$ collisions at $\sqrt{s_{NN}} = 2.76\,TeV$ with the ATLAS detector at the LHC*, *JHEP* **09** (2015) 050 [arXiv:1504.04337] [INSPIRE].

[53] ATLAS collaboration, *Measurement of the pseudorapidity and transverse momentum dependence of the elliptic flow of charged particles in lead-lead collisions at $\sqrt{s_{NN}} = 2.76\,TeV$ with the ATLAS detector*, *Phys. Lett.* **B 707** (2012) 330 [arXiv:1108.6018] [INSPIRE].

[54] M. Gyulassy and X.-N. Wang, *HIJING 1.0: A Monte Carlo program for parton and particle production in high-energy hadronic and nuclear collisions*, *Comput. Phys. Commun.* **83** (1994) 307 [nucl-th/9502021] [INSPIRE].

[55] M. Masera, G. Ortona, M.G. Poghosyan and F. Prino, *Anisotropic transverse flow introduction in Monte Carlo generators for heavy ion collisions*, *Phys. Rev.* **C 79** (2009) 064909 [INSPIRE].

[56] GEANT4 collaboration, *GEANT4: A Simulation toolkit*, *Nucl. Instrum. Meth.* **A 506** (2003) 250 [INSPIRE].

[57] ATLAS collaboration, *The ATLAS Simulation Infrastructure*, *Eur. Phys. J.* **C 70** (2010) 823 [arXiv:1005.4568] [INSPIRE].

[58] ATLAS collaboration, *Correlated long-range mixed-harmonic fluctuations measured in pp, p + Pb and low-multiplicity Pb + Pb collisions with the ATLAS detector*, *Phys. Lett.* **B 789** (2019) 444 [arXiv:1807.02012] [INSPIRE].

[59] P. Di Francesco, M. Guilbaud, M. Luzum and J.-Y. Ollitrault, *Systematic procedure for analyzing cumulants at any order*, *Phys. Rev.* **C 95** (2017) 044911 [arXiv:1612.05634] [INSPIRE].

[60] S.A. Voloshin, A.M. Poskanzer and R. Snellings, *Collective phenomena in non-central nuclear collisions*, *Landolt-Bornstein* **23** (2010) 293 [arXiv:0809.2949] [INSPIRE].

[61] J. Jia and S. Radhakrishnan, *Limitation of multiparticle correlations for studying the event-by-event distribution of harmonic flow in heavy-ion collisions*, *Phys. Rev.* **C 92** (2015) 024911 [arXiv:1412.4759] [INSPIRE].

[62] ATLAS collaboration, *Measurement of multi-particle azimuthal correlations in pp, p + Pb and low-multiplicity Pb + Pb collisions with the ATLAS detector*, *Eur. Phys. J.* **C 77** (2017) 428 [arXiv:1705.04176] [INSPIRE].

[63] P. Huo, K. Gajdošová, J. Jia and Y. Zhou, *Importance of non-flow in mixed-harmonic multi-particle correlations in small collision systems*, *Phys. Lett.* **B 777** (2018) 201 [arXiv:1710.07567] [INSPIRE].

[64] C. Zhang, J. Jia and J. Xu, *Non-flow effects in three-particle mixed-harmonic azimuthal correlations in small collision systems*, *Phys. Lett.* **B 792** (2019) 138 [arXiv:1812.03536] [INSPIRE].

[65] G. Giacalone, L. Yan, J. Noronha-Hostler and J.-Y. Ollitrault, *Symmetric cumulants and event-plane correlations in Pb + Pb collisions*, *Phys. Rev.* **C 94** (2016) 014906 [arXiv:1605.08303] [INSPIRE].

[66] S.J. Das, G. Giacalone, P.-A. Monard and J.-Y. Ollitrault, *Relating centrality to impact parameter in nucleus-nucleus collisions*, *Phys. Rev.* **C 97** (2018) 014905 [arXiv:1708.00081] [INSPIRE].

[67] Y. Akamatsu, A. Mazeliauskas and D. Teaney, *A kinetic regime of hydrodynamic fluctuations and long time tails for a Bjorken expansion*, *Phys. Rev.* **C 95** (2017) 014909 [arXiv:1606.07742] [INSPIRE].

[68] D. Teaney and L. Yan, *Non linearities in the harmonic spectrum of heavy ion collisions with ideal and viscous hydrodynamics*, *Phys. Rev.* **C 86** (2012) 044908 [arXiv:1206.1905] [INSPIRE].

[69] STAR collaboration, *Elliptic flow from two and four particle correlations in Au + Au collisions at $\sqrt{s_{NN}} = 130\,GeV$*, *Phys. Rev.* **C 66** (2002) 034904 [nucl-ex/0206001] [INSPIRE].

[70] PHOBOS collaboration, *Importance of correlations and fluctuations on the initial source eccentricity in high-energy nucleus-nucleus collisions*, *Phys. Rev.* **C 77** (2008) 014906 [arXiv:0711.3724] [INSPIRE].

[71] G. Giacalone, L. Yan, J. Noronha-Hostler and J.-Y. Ollitrault, *The fluctuations of quadrangular flow*, *J. Phys. Conf. Ser.* **779** (2017) 012064 [`arXiv:1608.06022`] [InSPIRE].

[72] N. Borghini, P.M. Dinh, J.-Y. Ollitrault, A.M. Poskanzer and S.A. Voloshin, *Effects of momentum conservation on the analysis of anisotropic flow*, *Phys. Rev.* **C 66** (2002) 014901 [`nucl-th/0202013`] [InSPIRE].

[73] X. Zhu, Y. Zhou, H. Xu and H. Song, *Correlations of flow harmonics in* 2.76 *A TeV Pb-Pb collisions*, *Phys. Rev.* **C 95** (2017) 044902 [`arXiv:1608.05305`] [InSPIRE].

[74] STAR collaboration, *Energy and system-size dependence of two- and four-particle v_2 measurements in heavy-ion collisions at RHIC and their implications on flow fluctuations and nonflow*, *Phys. Rev.* **C 86** (2012) 014904 [`arXiv:1111.5637`] [InSPIRE].

[75] ATLAS collaboration, *Measurement of longitudinal flow decorrelations in Pb + Pb collisions at $\sqrt{s_{\mathrm{NN}}} = 2.76$ and 5.02 TeV with the ATLAS detector*, *Eur. Phys. J.* **C 78** (2018) 142 [`arXiv:1709.02301`] [InSPIRE].

[76] ATLAS collaboration, *ATLAS Computing Acknowledgements*, ATL-GEN-PUB-2016-002 (2016).

The ATLAS collaboration

M. Aaboud[35d], G. Aad[101], B. Abbott[128], D.C. Abbott[102], O. Abdinov[13,*], A. Abed Abud[70a,70b],
D.K. Abhayasinghe[93], S.H. Abidi[167], O.S. AbouZeid[40], N.L. Abraham[156], H. Abramowicz[161],
H. Abreu[160], Y. Abulaiti[6], B.S. Acharya[66a,66b,o], S. Adachi[163], L. Adam[99],
C. Adam Bourdarios[132], L. Adamczyk[83a], L. Adamek[167], J. Adelman[120], M. Adersberger[113],
A. Adiguzel[12c,ai], S. Adorni[54], T. Adye[144], A.A. Affolder[146], Y. Afik[160], C. Agapopoulou[132],
M.N. Agaras[38], A. Aggarwal[118], C. Agheorghiesei[27c], J.A. Aguilar-Saavedra[140f,140a,ah],
F. Ahmadov[79], X. Ai[15a], G. Aielli[73a,73b], S. Akatsuka[85], T.P.A. Åkesson[96], E. Akilli[54],
A.V. Akimov[110], K. Al Khoury[132], G.L. Alberghi[23b,23a], J. Albert[176], M.J. Alconada Verzini[161],
S. Alderweireldt[118], M. Aleksa[36], I.N. Aleksandrov[79], C. Alexa[27b], D. Alexandre[19],
T. Alexopoulos[10], A. Alfonsi[119], M. Alhroob[128], B. Ali[142], G. Alimonti[68a], J. Alison[37],
S.P. Alkire[148], C. Allaire[132], B.M.M. Allbrooke[156], B.W. Allen[131], P.P. Allport[21],
A. Aloisio[69a,69b], A. Alonso[40], F. Alonso[88], C. Alpigiani[148], A.A. Alshehri[57], M.I. Alstaty[101],
M. Alvarez Estevez[98], B. Alvarez Gonzalez[36], D. Álvarez Piqueras[174], M.G. Alviggi[69a,69b],
Y. Amaral Coutinho[80b], A. Ambler[103], L. Ambroz[135], C. Amelung[26], D. Amidei[105],
S.P. Amor Dos Santos[140a,140c], S. Amoroso[46], C.S. Amrouche[54], F. An[78], C. Anastopoulos[149],
N. Andari[145], T. Andeen[11], C.F. Anders[61b], J.K. Anders[20], A. Andreazza[68a,68b], V. Andrei[61a],
C.R. Anelli[176], S. Angelidakis[38], I. Angelozzi[119], A. Angerami[39], A.V. Anisenkov[121b,121a],
A. Annovi[71a], C. Antel[61a], M.T. Anthony[149], M. Antonelli[51], D.J.A. Antrim[171], F. Anulli[72a],
M. Aoki[81], J.A. Aparisi Pozo[174], L. Aperio Bella[36], G. Arabidze[106], J.P. Araque[140a],
V. Araujo Ferraz[80b], R. Araujo Pereira[80b], A.T.H. Arce[49], F.A. Arduh[88], J-F. Arguin[109],
S. Argyropoulos[77], J.-H. Arling[46], A.J. Armbruster[36], L.J. Armitage[92], A. Armstrong[171],
O. Arnaez[167], H. Arnold[119], A. Artamonov[123,*], G. Artoni[135], S. Artz[99], S. Asai[163], N. Asbah[59],
E.M. Asimakopoulou[172], L. Asquith[156], K. Assamagan[29], R. Astalos[28a], R.J. Atkin[33a],
M. Atkinson[173], N.B. Atlay[151], H. Atmani[132], K. Augsten[142], G. Avolio[36], R. Avramidou[60a],
M.K. Ayoub[15a], A.M. Azoulay[168b], G. Azuelos[109,ax], A.E. Baas[61a], M.J. Baca[21], H. Bachacou[145],
K. Bachas[67a,67b], M. Backes[135], F. Backman[45a,45b], P. Bagnaia[72a,72b], M. Bahmani[84],
H. Bahrasemani[152], A.J. Bailey[174], V.R. Bailey[173], J.T. Baines[144], M. Bajic[40], C. Bakalis[10],
O.K. Baker[183], P.J. Bakker[119], D. Bakshi Gupta[8], S. Balaji[157], E.M. Baldin[121b,121a], P. Balek[180],
F. Balli[145], W.K. Balunas[135], J. Balz[99], E. Banas[84], A. Bandyopadhyay[24], Sw. Banerjee[181,j],
A.A.E. Bannoura[182], L. Barak[161], W.M. Barbe[38], E.L. Barberio[104], D. Barberis[55b,55a],
M. Barbero[101], T. Barillari[114], M-S. Barisits[36], J. Barkeloo[131], T. Barklow[153], R. Barnea[160],
S.L. Barnes[60c], B.M. Barnett[144], R.M. Barnett[18], Z. Barnovska-Blenessy[60a], A. Baroncelli[60a],
G. Barone[29], A.J. Barr[135], L. Barranco Navarro[174], F. Barreiro[98],
J. Barreiro Guimarães da Costa[15a], R. Bartoldus[153], G. Bartolini[101], A.E. Barton[89], P. Bartos[28a],
A. Basalaev[46], A. Bassalat[132,aq], R.L. Bates[57], S.J. Batista[167], S. Batlamous[35e], J.R. Batley[32],
B. Batool[151], M. Battaglia[146], M. Bauce[72a,72b], F. Bauer[145], K.T. Bauer[171], H.S. Bawa[31,m],
J.B. Beacham[49], T. Beau[136], P.H. Beauchemin[170], P. Bechtle[24], H.C. Beck[53], H.P. Beck[20,r],
K. Becker[52], M. Becker[99], C. Becot[46], A. Beddall[12d], A.J. Beddall[12a], V.A. Bednyakov[79],
M. Bedognetti[119], C.P. Bee[155], T.A. Beermann[76], M. Begalli[80b], M. Begel[29], A. Behera[155],
J.K. Behr[46], F. Beisiegel[24], A.S. Bell[94], G. Bella[161], L. Bellagamba[23b], A. Bellerive[34], P. Bellos[9],
K. Beloborodov[121b,121a], K. Belotskiy[111], N.L. Belyaev[111], O. Benary[161,*], D. Benchekroun[35a],
N. Benekos[10], Y. Benhammou[161], D.P. Benjamin[6], M. Benoit[54], J.R. Bensinger[26],
S. Bentvelsen[119], L. Beresford[135], M. Beretta[51], D. Berge[46], E. Bergeaas Kuutmann[172],
N. Berger[5], B. Bergmann[142], L.J. Bergsten[26], J. Beringer[18], S. Berlendis[7], N.R. Bernard[102],
G. Bernardi[136], C. Bernius[153], F.U. Bernlochner[24], T. Berry[93], P. Berta[99], C. Bertella[15a],
G. Bertoli[45a,45b], I.A. Bertram[89], G.J. Besjes[40], O. Bessidskaia Bylund[182], N. Besson[145],

A. Bethani[100], S. Bethke[114], A. Betti[24], A.J. Bevan[92], J. Beyer[114], R. Bi[139], R.M. Bianchi[139],
O. Biebel[113], D. Biedermann[19], R. Bielski[36], K. Bierwagen[99], N.V. Biesuz[71a,71b], M. Biglietti[74a],
T.R.V. Billoud[109], M. Bindi[53], A. Bingul[12d], C. Bini[72a,72b], S. Biondi[23b,23a], M. Birman[180],
T. Bisanz[53], J.P. Biswal[161], A. Bitadze[100], C. Bittrich[48], D.M. Bjergaard[49], J.E. Black[153],
K.M. Black[25], T. Blazek[28a], I. Bloch[46], C. Blocker[26], A. Blue[57], U. Blumenschein[92],
G.J. Bobbink[119], V.S. Bobrovnikov[121b,121a], S.S. Bocchetta[96], A. Bocci[49], D. Boerner[46],
D. Bogavac[14], A.G. Bogdanchikov[121b,121a], C. Bohm[45a], V. Boisvert[93], P. Bokan[53,172], T. Bold[83a],
A.S. Boldyrev[112], A.E. Bolz[61b], M. Bomben[136], M. Bona[92], J.S. Bonilla[131], M. Boonekamp[145],
H.M. Borecka-Bielska[90], A. Borisov[122], G. Borissov[89], J. Bortfeldt[36], D. Bortoletto[135],
V. Bortolotto[73a,73b], D. Boscherini[23b], M. Bosman[14], J.D. Bossio Sola[30], K. Bouaouda[35a],
J. Boudreau[139], E.V. Bouhova-Thacker[89], D. Boumediene[38], S.K. Boutle[57], A. Boveia[126],
J. Boyd[36], D. Boye[33b,ar], I.R. Boyko[79], A.J. Bozson[93], J. Bracinik[21], N. Brahimi[101], G. Brandt[182],
O. Brandt[61a], F. Braren[46], U. Bratzler[164], B. Brau[102], J.E. Brau[131], W.D. Breaden Madden[57],
K. Brendlinger[46], L. Brenner[46], R. Brenner[172], S. Bressler[180], B. Brickwedde[99], D.L. Briglin[21],
D. Britton[57], D. Britzger[114], I. Brock[24], R. Brock[106], G. Brooijmans[39], T. Brooks[93],
W.K. Brooks[147c], E. Brost[120], J.H Broughton[21], P.A. Bruckman de Renstrom[84], D. Bruncko[28b],
A. Bruni[23b], G. Bruni[23b], L.S. Bruni[119], S. Bruno[73a,73b], B.H. Brunt[32], M. Bruschi[23b],
N. Bruscino[139], P. Bryant[37], L. Bryngemark[96], T. Buanes[17], Q. Buat[36], P. Buchholz[151],
A.G. Buckley[57], I.A. Budagov[79], M.K. Bugge[134], F. Bührer[52], O. Bulekov[111], T.J. Burch[120],
S. Burdin[90], C.D. Burgard[119], A.M. Burger[129], B. Burghgrave[8], J.T.P. Burr[46], V. Büscher[99],
E. Buschmann[53], P.J. Bussey[57], J.M. Butler[25], C.M. Buttar[57], J.M. Butterworth[94], P. Butti[36],
W. Buttinger[36], A. Buzatu[158], A.R. Buzykaev[121b,121a], G. Cabras[23b,23a], S. Cabrera Urbán[174],
D. Caforio[142], H. Cai[173], V.M.M. Cairo[153], O. Cakir[4a], N. Calace[36], P. Calafiura[18],
A. Calandri[101], G. Calderini[136], P. Calfayan[65], G. Callea[57], L.P. Caloba[80b], S. Calvente Lopez[98],
D. Calvet[38], S. Calvet[38], T.P. Calvet[155], M. Calvetti[71a,71b], R. Camacho Toro[136], S. Camarda[36],
D. Camarero Munoz[98], P. Camarri[73a,73b], D. Cameron[134], R. Caminal Armadans[102],
C. Camincher[36], S. Campana[36], M. Campanelli[94], A. Camplani[40], A. Campoverde[151],
V. Canale[69a,69b], A. Canesse[103], M. Cano Bret[60c], J. Cantero[129], T. Cao[161], Y. Cao[173],
M.D.M. Capeans Garrido[36], M. Capua[41b,41a], R. Cardarelli[73a], F. Cardillo[149], I. Carli[143],
T. Carli[36], G. Carlino[69a], B.T. Carlson[139], L. Carminati[68a,68b], R.M.D. Carney[45a,45b],
S. Caron[118], E. Carquin[147c], S. Carrá[68a,68b], J.W.S. Carter[167], M.P. Casado[14,f], A.F. Casha[167],
D.W. Casper[171], R. Castelijn[119], F.L. Castillo[174], V. Castillo Gimenez[174], N.F. Castro[140a,140e],
A. Catinaccio[36], J.R. Catmore[134], A. Cattai[36], J. Caudron[24], V. Cavaliere[29], E. Cavallaro[14],
D. Cavalli[68a], M. Cavalli-Sforza[14], V. Cavasinni[71a,71b], E. Celebi[12b], F. Ceradini[74a,74b],
L. Cerda Alberich[174], A.S. Cerqueira[80a], A. Cerri[156], L. Cerrito[73a,73b], F. Cerutti[18],
A. Cervelli[23b,23a], S.A. Cetin[12b], A. Chafaq[35a], D. Chakraborty[120], S.K. Chan[59], W.S. Chan[119],
W.Y. Chan[90], J.D. Chapman[32], B. Chargeishvili[159b], D.G. Charlton[21], C.C. Chau[34],
C.A. Chavez Barajas[156], S. Che[126], A. Chegwidden[106], S. Chekanov[6], S.V. Chekulaev[168a],
G.A. Chelkov[79,aw], M.A. Chelstowska[36], B. Chen[78], C. Chen[60a], C.H. Chen[78], H. Chen[29],
J. Chen[60a], J. Chen[39], S. Chen[137], S.J. Chen[15c], X. Chen[15b,av], Y. Chen[82], Y-H. Chen[46],
H.C. Cheng[63a], H.J. Cheng[15a], A. Cheplakov[79], E. Cheremushkina[122],
R. Cherkaoui El Moursli[35e], E. Cheu[7], K. Cheung[64], T.J.A. Chevalérias[145], L. Chevalier[145],
V. Chiarella[51], G. Chiarelli[71a], G. Chiodini[67a], A.S. Chisholm[36,21], A. Chitan[27b], I. Chiu[163],
Y.H. Chiu[176], M.V. Chizhov[79], K. Choi[65], A.R. Chomont[132], S. Chouridou[162], Y.S. Chow[119],
M.C. Chu[63a], J. Chudoba[141], A.J. Chuinard[103], J.J. Chwastowski[84], L. Chytka[130], D. Cinca[47],
V. Cindro[91], I.A. Cioară[27b], A. Ciocio[18], F. Cirotto[69a,69b], Z.H. Citron[180], M. Citterio[68a],
B.M. Ciungu[167], A. Clark[54], M.R. Clark[39], P.J. Clark[50], C. Clement[45a,45b], Y. Coadou[101],
M. Cobal[66a,66c], A. Coccaro[55b], J. Cochran[78], H. Cohen[161], A.E.C. Coimbra[180], L. Colasurdo[118],

B. Cole[39], A.P. Colijn[119], J. Collot[58], P. Conde Muiño[140a,g], E. Coniavitis[52], S.H. Connell[33b],
I.A. Connelly[57], S. Constantinescu[27b], F. Conventi[69a,ay], A.M. Cooper-Sarkar[135], F. Cormier[175],
K.J.R. Cormier[167], L.D. Corpe[94], M. Corradi[72a,72b], E.E. Corrigan[96], F. Corriveau[103,ad],
A. Cortes-Gonzalez[36], M.J. Costa[174], F. Costanza[5], D. Costanzo[149], G. Cowan[93], J.W. Cowley[32],
J. Crane[100], K. Cranmer[124], S.J. Crawley[57], R.A. Creager[137], S. Crépe-Renaudin[58],
F. Crescioli[136], M. Cristinziani[24], V. Croft[119], G. Crosetti[41b,41a], A. Cueto[5],
T. Cuhadar Donszelmann[149], A.R. Cukierman[153], S. Czekierda[84], P. Czodrowski[36],
M.J. Da Cunha Sargedas De Sousa[60b], J.V. Da Fonseca Pinto[80b], C. Da Via[100], W. Dabrowski[83a],
T. Dado[28a], S. Dahbi[35e], T. Dai[105], C. Dallapiccola[102], M. Dam[40], G. D'amen[23b,23a], J. Damp[99],
J.R. Dandoy[137], M.F. Daneri[30], N.P. Dang[181,j], N.S. Dann[100], M. Danninger[175], V. Dao[36],
G. Darbo[55b], O. Dartsi[5], A. Dattagupta[131], T. Daubney[46], S. D'Auria[68a,68b], W. Davey[24],
C. David[46], T. Davidek[143], D.R. Davis[49], E. Dawe[104], I. Dawson[149], K. De[8], R. De Asmundis[69a],
A. De Benedetti[128], M. De Beurs[119], S. De Castro[23b,23a], S. De Cecco[72a,72b], N. De Groot[118],
P. de Jong[119], H. De la Torre[106], A. De Maria[15c], D. De Pedis[72a], A. De Salvo[72a],
U. De Sanctis[73a,73b], M. De Santis[73a,73b], A. De Santo[156], K. De Vasconcelos Corga[101],
J.B. De Vivie De Regie[132], C. Debenedetti[146], D.V. Dedovich[79], A.M. Deiana[42],
M. Del Gaudio[41b,41a], J. Del Peso[98], Y. Delabat Diaz[46], D. Delgove[132], F. Deliot[145],
C.M. Delitzsch[7], M. Della Pietra[69a,69b], D. Della Volpe[54], A. Dell'Acqua[36], L. Dell'Asta[25],
M. Delmastro[5], C. Delporte[132], P.A. Delsart[58], D.A. DeMarco[167], S. Demers[183], M. Demichev[79],
G. Demontigny[109], S.P. Denisov[122], D. Denysiuk[119], L. D'Eramo[136], D. Derendarz[84],
J.E. Derkaoui[35d], F. Derue[136], P. Dervan[90], K. Desch[24], C. Deterre[46], K. Dette[167],
M.R. Devesa[30], P.O. Deviveiros[36], A. Dewhurst[144], S. Dhaliwal[26], F.A. Di Bello[54],
A. Di Ciaccio[73a,73b], L. Di Ciaccio[5], W.K. Di Clemente[137], C. Di Donato[69a,69b], A. Di Girolamo[36],
G. Di Gregorio[71a,71b], B. Di Micco[74a,74b], R. Di Nardo[102], K.F. Di Petrillo[59], R. Di Sipio[167],
D. Di Valentino[34], C. Diaconu[101], F.A. Dias[40], T. Dias Do Vale[140a,140e], M.A. Diaz[147a],
J. Dickinson[18], E.B. Diehl[105], J. Dietrich[19], S. Díez Cornell[46], A. Dimitrievska[18], W. Ding[15b],
J. Dingfelder[24], F. Dittus[36], F. Djama[101], T. Djobava[159b], J.I. Djuvsland[17], M.A.B. Do Vale[80c],
M. Dobre[27b], D. Dodsworth[26], C. Doglioni[96], J. Dolejsi[143], Z. Dolezal[143], M. Donadelli[80d],
J. Donini[38], A. D'onofrio[92], M. D'Onofrio[90], J. Dopke[144], A. Doria[69a], M.T. Dova[88],
A.T. Doyle[57], E. Drechsler[152], E. Dreyer[152], T. Dreyer[53], Y. Du[60b], Y. Duan[60b], F. Dubinin[110],
M. Dubovsky[28a], A. Dubreuil[54], E. Duchovni[180], G. Duckeck[113], A. Ducourthial[136],
O.A. Ducu[109,x], D. Duda[114], A. Dudarev[36], A.C. Dudder[99], E.M. Duffield[18], L. Duflot[132],
M. Dührssen[36], C. Dülsen[182], M. Dumancic[180], A.E. Dumitriu[27b], A.K. Duncan[57], M. Dunford[61a],
A. Duperrin[101], H. Duran Yildiz[4a], M. Düren[56], A. Durglishvili[159b], D. Duschinger[48], B. Dutta[46],
D. Duvnjak[1], G.I. Dyckes[137], M. Dyndal[46], S. Dysch[100], B.S. Dziedzic[84], K.M. Ecker[114],
R.C. Edgar[105], T. Eifert[36], G. Eigen[17], K. Einsweiler[18], T. Ekelof[172], M. El Kacimi[35c],
R. El Kosseifi[101], V. Ellajosyula[172], M. Ellert[172], F. Ellinghaus[182], A.A. Elliot[92], N. Ellis[36],
J. Elmsheuser[29], M. Elsing[36], D. Emeliyanov[144], A. Emerman[39], Y. Enari[163], J.S. Ennis[178],
M.B. Epland[49], J. Erdmann[47], A. Ereditato[20], M. Escalier[132], C. Escobar[174],
O. Estrada Pastor[174], A.I. Etienvre[145], E. Etzion[161], H. Evans[65], A. Ezhilov[138], F. Fabbri[57],
L. Fabbri[23b,23a], V. Fabiani[118], G. Facini[94], R.M. Faisca Rodrigues Pereira[140a],
R.M. Fakhrutdinov[122], S. Falciano[72a], P.J. Falke[5], S. Falke[5], J. Faltova[143], Y. Fang[15a],
Y. Fang[15a], G. Fanourakis[44], M. Fanti[68a,68b], A. Farbin[8], A. Farilla[74a], E.M. Farina[70a,70b],
T. Farooque[106], S. Farrell[18], S.M. Farrington[178], P. Farthouat[36], F. Fassi[35e], P. Fassnacht[36],
D. Fassouliotis[9], M. Faucci Giannelli[50], W.J. Fawcett[32], L. Fayard[132], O.L. Fedin[138,p],
W. Fedorko[175], M. Feickert[42], S. Feigl[134], L. Feligioni[101], A. Fell[149], C. Feng[60b], E.J. Feng[36],
M. Feng[49], M.J. Fenton[57], A.B. Fenyuk[122], J. Ferrando[46], A. Ferrari[172], P. Ferrari[119],
R. Ferrari[70a], D.E. Ferreira de Lima[61b], A. Ferrer[174], D. Ferrere[54], C. Ferretti[105], F. Fiedler[99],

A. Filipčič[91], F. Filthaut[118], K.D. Finelli[25], M.C.N. Fiolhais[140a,140c,a], L. Fiorini[174], C. Fischer[14],
F. Fischer[113], W.C. Fisher[106], I. Fleck[151], P. Fleischmann[105], R.R.M. Fletcher[137], T. Flick[182],
B.M. Flierl[113], L. Flores[137], L.R. Flores Castillo[63a], F.M. Follega[75a,75b], N. Fomin[17],
G.T. Forcolin[75a,75b], A. Formica[145], F.A. Förster[14], A.C. Forti[100], A.G. Foster[21], D. Fournier[132],
H. Fox[89], S. Fracchia[149], P. Francavilla[71a,71b], M. Franchini[23b,23a], S. Franchino[61a], D. Francis[36],
L. Franconi[20], M. Franklin[59], M. Frate[171], A.N. Fray[92], B. Freund[109], W.S. Freund[80b],
E.M. Freundlich[47], D.C. Frizzell[128], D. Froidevaux[36], J.A. Frost[135], C. Fukunaga[164],
E. Fullana Torregrosa[174], E. Fumagalli[55b,55a], T. Fusayasu[115], J. Fuster[174], A. Gabrielli[23b,23a],
A. Gabrielli[18], G.P. Gach[83a], S. Gadatsch[54], P. Gadow[114], G. Gagliardi[55b,55a], L.G. Gagnon[109],
C. Galea[27b], B. Galhardo[140a,140c], E.J. Gallas[135], B.J. Gallop[144], P. Gallus[142], G. Galster[40],
R. Gamboa Goni[92], K.K. Gan[126], S. Ganguly[180], J. Gao[60a], Y. Gao[90], Y.S. Gao[31,m], C. García[174],
J.E. García Navarro[174], J.A. García Pascual[15a], C. Garcia-Argos[52], M. Garcia-Sciveres[18],
R.W. Gardner[37], N. Garelli[153], S. Gargiulo[52], V. Garonne[134], A. Gaudiello[55b,55a], G. Gaudio[70a],
I.L. Gavrilenko[110], A. Gavrilyuk[123], C. Gay[175], G. Gaycken[24], E.N. Gazis[10], A.A. Geanta[27b],
C.N.P. Gee[144], J. Geisen[53], M. Geisen[99], M.P. Geisler[61a], C. Gemme[55b], M.H. Genest[58],
C. Geng[105], S. Gentile[72a,72b], S. George[93], T. Geralis[44], D. Gerbaudo[14], L.O. Gerlach[53],
G. Gessner[47], S. Ghasemi[151], M. Ghasemi Bostanabad[176], A. Ghosh[77], B. Giacobbe[23b],
S. Giagu[72a,72b], N. Giangiacomi[23b,23a], P. Giannetti[71a], A. Giannini[69a,69b], S.M. Gibson[93],
M. Gignac[146], D. Gillberg[34], G. Gilles[182], D.M. Gingrich[3,ax], M.P. Giordani[66a,66c], F.M. Giorgi[23b],
P.F. Giraud[145], G. Giugliarelli[66a,66c], D. Giugni[68a], F. Giuli[73a,73b], M. Giulini[61b], S. Gkaitatzis[162],
I. Gkialas[9,i], E.L. Gkougkousis[14], P. Gkountoumis[10], L.K. Gladilin[112], C. Glasman[98], J. Glatzer[14],
P.C.F. Glaysher[46], A. Glazov[46], M. Goblirsch-Kolb[26], S. Goldfarb[104], T. Golling[54],
D. Golubkov[122], A. Gomes[140a,140b], R. Goncalves Gama[53], R. Gonçalo[140a,140b], G. Gonella[52],
L. Gonella[21], A. Gongadze[79], F. Gonnella[21], J.L. Gonski[59], S. González de la Hoz[174],
S. Gonzalez-Sevilla[54], G.R. Gonzalvo Rodriguez[174], L. Goossens[36], P.A. Gorbounov[123],
H.A. Gordon[29], B. Gorini[36], E. Gorini[67a,67b], A. Gorišek[91], A.T. Goshaw[49], M.I. Gostkin[79],
C.A. Gottardo[24], C.R. Goudet[132], M. Gouighri[35b], D. Goujdami[35c], A.G. Goussiou[148],
N. Govender[33b,b], C. Goy[5], E. Gozani[160], I. Grabowska-Bold[83a], P.O.J. Gradin[172],
E.C. Graham[90], J. Gramling[171], E. Gramstad[134], S. Grancagnolo[19], M. Grandi[156],
V. Gratchev[138], P.M. Gravila[27f], F.G. Gravili[67a,67b], C. Gray[57], H.M. Gray[18], C. Grefe[24],
K. Gregersen[96], I.M. Gregor[46], P. Grenier[153], K. Grevtsov[46], N.A. Grieser[128], J. Griffiths[8],
A.A. Grillo[146], K. Grimm[31,l], S. Grinstein[14,y], J.-F. Grivaz[132], S. Groh[99], E. Gross[180],
J. Grosse-Knetter[53], Z.J. Grout[94], A. Grummer[117], L. Guan[105], W. Guan[181],
J. Guenther[36], A. Guerguichon[132], F. Guescini[168a], D. Guest[171], R. Gugel[52], B. Gui[126],
T. Guillemin[5], S. Guindon[36], U. Gul[57], J. Guo[60c], W. Guo[105], Y. Guo[60a,s], Z. Guo[101], R. Gupta[46],
S. Gurbuz[12c], G. Gustavino[128], P. Gutierrez[128], C. Gutschow[94], C. Guyot[145], M.P. Guzik[83a],
C. Gwenlan[135], C.B. Gwilliam[90], A. Haas[124], C. Haber[18], H.K. Hadavand[8], N. Haddad[35e],
A. Hadef[60a], S. Hageböck[36], M. Hagihara[169], M. Haleem[177], J. Haley[129], G. Halladjian[106],
G.D. Hallewell[101], K. Hamacher[182], P. Hamal[130], K. Hamano[176], H. Hamdaoui[35e],
G.N. Hamity[149], K. Han[60a,ak], L. Han[60a], S. Han[15a], K. Hanagaki[81,v], M. Hance[146],
D.M. Handl[113], B. Haney[137], R. Hankache[136], E. Hansen[96], J.B. Hansen[40], J.D. Hansen[40],
M.C. Hansen[24], P.H. Hansen[40], E.C. Hanson[100], K. Hara[169], A.S. Hard[181], T. Harenberg[182],
S. Harkusha[107], P.F. Harrison[178], N.M. Hartmann[113], Y. Hasegawa[150], A. Hasib[50], S. Hassani[145],
S. Haug[20], R. Hauser[106], L. Hauswald[48], L.B. Havener[39], M. Havranek[142], C.M. Hawkes[21],
R.J. Hawkings[36], D. Hayden[106], C. Hayes[155], R.L. Hayes[175], C.P. Hays[135], J.M. Hays[92],
H.S. Hayward[90], S.J. Haywood[144], F. He[60a], M.P. Heath[50], V. Hedberg[96], L. Heelan[8], S. Heer[24],
K.K. Heidegger[52], J. Heilman[34], S. Heim[46], T. Heim[18], B. Heinemann[46,as], J.J. Heinrich[131],
L. Heinrich[36], C. Heinz[56], J. Hejbal[141], L. Helary[61b], A. Held[175], S. Hellesund[134], C.M. Helling[146],

S. Hellman[45a,45b], C. Helsens[36], R.C.W. Henderson[89], Y. Heng[181], S. Henkelmann[175],
A.M. Henriques Correia[36], G.H. Herbert[19], H. Herde[26], V. Herget[177], Y. Hernández Jiménez[33d],
H. Herr[99], M.G. Herrmann[113], T. Herrmann[48], G. Herten[52], R. Hertenberger[113], L. Hervas[36],
T.C. Herwig[137], G.G. Hesketh[94], N.P. Hessey[168a], A. Higashida[163], S. Higashino[81],
E. Higón-Rodriguez[174], K. Hildebrand[37], E. Hill[176], J.C. Hill[32], K.K. Hill[29], K.H. Hiller[46],
S.J. Hillier[21], M. Hils[48], I. Hinchliffe[18], F. Hinterkeuser[24], M. Hirose[133], S. Hirose[52],
D. Hirschbuehl[182], B. Hiti[91], O. Hladik[141], D.R. Hlaluku[33d], X. Hoad[50], J. Hobbs[155], N. Hod[180],
M.C. Hodgkinson[149], A. Hoecker[36], F. Hoenig[113], D. Hohn[52], D. Hohov[132], T.R. Holmes[37],
M. Holzbock[113], L.B.A.H. Hommels[32], S. Honda[169], T. Honda[81], T.M. Hong[139], A. Hönle[114],
B.H. Hooberman[173], W.H. Hopkins[6], Y. Horii[116], P. Horn[48], A.J. Horton[152], L.A. Horyn[37],
J-Y. Hostachy[58], A. Hostiuc[148], S. Hou[158], A. Hoummada[35a], J. Howarth[100], J. Hoya[88],
M. Hrabovsky[130], J. Hrdinka[76], I. Hristova[19], J. Hrivnac[132], A. Hrynevich[108], T. Hryn'ova[5],
P.J. Hsu[64], S.-C. Hsu[148], Q. Hu[29], S. Hu[60c], Y. Huang[15a], Z. Hubacek[142], F. Hubaut[101],
M. Huebner[24], F. Huegging[24], T.B. Huffman[135], M. Huhtinen[36], R.F.H. Hunter[34], P. Huo[155],
A.M. Hupe[34], N. Huseynov[79,af], J. Huston[106], J. Huth[59], R. Hyneman[105], S. Hyrych[28a],
G. Iacobucci[54], G. Iakovidis[29], I. Ibragimov[151], L. Iconomidou-Fayard[132], Z. Idrissi[35e], P. Iengo[36],
R. Ignazzi[40], O. Igonkina[119,aa,*], R. Iguchi[163], T. Iizawa[54], Y. Ikegami[81], M. Ikeno[81], D. Iliadis[162],
N. Ilic[118], F. Iltzsche[48], G. Introzzi[70a,70b], M. Iodice[74a], K. Iordanidou[39], V. Ippolito[72a,72b],
M.F. Isacson[172], N. Ishijima[133], M. Ishino[163], M. Ishitsuka[165], W. Islam[129], C. Issever[135],
S. Istin[160], F. Ito[169], J.M. Iturbe Ponce[63a], R. Iuppa[75a,75b], A. Ivina[180], H. Iwasaki[81], J.M. Izen[43],
V. Izzo[69a], P. Jacka[141], P. Jackson[1], R.M. Jacobs[24], V. Jain[2], G. Jäkel[182], K.B. Jakobi[99],
K. Jakobs[52], S. Jakobsen[76], T. Jakoubek[141], J. Jamieson[57], D.O. Jamin[129], R. Jansky[54],
J. Janssen[24], M. Janus[53], P.A. Janus[83a], G. Jarlskog[96], N. Javadov[79,af], T. Javůrek[36],
M. Javurkova[52], F. Jeanneau[145], L. Jeanty[131], J. Jejelava[159a,ag], A. Jelinskas[178], P. Jenni[52,c],
J. Jeong[46], N. Jeong[46], S. Jézéquel[5], H. Ji[181], J. Jia[155], H. Jiang[78], Y. Jiang[60a], Z. Jiang[153,q],
S. Jiggins[52], F.A. Jimenez Morales[38], J. Jimenez Pena[174], S. Jin[15c], A. Jinaru[27b], O. Jinnouchi[165],
H. Jivan[33d], P. Johansson[149], K.A. Johns[7], C.A. Johnson[65], K. Jon-And[45a,45b], R.W.L. Jones[89],
S.D. Jones[156], S. Jones[7], T.J. Jones[90], J. Jongmanns[61a], P.M. Jorge[140a,140b], J. Jovicevic[168a],
X. Ju[18], J.J. Junggeburth[114], A. Juste Rozas[14,y], A. Kaczmarska[84], M. Kado[132], H. Kagan[126],
M. Kagan[153], T. Kaji[179], E. Kajomovitz[160], C.W. Kalderon[96], A. Kaluza[99],
A. Kamenshchikov[122], L. Kanjir[91], Y. Kano[163], V.A. Kantserov[111], J. Kanzaki[81], L.S. Kaplan[181],
D. Kar[33d], M.J. Kareem[168b], E. Karentzos[10], S.N. Karpov[79], Z.M. Karpova[79], V. Kartvelishvili[89],
A.N. Karyukhin[122], L. Kashif[181], R.D. Kass[126], A. Kastanas[45a,45b], Y. Kataoka[163], C. Kato[60d,60c],
J. Katzy[46], K. Kawade[82], K. Kawagoe[87], T. Kawaguchi[116], T. Kawamoto[163], G. Kawamura[53],
E.F. Kay[176], V.F. Kazanin[121b,121a], R. Keeler[176], R. Kehoe[42], J.S. Keller[34], E. Kellermann[96],
J.J. Kempster[21], J. Kendrick[21], O. Kepka[141], S. Kersten[182], B.P. Kerševan[91],
S. Ketabchi Haghighat[167], R.A. Keyes[103], M. Khader[173], F. Khalil-Zada[13], A. Khanov[129],
A.G. Kharlamov[121b,121a], T. Kharlamova[121b,121a], E.E. Khoda[175], A. Khodinov[166], T.J. Khoo[54],
E. Khramov[79], J. Khubua[159b], S. Kido[82], M. Kiehn[54], C.R. Kilby[93], Y.K. Kim[37],
N. Kimura[66a,66c], O.M. Kind[19], B.T. King[90,*], D. Kirchmeier[48], J. Kirk[144], A.E. Kiryunin[114],
T. Kishimoto[163], D.P. Kisliuk[167], V. Kitali[46], O. Kivernyk[5], E. Kladiva[28b,*],
T. Klapdor-Kleingrothaus[52], M.H. Klein[105], M. Klein[90], U. Klein[90], K. Kleinknecht[99],
P. Klimek[120], A. Klimentov[29], T. Klingl[24], T. Klioutchnikova[36], F.F. Klitzner[113], P. Kluit[119],
S. Kluth[114], E. Kneringer[76], E.B.F.G. Knoops[101], A. Knue[52], D. Kobayashi[87], T. Kobayashi[163],
M. Kobel[48], M. Kocian[153], P. Kodys[143], P.T. Koenig[24], T. Koffas[34], N.M. Köhler[114], T. Koi[153],
M. Kolb[61b], I. Koletsou[5], T. Kondo[81], N. Kondrashova[60c], K. Köneke[52], A.C. König[118],
T. Kono[125], R. Konoplich[124,an], V. Konstantinides[94], N. Konstantinidis[94], B. Konya[96],
R. Kopeliansky[65], S. Koperny[83a], K. Korcyl[84], K. Kordas[162], G. Koren[161], A. Korn[94],

I. Korolkov[14], E.V. Korolkova[149], N. Korotkova[112], O. Kortner[114], S. Kortner[114], T. Kosek[143], V.V. Kostyukhin[24], A. Kotwal[49], A. Koulouris[10], A. Kourkoumeli-Charalampidi[70a,70b], C. Kourkoumelis[9], E. Kourlitis[149], V. Kouskoura[29], A.B. Kowalewska[84], R. Kowalewski[176], C. Kozakai[163], W. Kozanecki[145], A.S. Kozhin[122], V.A. Kramarenko[112], G. Kramberger[91], D. Krasnopevtsev[60a], M.W. Krasny[136], A. Krasznahorkay[36], D. Krauss[114], J.A. Kremer[83a], J. Kretzschmar[90], P. Krieger[167], A. Krishnan[61b], K. Krizka[18], K. Kroeninger[47], H. Kroha[114], J. Kroll[141], J. Kroll[137], J. Krstic[16], U. Kruchonak[79], H. Krüger[24], N. Krumnack[78], M.C. Kruse[49], T. Kubota[104], S. Kuday[4b], J.T. Kuechler[46], S. Kuehn[36], A. Kugel[61a], T. Kuhl[46], V. Kukhtin[79], R. Kukla[101], Y. Kulchitsky[107,aj], S. Kuleshov[147c], Y.P. Kulinich[173], M. Kuna[58], T. Kunigo[85], A. Kupco[141], T. Kupfer[47], O. Kuprash[52], H. Kurashige[82], L.L. Kurchaninov[168a], Y.A. Kurochkin[107], A. Kurova[111], M.G. Kurth[15a,15d], E.S. Kuwertz[36], M. Kuze[165], A.K. Kvam[148], J. Kvita[130], T. Kwan[103], A. La Rosa[114], J.L. La Rosa Navarro[80d], L. La Rotonda[41b,41a], F. La Ruffa[41b,41a], C. Lacasta[174], F. Lacava[72a,72b], D.P.J. Lack[100], H. Lacker[19], D. Lacour[136], E. Ladygin[79], R. Lafaye[5], B. Laforge[136], T. Lagouri[33d], S. Lai[53], S. Lammers[65], W. Lampl[7], E. Lançon[29], U. Landgraf[52], M.P.J. Landon[92], M.C. Lanfermann[54], V.S. Lang[46], J.C. Lange[53], R.J. Langenberg[36], A.J. Lankford[171], F. Lanni[29], K. Lantzsch[24], A. Lanza[70a], A. Lapertosa[55b,55a], S. Laplace[136], J.F. Laporte[145], T. Lari[68a], F. Lasagni Manghi[23b,23a], M. Lassnig[36], T.S. Lau[63a], A. Laudrain[132], A. Laurier[34], M. Lavorgna[69a,69b], M. Lazzaroni[68a,68b], B. Le[104], O. Le Dortz[136], E. Le Guirriec[101], M. LeBlanc[7], T. LeCompte[6], F. Ledroit-Guillon[58], C.A. Lee[29], G.R. Lee[17], L. Lee[59], S.C. Lee[158], S.J. Lee[34], B. Lefebvre[168a], M. Lefebvre[176], F. Legger[113], C. Leggett[18], K. Lehmann[152], N. Lehmann[182], G. Lehmann Miotto[36], W.A. Leight[46], A. Leisos[162,w], M.A.L. Leite[80d], R. Leitner[143], D. Lellouch[180,*], K.J.C. Leney[42], T. Lenz[24], B. Lenzi[36], R. Leone[7], S. Leone[71a], C. Leonidopoulos[50], A. Leopold[136], G. Lerner[156], C. Leroy[109], R. Les[167], C.G. Lester[32], M. Levchenko[138], J. Levêque[5], D. Levin[105], L.J. Levinson[180], D.J. Lewis[21], B. Li[15b], B. Li[105], C-Q. Li[60a,am], F. Li[60c], H. Li[60a], H. Li[60b], J. Li[60c], K. Li[153], L. Li[60c], M. Li[15a,15d], Q. Li[15a,15d], Q.Y. Li[60a], S. Li[60d,60c], X. Li[46], Y. Li[46], Z. Liang[15a], B. Liberti[73a], A. Liblong[167], K. Lie[63c], S. Liem[119], C.Y. Lin[32], K. Lin[106], T.H. Lin[99], R.A. Linck[65], J.H. Lindon[21], A.L. Lionti[54], E. Lipeles[137], A. Lipniacka[17], M. Lisovyi[61b], T.M. Liss[173,au], A. Lister[175], A.M. Litke[146], J.D. Little[8], B. Liu[78], B.L. Liu[6], H.B. Liu[29], H. Liu[105], J.B. Liu[60a], J.K.K. Liu[135], K. Liu[136], M. Liu[60a], P. Liu[18], Y. Liu[15a,15d], Y.L. Liu[105], Y.W. Liu[60a], M. Livan[70a,70b], A. Lleres[58], J. Llorente Merino[15a], S.L. Lloyd[92], C.Y. Lo[63b], F. Lo Sterzo[42], E.M. Lobodzinska[46], P. Loch[7], S. Loffredo[73a,73b], T. Lohse[19], K. Lohwasser[149], M. Lokajicek[141], J.D. Long[173], R.E. Long[89], L. Longo[36], K.A. Looper[126], J.A. Lopez[147c], I. Lopez Paz[100], A. Lopez Solis[149], J. Lorenz[113], N. Lorenzo Martinez[5], M. Losada[22], P.J. Lösel[113], A. Lösle[52], X. Lou[46], X. Lou[15a], A. Lounis[132], J. Love[6], P.A. Love[89], J.J. Lozano Bahilo[174], H. Lu[63a], M. Lu[60a], Y.J. Lu[64], H.J. Lubatti[148], C. Luci[72a,72b], A. Lucotte[58], C. Luedtke[52], F. Luehring[65], I. Luise[136], L. Luminari[72a], B. Lund-Jensen[154], M.S. Lutz[102], D. Lynn[29], R. Lysak[141], E. Lytken[96], F. Lyu[15a], V. Lyubushkin[79], T. Lyubushkina[79], H. Ma[29], L.L. Ma[60b], Y. Ma[60b], G. Maccarrone[51], A. Macchiolo[114], C.M. Macdonald[149], J. Machado Miguens[137,140b], D. Madaffari[174], R. Madar[38], W.F. Mader[48], N. Madysa[48], J. Maeda[82], K. Maekawa[163], S. Maeland[17], T. Maeno[29], M. Maerker[48], A.S. Maevskiy[112], V. Magerl[52], N. Magini[78], D.J. Mahon[39], C. Maidantchik[80b], T. Maier[113], A. Maio[140a,140b,140d], K. Maj[84], O. Majersky[28a], S. Majewski[131], Y. Makida[81], N. Makovec[132], B. Malaescu[136], Pa. Malecki[84], V.P. Maleev[138], F. Malek[58], U. Mallik[77], D. Malon[6], C. Malone[32], S. Maltezos[10], S. Malyukov[79], J. Mamuzic[174], G. Mancini[51], I. Mandić[91], L. Manhaes de Andrade Filho[80a], I.M. Maniatis[162], J. Manjarres Ramos[48], K.H. Mankinen[96], A. Mann[113], A. Manousos[76], B. Mansoulie[145], I. Manthos[162], S. Manzoni[119], A. Marantis[162], G. Marceca[30], L. Marchese[135], G. Marchiori[136], M. Marcisovsky[141], C. Marcon[96], C.A. Marin Tobon[36], M. Marjanovic[38], Z. Marshall[18],

M.U.F. Martensson[172], S. Marti-Garcia[174], C.B. Martin[126], T.A. Martin[178], V.J. Martin[50], B. Martin dit Latour[17], M. Martinez[14,y], V.I. Martinez Outschoorn[102], S. Martin-Haugh[144], V.S. Martoiu[27b], A.C. Martyniuk[94], A. Marzin[36], L. Masetti[99], T. Mashimo[163], R. Mashinistov[110], J. Masik[100], A.L. Maslennikov[121b,121a], L.H. Mason[104], L. Massa[73a,73b], P. Massarotti[69a,69b], P. Mastrandrea[71a,71b], A. Mastroberardino[41b,41a], T. Masubuchi[163], A. Matic[113], P. Mättig[24], J. Maurer[27b], B. Maček[91], D.A. Maximov[121b,121a], R. Mazini[158], I. Maznas[162], S.M. Mazza[146], S.P. Mc Kee[105], T.G. McCarthy[114], L.I. McClymont[94], W.P. McCormack[18], E.F. McDonald[104], J.A. Mcfayden[36], M.A. McKay[42], K.D. McLean[176], S.J. McMahon[144], P.C. McNamara[104], C.J. McNicol[178], R.A. McPherson[176,ad], J.E. Mdhluli[33d], Z.A. Meadows[102], S. Meehan[148], T. Megy[52], S. Mehlhase[113], A. Mehta[90], T. Meideck[58], B. Meirose[43], D. Melini[174], B.R. Mellado Garcia[33d], J.D. Mellenthin[53], M. Melo[28a], F. Meloni[46], A. Melzer[24], S.B. Menary[100], E.D. Mendes Gouveia[140a,140e], L. Meng[36], X.T. Meng[105], S. Menke[114], E. Meoni[41b,41a], S. Mergelmeyer[19], S.A.M. Merkt[139], C. Merlassino[20], P. Mermod[54], L. Merola[69a,69b], C. Meroni[68a], O. Meshkov[112], J.K.R. Meshreki[151], A. Messina[72a,72b], J. Metcalfe[6], A.S. Mete[171], C. Meyer[65], J. Meyer[160], J-P. Meyer[145], H. Meyer Zu Theenhausen[61a], F. Miano[156], R.P. Middleton[144], L. Mijović[50], G. Mikenberg[180], M. Mikestikova[141], M. Mikuž[91], H. Mildner[149], M. Milesi[104], A. Milic[167], D.A. Millar[92], D.W. Miller[37], A. Milov[180], D.A. Milstead[45a,45b], R.A. Mina[153,q], A.A. Minaenko[122], M. Miñano Moya[174], I.A. Minashvili[159b], A.I. Mincer[124], B. Mindur[83a], M. Mineev[79], Y. Minegishi[163], Y. Ming[181], L.M. Mir[14], A. Mirto[67a,67b], K.P. Mistry[137], T. Mitani[179], J. Mitrevski[113], V.A. Mitsou[174], M. Mittal[60c], A. Miucci[20], P.S. Miyagawa[149], A. Mizukami[81], J.U. Mjörnmark[96], T. Mkrtchyan[184], M. Mlynarikova[143], T. Moa[45a,45b], K. Mochizuki[109], P. Mogg[52], S. Mohapatra[39], R. Moles-Valls[24], M.C. Mondragon[106], K. Mönig[46], J. Monk[40], E. Monnier[101], A. Montalbano[152], J. Montejo Berlingen[36], M. Montella[94], F. Monticelli[88], S. Monzani[68a], N. Morange[132], D. Moreno[22], M. Moreno Llácer[36], P. Morettini[55b], M. Morgenstern[119], S. Morgenstern[48], D. Mori[152], M. Morii[59], M. Morinaga[179], V. Morisbak[134], A.K. Morley[36], G. Mornacchi[36], A.P. Morris[94], L. Morvaj[155], P. Moschovakos[10], B. Moser[119], M. Mosidze[159b], H.J. Moss[149], J. Moss[31,n], K. Motohashi[165], E. Mountricha[36], E.J.W. Moyse[102], S. Muanza[101], F. Mueller[114], J. Mueller[139], R.S.P. Mueller[113], D. Muenstermann[89], G.A. Mullier[96], J.L. Munoz Martinez[14], F.J. Munoz Sanchez[100], P. Murin[28b], W.J. Murray[178,144], A. Murrone[68a,68b], M. Muškinja[18], C. Mwewa[33a], A.G. Myagkov[122,ao], J. Myers[131], M. Myska[142], B.P. Nachman[18], O. Nackenhorst[47], A.Nag Nag[48], K. Nagai[135], K. Nagano[81], Y. Nagasaka[62], M. Nagel[52], E. Nagy[101], A.M. Nairz[36], Y. Nakahama[116], K. Nakamura[81], T. Nakamura[163], I. Nakano[127], H. Nanjo[133], F. Napolitano[61a], R.F. Naranjo Garcia[46], R. Narayan[11], D.I. Narrias Villar[61a], I. Naryshkin[138], T. Naumann[46], G. Navarro[22], H.A. Neal[105,*], P.Y. Nechaeva[110], F. Nechansky[46], T.J. Neep[21], A. Negri[70a,70b], M. Negrini[23b], S. Nektarijevic[118], C. Nellist[53], M.E. Nelson[135], S. Nemecek[141], P. Nemethy[124], M. Nessi[36,e], M.S. Neubauer[173], M. Neumann[182], P.R. Newman[21], T.Y. Ng[63c], Y.S. Ng[19], Y.W.Y. Ng[171], H.D.N. Nguyen[101], T. Nguyen Manh[109], E. Nibigira[38], R.B. Nickerson[135], R. Nicolaidou[145], D.S. Nielsen[40], J. Nielsen[146], N. Nikiforou[11], V. Nikolaenko[122,ao], I. Nikolic-Audit[136], K. Nikolopoulos[21], P. Nilsson[29], H.R. Nindhito[54], Y. Ninomiya[81], A. Nisati[72a], N. Nishu[60c], R. Nisius[114], I. Nitsche[47], T. Nitta[179], T. Nobe[163], Y. Noguchi[85], M. Nomachi[133], I. Nomidis[136], M.A. Nomura[29], M. Nordberg[36], N. Norjoharuddeen[135], T. Novak[91], O. Novgorodova[48], R. Novotny[142], L. Nozka[130], K. Ntekas[171], E. Nurse[94], F. Nuti[104], F.G. Oakham[34,ax], H. Oberlack[114], J. Ocariz[136], A. Ochi[82], I. Ochoa[39], J.P. Ochoa-Ricoux[147a], K. O'Connor[26], S. Oda[87], S. Odaka[81], S. Oerdek[53], A. Ogrodnik[83a], A. Oh[100], S.H. Oh[49], C.C. Ohm[154], H. Oide[55b,55a], M.L. Ojeda[167], H. Okawa[169], Y. Okazaki[85], Y. Okumura[163], T. Okuyama[81], A. Olariu[27b], L.F. Oleiro Seabra[140a], S.A. Olivares Pino[147a], D. Oliveira Damazio[29], J.L. Oliver[1], M.J.R. Olsson[171], A. Olszewski[84], J. Olszowska[84],

D.C. O'Neil[152], A. Onofre[140a,140e], K. Onogi[116], P.U.E. Onyisi[11], H. Oppen[134], M.J. Oreglia[37],
G.E. Orellana[88], D. Orestano[74a,74b], N. Orlando[14], R.S. Orr[167], B. Osculati[55b,55a,*], V. O'Shea[57],
R. Ospanov[60a], G. Otero y Garzon[30], H. Otono[87], M. Ouchrif[35d], F. Ould-Saada[134],
A. Ouraou[145], Q. Ouyang[15a], M. Owen[57], R.E. Owen[21], V.E. Ozcan[12c], N. Ozturk[8], J. Pacalt[130],
H.A. Pacey[32], K. Pachal[49], A. Pacheco Pages[14], C. Padilla Aranda[14], S. Pagan Griso[18],
M. Paganini[183], G. Palacino[65], S. Palazzo[50], S. Palestini[36], M. Palka[83b], D. Pallin[38],
I. Panagoulias[10], C.E. Pandini[36], J.G. Panduro Vazquez[93], P. Pani[46], G. Panizzo[66a,66c],
L. Paolozzi[54], C. Papadatos[109], K. Papageorgiou[9,i], A. Paramonov[6], D. Paredes Hernandez[63b],
S.R. Paredes Saenz[135], B. Parida[166], T.H. Park[167], A.J. Parker[89], M.A. Parker[32], F. Parodi[55b,55a],
E.W. Parrish[120], J.A. Parsons[39], U. Parzefall[52], L. Pascual Dominguez[136], V.R. Pascuzzi[167],
J.M.P. Pasner[146], E. Pasqualucci[72a], S. Passaggio[55b], F. Pastore[93], P. Pasuwan[45a,45b],
S. Pataraia[99], J.R. Pater[100], A. Pathak[181], T. Pauly[36], B. Pearson[114], M. Pedersen[134],
L. Pedraza Diaz[118], R. Pedro[140a,140b], S.V. Peleganchuk[121b,121a], O. Penc[141], C. Peng[15a],
H. Peng[60a], B.S. Peralva[80a], M.M. Perego[132], A.P. Pereira Peixoto[140a,140e], D.V. Perepelitsa[29],
F. Peri[19], L. Perini[68a,68b], H. Pernegger[36], S. Perrella[69a,69b], V.D. Peshekhonov[79,*], K. Peters[46],
R.F.Y. Peters[100], B.A. Petersen[36], T.C. Petersen[40], E. Petit[58], A. Petridis[1], C. Petridou[162],
P. Petroff[132], M. Petrov[135], F. Petrucci[74a,74b], M. Pettee[183], N.E. Pettersson[102], K. Petukhova[143],
A. Peyaud[145], R. Pezoa[147c], T. Pham[104], F.H. Phillips[106], P.W. Phillips[144], M.W. Phipps[173],
G. Piacquadio[155], E. Pianori[18], A. Picazio[102], R.H. Pickles[100], R. Piegaia[30], D. Pietreanu[27b],
J.E. Pilcher[37], A.D. Pilkington[100], M. Pinamonti[73a,73b], J.L. Pinfold[3], M. Pitt[180],
L. Pizzimento[73a,73b], M.-A. Pleier[29], V. Pleskot[143], E. Plotnikova[79], D. Pluth[78],
P. Podberezko[121b,121a], R. Poettgen[96], R. Poggi[54], L. Poggioli[132], I. Pogrebnyak[106], D. Pohl[24],
I. Pokharel[53], G. Polesello[70a], A. Poley[18], A. Policicchio[72a,72b], R. Polifka[36], A. Polini[23b],
C.S. Pollard[46], V. Polychronakos[29], D. Ponomarenko[111], L. Pontecorvo[36], S. Popa[27a],
G.A. Popeneciu[27d], D.M. Portillo Quintero[136], S. Pospisil[142], K. Potamianos[46], I.N. Potrap[79],
C.J. Potter[32], H. Potti[11], T. Poulsen[96], J. Poveda[36], T.D. Powell[149], G. Pownall[46],
M.E. Pozo Astigarraga[36], P. Pralavorio[101], S. Prell[78], D. Price[100], M. Primavera[67a], S. Prince[103],
M.L. Proffitt[148], N. Proklova[111], K. Prokofiev[63c], F. Prokoshin[147c], S. Protopopescu[29],
J. Proudfoot[6], M. Przybycien[83a], A. Puri[173], P. Puzo[132], J. Qian[105], Y. Qin[100], A. Quadt[53],
M. Queitsch-Maitland[46], A. Qureshi[1], P. Rados[104], F. Ragusa[68a,68b], G. Rahal[97], J.A. Raine[54],
S. Rajagopalan[29], A. Ramirez Morales[92], K. Ran[15a,15d], T. Rashid[132], S. Raspopov[5],
M.G. Ratti[68a,68b], D.M. Rauch[46], F. Rauscher[113], S. Rave[99], B. Ravina[149], I. Ravinovich[180],
J.H. Rawling[100], M. Raymond[36], A.L. Read[134], N.P. Readioff[58], M. Reale[67a,67b],
D.M. Rebuzzi[70a,70b], A. Redelbach[177], G. Redlinger[29], R.G. Reed[33d], K. Reeves[43], L. Rehnisch[19],
J. Reichert[137], D. Reikher[161], A. Reiss[99], A. Rej[151], C. Rembser[36], H. Ren[15a], M. Rescigno[72a],
S. Resconi[68a], E.D. Resseguie[137], S. Rettie[175], E. Reynolds[21], O.L. Rezanova[121b,121a],
P. Reznicek[143], E. Ricci[75a,75b], R. Richter[114], S. Richter[46], E. Richter-Was[83b], O. Ricken[24],
M. Ridel[136], P. Rieck[114], C.J. Riegel[182], O. Rifki[46], M. Rijssenbeek[155], A. Rimoldi[70a,70b],
M. Rimoldi[20], L. Rinaldi[23b], G. Ripellino[154], B. Ristić[89], E. Ritsch[36], I. Riu[14],
J.C. Rivera Vergara[147a], F. Rizatdinova[129], E. Rizvi[92], C. Rizzi[36], R.T. Roberts[100],
S.H. Robertson[103,ad], M. Robin[46], D. Robinson[32], J.E.M. Robinson[46], A. Robson[57], E. Rocco[99],
C. Roda[71a,71b], Y. Rodina[101], S. Rodriguez Bosca[174], A. Rodriguez Perez[14],
D. Rodriguez Rodriguez[174], A.M. Rodríguez Vera[168b], S. Roe[36], O. Røhne[134], R. Röhrig[114],
C.P.A. Roland[65], J. Roloff[59], A. Romaniouk[111], M. Romano[23b,23a], N. Rompotis[90], M. Ronzani[124],
L. Roos[136], S. Rosati[72a], K. Rosbach[52], N-A. Rosien[53], G. Rosin[102], B.J. Rosser[137], E. Rossi[46],
E. Rossi[74a,74b], E. Rossi[69a,69b], L.P. Rossi[55b], L. Rossini[68a,68b], J.H.N. Rosten[32], R. Rosten[14],
M. Rotaru[27b], J. Rothberg[148], D. Rousseau[132], D. Roy[33d], A. Rozanov[101], Y. Rozen[160],
X. Ruan[33d], F. Rubbo[153], F. Rühr[52], A. Ruiz-Martinez[174], A. Rummler[36], Z. Rurikova[52],

N.A. Rusakovich[79], H.L. Russell[103], L. Rustige[38,47], J.P. Rutherfoord[7], E.M. Rüttinger[46,k], Y.F. Ryabov[138,*], M. Rybar[39], G. Rybkin[132], A. Ryzhov[122], G.F. Rzehorz[53], P. Sabatini[53], G. Sabato[119], S. Sacerdoti[132], H.F-W. Sadrozinski[146], R. Sadykov[79], F. Safai Tehrani[72a], B. Safarzadeh Samani[156], P. Saha[120], S. Saha[103], M. Sahinsoy[61a], A. Sahu[182], M. Saimpert[46], M. Saito[163], T. Saito[163], H. Sakamoto[163], A. Sakharov[124,an], D. Salamani[54], G. Salamanna[74a,74b], J.E. Salazar Loyola[147c], P.H. Sales De Bruin[172], D. Salihagic[114,*], A. Salnikov[153], J. Salt[174], D. Salvatore[41b,41a], F. Salvatore[156], A. Salvucci[63a,63b,63c], A. Salzburger[36], J. Samarati[36], D. Sammel[52], D. Sampsonidis[162], D. Sampsonidou[162], J. Sánchez[174], A. Sanchez Pineda[66a,66c], H. Sandaker[134], C.O. Sander[46], M. Sandhoff[182], C. Sandoval[22], D.P.C. Sankey[144], M. Sannino[55b,55a], Y. Sano[116], A. Sansoni[51], C. Santoni[38], H. Santos[140a,140b], S.N. Santpur[18], A. Santra[174], A. Sapronov[79], J.G. Saraiva[140a,140d], O. Sasaki[81], K. Sato[169], E. Sauvan[5], P. Savard[167,ax], N. Savic[114], R. Sawada[163], C. Sawyer[144], L. Sawyer[95,al], C. Sbarra[23b], A. Sbrizzi[23a], T. Scanlon[94], J. Schaarschmidt[148], P. Schacht[114], B.M. Schachtner[113], D. Schaefer[37], L. Schaefer[137], J. Schaeffer[99], S. Schaepe[36], U. Schäfer[99], A.C. Schaffer[132], D. Schaile[113], R.D. Schamberger[155], N. Scharmberg[100], V.A. Schegelsky[138], D. Scheirich[143], F. Schenck[19], M. Schernau[171], C. Schiavi[55b,55a], S. Schier[146], L.K. Schildgen[24], Z.M. Schillaci[26], E.J. Schioppa[36], M. Schioppa[41b,41a], K.E. Schleicher[52], S. Schlenker[36], K.R. Schmidt-Sommerfeld[114], K. Schmieden[36], C. Schmitt[99], S. Schmitt[46], S. Schmitz[99], J.C. Schmoeckel[46], U. Schnoor[52], L. Schoeffel[145], A. Schoening[61b], E. Schopf[135], M. Schott[99], J.F.P. Schouwenberg[118], J. Schovancova[36], S. Schramm[54], F. Schroeder[182], A. Schulte[99], H-C. Schultz-Coulon[61a], M. Schumacher[52], B.A. Schumm[146], Ph. Schune[145], A. Schwartzman[153], T.A. Schwarz[105], Ph. Schwemling[145], R. Schwienhorst[106], A. Sciandra[24], G. Sciolla[26], M. Scornajenghi[41b,41a], F. Scuri[71a], F. Scutti[104], L.M. Scyboz[114], C.D. Sebastiani[72a,72b], P. Seema[19], S.C. Seidel[117], A. Seiden[146], T. Seiss[37], J.M. Seixas[80b], G. Sekhniaidze[69a], K. Sekhon[105], S.J. Sekula[42], N. Semprini-Cesari[23b,23a], S. Sen[49], S. Senkin[38], C. Serfon[76], L. Serin[132], L. Serkin[66a,66b], M. Sessa[60a], H. Severini[128], T. Šfiligoj[91], F. Sforza[170], A. Sfyrla[54], E. Shabalina[53], J.D. Shahinian[146], N.W. Shaikh[45a,45b], D. Shaked Renous[180], L.Y. Shan[15a], R. Shang[173], J.T. Shank[25], M. Shapiro[18], A. Sharma[135], A.S. Sharma[1], P.B. Shatalov[123], K. Shaw[156], S.M. Shaw[100], A. Shcherbakova[138], Y. Shen[128], N. Sherafati[34], A.D. Sherman[25], P. Sherwood[94], L. Shi[158,at], S. Shimizu[81], C.O. Shimmin[183], Y. Shimogama[179], M. Shimojima[115], I.P.J. Shipsey[135], S. Shirabe[87], M. Shiyakova[79,ab], J. Shlomi[180], A. Shmeleva[110], M.J. Shochet[37], J. Shojaii[104], D.R. Shope[128], S. Shrestha[126], E. Shulga[180], P. Sicho[141], A.M. Sickles[173], P.E. Sidebo[154], E. Sideras Haddad[33d], O. Sidiropoulou[36], A. Sidoti[23b,23a], F. Siegert[48], Dj. Sijacki[16], M.Jr. Silva[181], M.V. Silva Oliveira[80a], S.B. Silverstein[45a], S. Simion[132], E. Simioni[99], M. Simon[99], R. Simoniello[99], P. Sinervo[167], N.B. Sinev[131], M. Sioli[23b,23a], I. Siral[105], S.Yu. Sivoklokov[112], J. Sjölin[45a,45b], E. Skorda[96], P. Skubic[128], M. Slawinska[84], K. Sliwa[170], R. Slovak[143], V. Smakhtin[180], B.H. Smart[144], J. Smiesko[28a], N. Smirnov[111], S.Yu. Smirnov[111], Y. Smirnov[111], L.N. Smirnova[112,t], O. Smirnova[96], J.W. Smith[53], M. Smizanska[89], K. Smolek[142], A. Smykiewicz[84], A.A. Snesarev[110], H.L. Snoek[119], I.M. Snyder[131], S. Snyder[29], R. Sobie[176,ad], A.M. Soffa[171], A. Soffer[161], A. Søgaard[50], F. Sohns[53], G. Sokhrannyi[91], C.A. Solans Sanchez[36], E.Yu. Soldatov[111], U. Soldevila[174], A.A. Solodkov[122], A. Soloshenko[79], O.V. Solovyanov[122], V. Solovyev[138], P. Sommer[149], H. Son[170], W. Song[144], W.Y. Song[168b], A. Sopczak[142], F. Sopkova[28b], C.L. Sotiropoulou[71a,71b], S. Sottocornola[70a,70b], R. Soualah[66a,66c,h], A.M. Soukharev[121b,121a], D. South[46], S. Spagnolo[67a,67b], M. Spalla[114], M. Spangenberg[178], F. Spanò[93], D. Sperlich[19], T.M. Spieker[61a], R. Spighi[23b], G. Spigo[36], L.A. Spiller[104], M. Spina[156], D.P. Spiteri[57], M. Spousta[143], A. Stabile[68a,68b], B.L. Stamas[120], R. Stamen[61a], M. Stamenkovic[119], S. Stamm[19], E. Stanecka[84], R.W. Stanek[6], B. Stanislaus[135], M.M. Stanitzki[46], M. Stankaityte[135], B. Stapf[119], E.A. Starchenko[122], G.H. Stark[146], J. Stark[58],

S.H. Stark[40], P. Staroba[141], P. Starovoitov[61a], S. Stärz[103], R. Staszewski[84], G. Stavropoulos[44], M. Stegler[46], P. Steinberg[29], B. Stelzer[152], H.J. Stelzer[36], O. Stelzer-Chilton[168a], H. Stenzel[56], T.J. Stevenson[156], G.A. Stewart[36], M.C. Stockton[36], G. Stoicea[27b], M. Stolarski[140a], P. Stolte[53], S. Stonjek[114], A. Straessner[48], J. Strandberg[154], S. Strandberg[45a,45b], M. Strauss[128], P. Strizenec[28b], R. Ströhmer[177], D.M. Strom[131], R. Stroynowski[42], A. Strubig[50], S.A. Stucci[29], B. Stugu[17], J. Stupak[128], N.A. Styles[46], D. Su[153], S. Suchek[61a], Y. Sugaya[133], V.V. Sulin[110], M.J. Sullivan[90], D.M.S. Sultan[54], S. Sultansoy[4c], T. Sumida[85], S. Sun[105], X. Sun[3], K. Suruliz[156], C.J.E. Suster[157], M.R. Sutton[156], S. Suzuki[81], M. Svatos[141], M. Swiatlowski[37], S.P. Swift[2], A. Sydorenko[99], I. Sykora[28a], M. Sykora[143], T. Sykora[143], D. Ta[99], K. Tackmann[46,z], J. Taenzer[161], A. Taffard[171], R. Tafirout[168a], E. Tahirovic[92], H. Takai[29], R. Takashima[86], K. Takeda[82], T. Takeshita[150], E.P. Takeva[50], Y. Takubo[81], M. Talby[101], A.A. Talyshev[121b,121a], N.M. Tamir[161], J. Tanaka[163], M. Tanaka[165], R. Tanaka[132], B.B. Tannenwald[126], S. Tapia Araya[173], S. Tapprogge[99], A. Tarek Abouelfadl Mohamed[136], S. Tarem[160], G. Tarna[27b,d], G.F. Tartarelli[68a], P. Tas[143], M. Tasevsky[141], T. Tashiro[85], E. Tassi[41b,41a], A. Tavares Delgado[140a,140b], Y. Tayalati[35e], A.J. Taylor[50], G.N. Taylor[104], P.T.E. Taylor[104], W. Taylor[168b], A.S. Tee[89], R. Teixeira De Lima[153], P. Teixeira-Dias[93], H. Ten Kate[36], J.J. Teoh[119], S. Terada[81], K. Terashi[163], J. Terron[98], S. Terzo[14], M. Testa[51], R.J. Teuscher[167,ad], S.J. Thais[183], T. Theveneaux-Pelzer[46], F. Thiele[40], D.W. Thomas[93], J.O. Thomas[42], J.P. Thomas[21], A.S. Thompson[57], P.D. Thompson[21], L.A. Thomsen[183], E. Thomson[137], Y. Tian[39], R.E. Ticse Torres[53], V.O. Tikhomirov[110,ap], Yu.A. Tikhonov[121b,121a], S. Timoshenko[111], P. Tipton[183], S. Tisserant[101], K. Todome[23b,23a], S. Todorova-Nova[5], S. Todt[48], J. Tojo[87], S. Tokár[28a], K. Tokushuku[81], E. Tolley[126], K.G. Tomiwa[33d], M. Tomoto[116], L. Tompkins[153,q], B. Tong[59], P. Tornambe[102], E. Torrence[131], H. Torres[48], E. Torró Pastor[148], C. Tosciri[135], J. Toth[101,ac], D.R. Tovey[149], C.J. Treado[124], T. Trefzger[177], F. Tresoldi[156], A. Tricoli[29], I.M. Trigger[168a], S. Trincaz-Duvoid[136], W. Trischuk[167], B. Trocmé[58], A. Trofymov[132], C. Troncon[68a], M. Trovatelli[176], F. Trovato[156], L. Truong[33b], M. Trzebinski[84], A. Trzupek[84], F. Tsai[46], J.C-L. Tseng[135], P.V. Tsiareshka[107,aj], A. Tsirigotis[162], N. Tsirintanis[9], V. Tsiskaridze[155], E.G. Tskhadadze[159a], M. Tsopoulou[162], I.I. Tsukerman[123], V. Tsulaia[18], S. Tsuno[81], D. Tsybychev[155], Y. Tu[63b], A. Tudorache[27b], V. Tudorache[27b], T.T. Tulbure[27a], A.N. Tuna[59], S. Turchikhin[79], D. Turgeman[180], I. Turk Cakir[4b,u], R.J. Turner[21], R.T. Turra[68a], P.M. Tuts[39], S. Tzamarias[162], E. Tzovara[99], G. Ucchielli[47], I. Ueda[81], M. Ughetto[45a,45b], F. Ukegawa[169], G. Unal[36], A. Undrus[29], G. Unel[171], F.C. Ungaro[104], Y. Unno[81], K. Uno[163], J. Urban[28b], P. Urquijo[104], G. Usai[8], J. Usui[81], L. Vacavant[101], V. Vacek[142], B. Vachon[103], K.O.H. Vadla[134], A. Vaidya[94], C. Valderanis[113], E. Valdes Santurio[45a,45b], M. Valente[54], S. Valentinetti[23b,23a], A. Valero[174], L. Valéry[46], R.A. Vallance[21], A. Vallier[36], J.A. Valls Ferrer[174], T.R. Van Daalen[14], P. Van Gemmeren[6], I. Van Vulpen[119], M. Vanadia[73a,73b], W. Vandelli[36], A. Vaniachine[166], R. Vari[72a], E.W. Varnes[7], C. Varni[55b,55a], T. Varol[42], D. Varouchas[132], K.E. Varvell[157], M.E. Vasile[27b], G.A. Vasquez[176], J.G. Vasquez[183], F. Vazeille[38], D. Vazquez Furelos[14], T. Vazquez Schroeder[36], J. Veatch[53], V. Vecchio[74a,74b], L.M. Veloce[167], F. Veloso[140a,140c], S. Veneziano[72a], A. Ventura[67a,67b], N. Venturi[36], A. Verbytskyi[114], V. Vercesi[70a], M. Verducci[74a,74b], C.M. Vergel Infante[78], C. Vergis[24], W. Verkerke[119], A.T. Vermeulen[119], J.C. Vermeulen[119], M.C. Vetterli[152,ax], N. Viaux Maira[147c], M. Vicente Barreto Pinto[54], I. Vichou[173,*], T. Vickey[149], O.E. Vickey Boeriu[149], G.H.A. Viehhauser[135], L. Vigani[135], M. Villa[23b,23a], M. Villaplana Perez[68a,68b], E. Vilucchi[51], M.G. Vincter[34], V.B. Vinogradov[79], A. Vishwakarma[46], C. Vittori[23b,23a], I. Vivarelli[156], M. Vogel[182], P. Vokac[142], G. Volpi[14], S.E. von Buddenbrock[33d], E. Von Toerne[24], V. Vorobel[143], K. Vorobev[111], M. Vos[174], J.H. Vossebeld[90], N. Vranjes[16], M. Vranjes Milosavljevic[16], V. Vrba[142], M. Vreeswijk[119], R. Vuillermet[36], I. Vukotic[37], P. Wagner[24], W. Wagner[182], J. Wagner-Kuhr[113],

H. Wahlberg[88], S. Wahrmund[48], K. Wakamiya[82], V.M. Walbrecht[114], J. Walder[89], R. Walker[113],
S.D. Walker[93], W. Walkowiak[151], V. Wallangen[45a,45b], A.M. Wang[59], C. Wang[60b], F. Wang[181],
H. Wang[18], H. Wang[3], J. Wang[157], J. Wang[61b], P. Wang[42], Q. Wang[128], R.-J. Wang[136],
R. Wang[60a], R. Wang[6], S.M. Wang[158], W.T. Wang[60a], W. Wang[15c,ae], W.X. Wang[60a,ae],
Y. Wang[60a,am], Z. Wang[60c], C. Wanotayaroj[46], A. Warburton[103], C.P. Ward[32], D.R. Wardrope[94],
A. Washbrook[50], A.T. Watson[21], M.F. Watson[21], G. Watts[148], B.M. Waugh[94], A.F. Webb[11],
S. Webb[99], C. Weber[183], M.S. Weber[20], S.A. Weber[34], S.M. Weber[61a], A.R. Weidberg[135],
J. Weingarten[47], M. Weirich[99], C. Weiser[52], P.S. Wells[36], T. Wenaus[29], T. Wengler[36], S. Wenig[36],
N. Wermes[24], M.D. Werner[78], P. Werner[36], M. Wessels[61a], T.D. Weston[20], K. Whalen[131],
N.L. Whallon[148], A.M. Wharton[89], A.S. White[105], A. White[8], M.J. White[1], R. White[147c],
D. Whiteson[171], B.W. Whitmore[89], F.J. Wickens[144], W. Wiedenmann[181], M. Wielers[144],
C. Wiglesworth[40], L.A.M. Wiik-Fuchs[52], F. Wilk[100], H.G. Wilkens[36], L.J. Wilkins[93],
H.H. Williams[137], S. Williams[32], C. Willis[106], S. Willocq[102], J.A. Wilson[21], I. Wingerter-Seez[5],
E. Winkels[156], F. Winklmeier[131], O.J. Winston[156], B.T. Winter[52], M. Wittgen[153], M. Wobisch[95],
A. Wolf[99], T.M.H. Wolf[119], R. Wolff[101], R.W. Wölker[135], J. Wollrath[52], M.W. Wolter[84],
H. Wolters[140a,140c], V.W.S. Wong[175], N.L. Woods[146], S.D. Worm[21], B.K. Wosiek[84],
K.W. Woźniak[84], K. Wraight[57], S.L. Wu[181], X. Wu[54], Y. Wu[60a], T.R. Wyatt[100], B.M. Wynne[50],
S. Xella[40], Z. Xi[105], L. Xia[178], D. Xu[15a], H. Xu[60a,d], L. Xu[29], T. Xu[145], W. Xu[105], Z. Xu[60b],
Z. Xu[153], B. Yabsley[157], S. Yacoob[33a], K. Yajima[133], D.P. Yallup[94], D. Yamaguchi[165],
Y. Yamaguchi[165], A. Yamamoto[81], T. Yamanaka[163], F. Yamane[82], M. Yamatani[163],
T. Yamazaki[163], Y. Yamazaki[82], Z. Yan[25], H.J. Yang[60c,60d], H.T. Yang[18], S. Yang[77],
X. Yang[60b,58], Y. Yang[163], Z. Yang[17], W-M. Yao[18], Y.C. Yap[46], Y. Yasu[81], E. Yatsenko[60c,60d],
J. Ye[42], S. Ye[29], I. Yeletskikh[79], E. Yigitbasi[25], E. Yildirim[99], K. Yorita[179], K. Yoshihara[137],
C.J.S. Young[36], C. Young[153], J. Yu[78], X. Yue[61a], S.P.Y. Yuen[24], B. Zabinski[84], G. Zacharis[10],
E. Zaffaroni[54], J. Zahreddine[136], R. Zaidan[14], A.M. Zaitsev[122,ao], T. Zakareishvili[159b],
N. Zakharchuk[34], S. Zambito[59], D. Zanzi[36], D.R. Zaripovas[57], S.V. Zeißner[47], C. Zeitnitz[182],
G. Zemaityte[135], J.C. Zeng[173], O. Zenin[122], T. Ženiš[28a], D. Zerwas[132], M. Zgubič[135],
D.F. Zhang[15b], F. Zhang[181], G. Zhang[60a], G. Zhang[15b], H. Zhang[15c], J. Zhang[6], L. Zhang[15c],
L. Zhang[60a], M. Zhang[173], R. Zhang[60a], R. Zhang[24], X. Zhang[60b], Y. Zhang[15a,15d], Z. Zhang[63a],
Z. Zhang[132], P. Zhao[49], Y. Zhao[60b], Z. Zhao[60a], A. Zhemchugov[79], Z. Zheng[105], D. Zhong[173],
B. Zhou[105], C. Zhou[181], M.S. Zhou[15a,15d], M. Zhou[155], N. Zhou[60c], Y. Zhou[7], C.G. Zhu[60b],
H.L. Zhu[60a], H. Zhu[15a], J. Zhu[105], Y. Zhu[60a], X. Zhuang[15a], K. Zhukov[110], V. Zhulanov[121b,121a],
D. Zieminska[65], N.I. Zimine[79], S. Zimmermann[52], Z. Zinonos[114], M. Ziolkowski[151], L. Živković[16],
G. Zobernig[181], A. Zoccoli[23b,23a], K. Zoch[53], T.G. Zorbas[149], R. Zou[37], L. Zwalinski[36]

1 *Department of Physics, University of Adelaide, Adelaide, Australia*
2 *Physics Department, SUNY Albany, Albany NY, United States of America*
3 *Department of Physics, University of Alberta, Edmonton AB, Canada*
4 *(a) Department of Physics, Ankara University, Ankara; (b) Istanbul Aydin University, Istanbul; (c) Division of Physics, TOBB University of Economics and Technology, Ankara, Turkey*
5 *LAPP, Université Grenoble Alpes, Université Savoie Mont Blanc, CNRS/IN2P3, Annecy, France*
6 *High Energy Physics Division, Argonne National Laboratory, Argonne IL, United States of America*
7 *Department of Physics, University of Arizona, Tucson AZ, United States of America*
8 *Department of Physics, University of Texas at Arlington, Arlington TX, United States of America*
9 *Physics Department, National and Kapodistrian University of Athens, Athens, Greece*
10 *Physics Department, National Technical University of Athens, Zografou, Greece*
11 *Department of Physics, University of Texas at Austin, Austin TX, United States of America*
12 *(a) Bahcesehir University, Faculty of Engineering and Natural Sciences, Istanbul; (b) Istanbul Bilgi University, Faculty of Engineering and Natural Sciences, Istanbul; (c) Department of Physics, Bogazici University, Istanbul; (d) Department of Physics Engineering, Gaziantep University, Gaziantep, Turkey*

13 Institute of Physics, Azerbaijan Academy of Sciences, Baku, Azerbaijan

14 Institut de Física d'Altes Energies (IFAE), Barcelona Institute of Science and Technology, Barcelona, Spain

15 [a] Institute of High Energy Physics, Chinese Academy of Sciences, Beijing; [b] Physics Department, Tsinghua University, Beijing; [c] Department of Physics, Nanjing University, Nanjing; [d] University of Chinese Academy of Science (UCAS), Beijing, China

16 Institute of Physics, University of Belgrade, Belgrade, Serbia

17 Department for Physics and Technology, University of Bergen, Bergen, Norway

18 Physics Division, Lawrence Berkeley National Laboratory and University of California, Berkeley CA, United States of America

19 Institut für Physik, Humboldt Universität zu Berlin, Berlin, Germany

20 Albert Einstein Center for Fundamental Physics and Laboratory for High Energy Physics, University of Bern, Bern, Switzerland

21 School of Physics and Astronomy, University of Birmingham, Birmingham, United Kingdom

22 Facultad de Ciencias y Centro de Investigaciónes, Universidad Antonio Nariño, Bogota, Colombia

23 [a] INFN Bologna and Universita' di Bologna, Dipartimento di Fisica; [b] INFN Sezione di Bologna, Italy

24 Physikalisches Institut, Universität Bonn, Bonn, Germany

25 Department of Physics, Boston University, Boston MA, United States of America

26 Department of Physics, Brandeis University, Waltham MA, United States of America

27 [a] Transilvania University of Brasov, Brasov; [b] Horia Hulubei National Institute of Physics and Nuclear Engineering, Bucharest; [c] Department of Physics, Alexandru Ioan Cuza University of Iasi, Iasi; [d] National Institute for Research and Development of Isotopic and Molecular Technologies, Physics Department, Cluj-Napoca; [e] University Politehnica Bucharest, Bucharest; [f] West University in Timisoara, Timisoara, Romania

28 [a] Faculty of Mathematics, Physics and Informatics, Comenius University, Bratislava; [b] Department of Subnuclear Physics, Institute of Experimental Physics of the Slovak Academy of Sciences, Kosice, Slovak Republic

29 Physics Department, Brookhaven National Laboratory, Upton NY, United States of America

30 Departamento de Física, Universidad de Buenos Aires, Buenos Aires, Argentina

31 California State University, CA, United States of America

32 Cavendish Laboratory, University of Cambridge, Cambridge, United Kingdom

33 [a] Department of Physics, University of Cape Town, Cape Town; [b] Department of Mechanical Engineering Science, University of Johannesburg, Johannesburg; [c] Pretoria; [d] School of Physics, University of the Witwatersrand, Johannesburg, South Africa

34 Department of Physics, Carleton University, Ottawa ON, Canada

35 [a] Faculté des Sciences Ain Chock, Réseau Universitaire de Physique des Hautes Energies — Université Hassan II, Casablanca; [b] Faculté des Sciences, Université Ibn-Tofail, Kénitra; [c] Faculté des Sciences Semlalia, Université Cadi Ayyad, LPHEA-Marrakech; [d] Faculté des Sciences, Université Mohamed Premier and LPTPM, Oujda; [e] Faculté des sciences, Université Mohammed V, Rabat, Morocco

36 CERN, Geneva, Switzerland

37 Enrico Fermi Institute, University of Chicago, Chicago IL, United States of America

38 LPC, Université Clermont Auvergne, CNRS/IN2P3, Clermont-Ferrand, France

39 Nevis Laboratory, Columbia University, Irvington NY, United States of America

40 Niels Bohr Institute, University of Copenhagen, Copenhagen, Denmark

41 [a] Dipartimento di Fisica, Università della Calabria, Rende; [b] INFN Gruppo Collegato di Cosenza, Laboratori Nazionali di Frascati, Italy

42 Physics Department, Southern Methodist University, Dallas TX, United States of America

43 Physics Department, University of Texas at Dallas, Richardson TX, United States of America

44 National Centre for Scientific Research "Demokritos", Agia Paraskevi, Greece

45 [a] Department of Physics, Stockholm University; [b] Oskar Klein Centre, Stockholm, Sweden

46   *Deutsches Elektronen-Synchrotron DESY, Hamburg and Zeuthen, Germany*

47   *Lehrstuhl für Experimentelle Physik IV, Technische Universität Dortmund, Dortmund, Germany*

48   *Institut für Kern und Teilchenphysik, Technische Universität Dresden, Dresden, Germany*

49   *Department of Physics, Duke University, Durham NC, United States of America*

50   *SUPA — School of Physics and Astronomy, University of Edinburgh, Edinburgh, United Kingdom*

51   *INFN e Laboratori Nazionali di Frascati, Frascati, Italy*

52   *Physikalisches Institut, Albert-Ludwigs-Universität Freiburg, Freiburg, Germany*

53   *II. Physikalisches Institut, Georg-August-Universität Göttingen, Göttingen, Germany*

54   *Département de Physique Nucléaire et Corpusculaire, Université de Genève, Genève, Switzerland*

55   [a]*Dipartimento di Fisica, Università di Genova, Genova;* [b]*INFN Sezione di Genova, Italy*

56   *II. Physikalisches Institut, Justus-Liebig-Universität Giessen, Giessen, Germany*

57   *SUPA — School of Physics and Astronomy, University of Glasgow, Glasgow, United Kingdom*

58   *LPSC, Université Grenoble Alpes, CNRS/IN2P3, Grenoble INP, Grenoble, France*

59   *Laboratory for Particle Physics and Cosmology, Harvard University, Cambridge MA, United States of America*

60   [a]*Department of Modern Physics and State Key Laboratory of Particle Detection and Electronics, University of Science and Technology of China, Hefei;* [b]*Institute of Frontier and Interdisciplinary Science and Key Laboratory of Particle Physics and Particle Irradiation (MOE), Shandong University, Qingdao;* [c]*School of Physics and Astronomy, Shanghai Jiao Tong University, KLPPAC-MoE, SKLPPC, Shanghai;* [d]*Tsung-Dao Lee Institute, Shanghai, China*

61   [a]*Kirchhoff-Institut für Physik, Ruprecht-Karls-Universität Heidelberg, Heidelberg;* [b]*Physikalisches Institut, Ruprecht-Karls-Universität Heidelberg, Heidelberg, Germany*

62   *Faculty of Applied Information Science, Hiroshima Institute of Technology, Hiroshima, Japan*

63   [a]*Department of Physics, Chinese University of Hong Kong, Shatin, N.T., Hong Kong;* [b]*Department of Physics, University of Hong Kong, Hong Kong;* [c]*Department of Physics and Institute for Advanced Study, Hong Kong University of Science and Technology, Clear Water Bay, Kowloon, Hong Kong, China*

64   *Department of Physics, National Tsing Hua University, Hsinchu, Taiwan*

65   *Department of Physics, Indiana University, Bloomington IN, United States of America*

66   [a]*INFN Gruppo Collegato di Udine, Sezione di Trieste, Udine;* [b]*ICTP, Trieste;* [c]*Dipartimento Politecnico di Ingegneria e Architettura, Università di Udine, Udine, Italy*

67   [a]*INFN Sezione di Lecce;* [b]*Dipartimento di Matematica e Fisica, Università del Salento, Lecce, Italy*

68   [a]*INFN Sezione di Milano;* [b]*Dipartimento di Fisica, Università di Milano, Milano, Italy*

69   [a]*INFN Sezione di Napoli;* [b]*Dipartimento di Fisica, Università di Napoli, Napoli, Italy*

70   [a]*INFN Sezione di Pavia;* [b]*Dipartimento di Fisica, Università di Pavia, Pavia, Italy*

71   [a]*INFN Sezione di Pisa;* [b]*Dipartimento di Fisica E. Fermi, Università di Pisa, Pisa, Italy*

72   [a]*INFN Sezione di Roma;* [b]*Dipartimento di Fisica, Sapienza Università di Roma, Roma, Italy*

73   [a]*INFN Sezione di Roma Tor Vergata;* [b]*Dipartimento di Fisica, Università di Roma Tor Vergata, Roma, Italy*

74   [a]*INFN Sezione di Roma Tre;* [b]*Dipartimento di Matematica e Fisica, Università Roma Tre, Roma, Italy*

75   [a]*INFN-TIFPA;* [b]*Università degli Studi di Trento, Trento, Italy*

76   *Institut für Astro und Teilchenphysik, Leopold-Franzens-Universität, Innsbruck, Austria*

77   *University of Iowa, Iowa City IA, United States of America*

78   *Department of Physics and Astronomy, Iowa State University, Ames IA, United States of America*

79   *Joint Institute for Nuclear Research, Dubna, Russia*

80   [a]*Departamento de Engenharia Elétrica, Universidade Federal de Juiz de Fora (UFJF), Juiz de Fora;* [b]*Universidade Federal do Rio De Janeiro COPPE/EE/IF, Rio de Janeiro;* [c]*Universidade Federal de São João del Rei (UFSJ), São João del Rei;* [d]*Instituto de Física, Universidade de São Paulo, São Paulo, Brazil*

81   *KEK, High Energy Accelerator Research Organization, Tsukuba, Japan*

82 *Graduate School of Science, Kobe University, Kobe, Japan*

83 *(a) AGH University of Science and Technology, Faculty of Physics and Applied Computer Science, Krakow; (b) Marian Smoluchowski Institute of Physics, Jagiellonian University, Krakow, Poland*

84 *Institute of Nuclear Physics Polish Academy of Sciences, Krakow, Poland*

85 *Faculty of Science, Kyoto University, Kyoto, Japan*

86 *Kyoto University of Education, Kyoto, Japan*

87 *Research Center for Advanced Particle Physics and Department of Physics, Kyushu University, Fukuoka , Japan*

88 *Instituto de Física La Plata, Universidad Nacional de La Plata and CONICET, La Plata, Argentina*

89 *Physics Department, Lancaster University, Lancaster, United Kingdom*

90 *Oliver Lodge Laboratory, University of Liverpool, Liverpool, United Kingdom*

91 *Department of Experimental Particle Physics, Jožef Stefan Institute and Department of Physics, University of Ljubljana, Ljubljana, Slovenia*

92 *School of Physics and Astronomy, Queen Mary University of London, London, United Kingdom*

93 *Department of Physics, Royal Holloway University of London, Egham, United Kingdom*

94 *Department of Physics and Astronomy, University College London, London, United Kingdom*

95 *Louisiana Tech University, Ruston LA, United States of America*

96 *Fysiska institutionen, Lunds universitet, Lund, Sweden*

97 *Centre de Calcul de l'Institut National de Physique Nucléaire et de Physique des Particules (IN2P3), Villeurbanne, France*

98 *Departamento de Física Teorica C-15 and CIAFF, Universidad Autónoma de Madrid, Madrid, Spain*

99 *Institut für Physik, Universität Mainz, Mainz, Germany*

100 *School of Physics and Astronomy, University of Manchester, Manchester, United Kingdom*

101 *CPPM, Aix-Marseille Université, CNRS/IN2P3, Marseille, France*

102 *Department of Physics, University of Massachusetts, Amherst MA, United States of America*

103 *Department of Physics, McGill University, Montreal QC, Canada*

104 *School of Physics, University of Melbourne, Victoria, Australia*

105 *Department of Physics, University of Michigan, Ann Arbor MI, United States of America*

106 *Department of Physics and Astronomy, Michigan State University, East Lansing MI, United States of America*

107 *B.I. Stepanov Institute of Physics, National Academy of Sciences of Belarus, Minsk, Belarus*

108 *Research Institute for Nuclear Problems of Byelorussian State University, Minsk, Belarus*

109 *Group of Particle Physics, University of Montreal, Montreal QC, Canada*

110 *P.N. Lebedev Physical Institute of the Russian Academy of Sciences, Moscow, Russia*

111 *National Research Nuclear University MEPhI, Moscow, Russia*

112 *D.V. Skobeltsyn Institute of Nuclear Physics, M.V. Lomonosov Moscow State University, Moscow, Russia*

113 *Fakultät für Physik, Ludwig-Maximilians-Universität München, München, Germany*

114 *Max-Planck-Institut für Physik (Werner-Heisenberg-Institut), München, Germany*

115 *Nagasaki Institute of Applied Science, Nagasaki, Japan*

116 *Graduate School of Science and Kobayashi-Maskawa Institute, Nagoya University, Nagoya, Japan*

117 *Department of Physics and Astronomy, University of New Mexico, Albuquerque NM, United States of America*

118 *Institute for Mathematics, Astrophysics and Particle Physics, Radboud University Nijmegen/Nikhef, Nijmegen, Netherlands*

119 *Nikhef National Institute for Subatomic Physics and University of Amsterdam, Amsterdam, Netherlands*

120 *Department of Physics, Northern Illinois University, DeKalb IL, United States of America*

121 *(a) Budker Institute of Nuclear Physics and NSU, SB RAS, Novosibirsk; (b) Novosibirsk State University Novosibirsk, Russia*

122 *Institute for High Energy Physics of the National Research Centre Kurchatov Institute, Protvino, Russia*

123 *Institute for Theoretical and Experimental Physics named by A.I. Alikhanov of National Research Centre "Kurchatov Institute", Moscow, Russia*

124 *Department of Physics, New York University, New York NY, United States of America*

125 *Ochanomizu University, Otsuka, Bunkyo-ku, Tokyo, Japan*

126 *Ohio State University, Columbus OH, United States of America*

127 *Faculty of Science, Okayama University, Okayama, Japan*

128 *Homer L. Dodge Department of Physics and Astronomy, University of Oklahoma, Norman OK, United States of America*

129 *Department of Physics, Oklahoma State University, Stillwater OK, United States of America*

130 *Palacký University, RCPTM, Joint Laboratory of Optics, Olomouc, Czech Republic*

131 *Center for High Energy Physics, University of Oregon, Eugene OR, United States of America*

132 *LAL, Université Paris-Sud, CNRS/IN2P3, Université Paris-Saclay, Orsay, France*

133 *Graduate School of Science, Osaka University, Osaka, Japan*

134 *Department of Physics, University of Oslo, Oslo, Norway*

135 *Department of Physics, Oxford University, Oxford, United Kingdom*

136 *LPNHE, Sorbonne Université, Université de Paris, CNRS/IN2P3, Paris, France*

137 *Department of Physics, University of Pennsylvania, Philadelphia PA, United States of America*

138 *Konstantinov Nuclear Physics Institute of National Research Centre "Kurchatov Institute", PNPI, St. Petersburg, Russia*

139 *Department of Physics and Astronomy, University of Pittsburgh, Pittsburgh PA, United States of America*

140 [a] *Laboratório de Instrumentação e Física Experimental de Partículas — LIP, Lisboa;* [b] *Departamento de Física, Faculdade de Ciências, Universidade de Lisboa, Lisboa;* [c] *Departamento de Física, Universidade de Coimbra, Coimbra;* [d] *Centro de Física Nuclear da Universidade de Lisboa, Lisboa;* [e] *Departamento de Física, Universidade do Minho, Braga;* [f] *Departamento de Física Teórica y del Cosmos, Universidad de Granada, Granada (Spain);* [g] *Departamento de Física and CEFITEC of Faculdade de Ciências e Tecnologia, Universidade Nova de Lisboa, Caparica;* [h] *Instituto Superior Técnico, Universidade de Lisboa, Lisboa, Portugal*

141 *Institute of Physics of the Czech Academy of Sciences, Prague, Czech Republic*

142 *Czech Technical University in Prague, Prague, Czech Republic*

143 *Charles University, Faculty of Mathematics and Physics, Prague, Czech Republic*

144 *Particle Physics Department, Rutherford Appleton Laboratory, Didcot, United Kingdom*

145 *IRFU, CEA, Université Paris-Saclay, Gif-sur-Yvette, France*

146 *Santa Cruz Institute for Particle Physics, University of California Santa Cruz, Santa Cruz CA, United States of America*

147 [a] *Departamento de Física, Pontificia Universidad Católica de Chile, Santiago;* [b] *Universidad Andres Bello, Department of Physics, Santiago;* [c] *Departamento de Física, Universidad Técnica Federico Santa María, Valparaíso, Chile*

148 *Department of Physics, University of Washington, Seattle WA, United States of America*

149 *Department of Physics and Astronomy, University of Sheffield, Sheffield, United Kingdom*

150 *Department of Physics, Shinshu University, Nagano, Japan*

151 *Department Physik, Universität Siegen, Siegen, Germany*

152 *Department of Physics, Simon Fraser University, Burnaby BC, Canada*

153 *SLAC National Accelerator Laboratory, Stanford CA, United States of America*

154 *Physics Department, Royal Institute of Technology, Stockholm, Sweden*

155 *Departments of Physics and Astronomy, Stony Brook University, Stony Brook NY, United States of America*

156 *Department of Physics and Astronomy, University of Sussex, Brighton, United Kingdom*

157 *School of Physics, University of Sydney, Sydney, Australia*

158 *Institute of Physics, Academia Sinica, Taipei, Taiwan*

159 [a] *E. Andronikashvili Institute of Physics, Iv. Javakhishvili Tbilisi State University, Tbilisi;* [b] *High Energy Physics Institute, Tbilisi State University, Tbilisi, Georgia*

160   *Department of Physics, Technion, Israel Institute of Technology, Haifa, Israel*

161   *Raymond and Beverly Sackler School of Physics and Astronomy, Tel Aviv University, Tel Aviv, Israel*

162   *Department of Physics, Aristotle University of Thessaloniki, Thessaloniki, Greece*

163   *International Center for Elementary Particle Physics and Department of Physics, University of Tokyo, Tokyo, Japan*

164   *Graduate School of Science and Technology, Tokyo Metropolitan University, Tokyo, Japan*

165   *Department of Physics, Tokyo Institute of Technology, Tokyo, Japan*

166   *Tomsk State University, Tomsk, Russia*

167   *Department of Physics, University of Toronto, Toronto ON, Canada*

168   [a]*TRIUMF, Vancouver BC;* [b]*Department of Physics and Astronomy, York University, Toronto ON, Canada*

169   *Division of Physics and Tomonaga Center for the History of the Universe, Faculty of Pure and Applied Sciences, University of Tsukuba, Tsukuba, Japan*

170   *Department of Physics and Astronomy, Tufts University, Medford MA, United States of America*

171   *Department of Physics and Astronomy, University of California Irvine, Irvine CA, United States of America*

172   *Department of Physics and Astronomy, University of Uppsala, Uppsala, Sweden*

173   *Department of Physics, University of Illinois, Urbana IL, United States of America*

174   *Instituto de Física Corpuscular (IFIC), Centro Mixto Universidad de Valencia — CSIC, Valencia, Spain*

175   *Department of Physics, University of British Columbia, Vancouver BC, Canada*

176   *Department of Physics and Astronomy, University of Victoria, Victoria BC, Canada*

177   *Fakultät für Physik und Astronomie, Julius-Maximilians-Universität Würzburg, Würzburg, Germany*

178   *Department of Physics, University of Warwick, Coventry, United Kingdom*

179   *Waseda University, Tokyo, Japan*

180   *Department of Particle Physics, Weizmann Institute of Science, Rehovot, Israel*

181   *Department of Physics, University of Wisconsin, Madison WI, United States of America*

182   *Fakultät für Mathematik und Naturwissenschaften, Fachgruppe Physik, Bergische Universität Wuppertal, Wuppertal, Germany*

183   *Department of Physics, Yale University, New Haven CT, United States of America*

184   *Yerevan Physics Institute, Yerevan, Armenia*

[a]   *Also at Borough of Manhattan Community College, City University of New York, New York NY, United States of America*

[b]   *Also at Centre for High Performance Computing, CSIR Campus, Rosebank, Cape Town, South Africa*

[c]   *Also at CERN, Geneva, Switzerland*

[d]   *Also at CPPM, Aix-Marseille Université, CNRS/IN2P3, Marseille, France*

[e]   *Also at Département de Physique Nucléaire et Corpusculaire, Université de Genève, Genève, Switzerland*

[f]   *Also at Departament de Fisica de la Universitat Autonoma de Barcelona, Barcelona, Spain*

[g]   *Also at Departamento de Física, Instituto Superior Técnico, Universidade de Lisboa, Lisboa, Portugal*

[h]   *Also at Department of Applied Physics and Astronomy, University of Sharjah, Sharjah, United Arab Emirates*

[i]   *Also at Department of Financial and Management Engineering, University of the Aegean, Chios, Greece*

[j]   *Also at Department of Physics and Astronomy, University of Louisville, Louisville, KY, United States of America*

[k]   *Also at Department of Physics and Astronomy, University of Sheffield, Sheffield, United Kingdom*

^{l} Also at Department of Physics, California State University, East Bay, United States of America

^{m} Also at Department of Physics, California State University, Fresno, United States of America

^{n} Also at Department of Physics, California State University, Sacramento, United States of America

^{o} Also at Department of Physics, King's College London, London, United Kingdom

^{p} Also at Department of Physics, St. Petersburg State Polytechnical University, St. Petersburg, Russia

^{q} Also at Department of Physics, Stanford University, Stanford CA, United States of America

^{r} Also at Department of Physics, University of Fribourg, Fribourg, Switzerland

^{s} Also at Department of Physics, University of Michigan, Ann Arbor MI, United States of America

^{t} Also at Faculty of Physics, M.V. Lomonosov Moscow State University, Moscow, Russia

^{u} Also at Giresun University, Faculty of Engineering, Giresun, Turkey

^{v} Also at Graduate School of Science, Osaka University, Osaka, Japan

^{w} Also at Hellenic Open University, Patras, Greece

^{x} Also at Horia Hulubei National Institute of Physics and Nuclear Engineering, Bucharest, Romania

^{y} Also at Institucio Catalana de Recerca i Estudis Avancats, ICREA, Barcelona, Spain

^{z} Also at Institut für Experimentalphysik, Universität Hamburg, Hamburg, Germany

^{aa} Also at Institute for Mathematics, Astrophysics and Particle Physics, Radboud University Nijmegen/Nikhef, Nijmegen, Netherlands

^{ab} Also at Institute for Nuclear Research and Nuclear Energy (INRNE) of the Bulgarian Academy of Sciences, Sofia, Bulgaria

^{ac} Also at Institute for Particle and Nuclear Physics, Wigner Research Centre for Physics, Budapest, Hungary

^{ad} Also at Institute of Particle Physics (IPP), Vancouver, Canada

^{ae} Also at Institute of Physics, Academia Sinica, Taipei, Taiwan

^{af} Also at Institute of Physics, Azerbaijan Academy of Sciences, Baku, Azerbaijan

^{ag} Also at Institute of Theoretical Physics, Ilia State University, Tbilisi, Georgia

^{ah} Also at Instituto de Fisica Teorica, IFT-UAM/CSIC, Madrid, Spain

^{ai} Also at Istanbul University, Department of Physics, Istanbul, Turkey

^{aj} Also at Joint Institute for Nuclear Research, Dubna, Russia

^{ak} Also at LAL, Université Paris-Sud, CNRS/IN2P3, Université Paris-Saclay, Orsay, France

^{al} Also at Louisiana Tech University, Ruston LA, United States of America

^{am} Also at LPNHE, Sorbonne Université, Université de Paris, CNRS/IN2P3, Paris, France

^{an} Also at Manhattan College, New York NY, United States of America

^{ao} Also at Moscow Institute of Physics and Technology State University, Dolgoprudny, Russia

^{ap} Also at National Research Nuclear University MEPhI, Moscow, Russia

^{aq} Also at Physics Department, An-Najah National University, Nablus, Palestine

^{ar} Also at Physics Dept, University of South Africa, Pretoria, South Africa

^{as} Also at Physikalisches Institut, Albert-Ludwigs-Universität Freiburg, Freiburg, Germany

^{at} Also at School of Physics, Sun Yat-sen University, Guangzhou, China

^{au} Also at The City College of New York, New York NY, United States of America

^{av} Also at The Collaborative Innovation Center of Quantum Matter (CICQM), Beijing, China

^{aw} Also at Tomsk State University, Tomsk, and Moscow Institute of Physics and Technology State University, Dolgoprudny, Russia

^{ax} Also at TRIUMF, Vancouver BC, Canada

^{ay} Also at Universita di Napoli Parthenope, Napoli, Italy

* Deceased